



# PACIFIC EARTHQUAKE ENGINEERING RESEARCH CENTER

## **Modeling Soil Liquefaction Hazards for Performance-Based Earthquake Engineering**

**Steven L. Kramer**  
University of Washington

**Ahmed-W. Elgamal**  
University of California, San Diego

A report on research conducted under  
grant no. EEC-9701568 from the National Science Foundation

# **Modeling Soil Liquefaction Hazards for Performance-Based Earthquake Engineering**

**Steven L. Kramer**

Professor

Department of Civil and Environmental Engineering  
University of Washington

**and**

**Ahmed-W. Elgamal**

Professor

Department of Structural Engineering  
University of California, San Diego

A report on research conducted under  
grant no. EEC-9701568 from the National Science Foundation

PEER Report 2001/13  
Pacific Earthquake Engineering Research Center  
College of Engineering  
University of California, Berkeley

February 2001

# EXECUTIVE SUMMARY

## Introduction

The performance of structures such as buildings and bridges during earthquakes is strongly influenced by the performance of the soils that support them. Local soil conditions can influence structural performance in two primary ways — by influencing the ground motions that excite the structure and by imposing additional deformations on the structure through ground failure.

The first widespread observations of damage attributed to liquefaction were made in the 1964 Niigata, Japan, and 1964 Alaska earthquakes. In numerous earthquakes since, liquefaction has been deemed responsible for significant damage to buildings and bridges. Liquefaction has been studied extensively over the past 35 years, and substantial advances have been made in understanding the development and effects of this phenomenon. These advances have led to a series of practical procedures for evaluating the potential for occurrence and for estimating its effects. These procedures, however, are almost entirely empirical in nature and, as such, are difficult to apply to the problem of performance prediction for individual structures.

The Pacific Earthquake Engineering Research (PEER) Center is committed to the development of methods and procedures for performance-based earthquake engineering (PBEE). The use of PBEE requires the ability to predict a nearly continuous spectrum of performance states for individual structures. This requirement implies the need for tools and procedures for evaluation of the entire process of liquefaction, from initiation to effects. Recent advances in the understanding of liquefaction-related phenomena offer the promise of improved analytical predictions of the initiation and effects of soil liquefaction.

## Background

Soil liquefaction is a complicated phenomenon that can manifest itself in several different ways in the field. When high porewater pressures are generated in a substantially thick soil layer that is relatively near the ground surface, the upward flowing porewater may carry sand particles up to the ground surface where they are deposited in a generally conical pile called a sand boil. While sand boils represent the most common evidence of subsurface soil liquefaction, they are not damaging by themselves. Liquefaction can, however, produce significant soil deformations, both horizontal and vertical, that can cause significant damage to a variety of structures.

Soil liquefaction has attracted considerable attention from geotechnical engineering researchers over the past 35 years. Liquefaction research has been undertaken from several different perspectives, which has led to some ambiguity and inconsistency in the terminology used to describe various liquefaction-related phenomena. For example, liquefaction was viewed by one group of researchers to correspond to the condition at which the effective stress reaches (temporarily) a value of zero, while another group considered liquefaction to have occurred when the soil deforms to large strains under constant shearing resistance. The first phenomenon is now referred to as cyclic mobility and the second as flow liquefaction. In the field, significant lateral deformations can be caused by either of these phenomena. The deformations produced by flow liquefaction are usually referred to as flow slides, and those produced by cyclic mobility as lateral spreads, but it is frequently impossible to distinguish between the two in the field. Further complicating matters is the fact that some flow slides begin as lateral spreads, so that the final deformations reflect both phenomena.

To date, most research into liquefaction hazards has concentrated on the question of liquefaction potential, i.e., whether or not liquefaction will occur. The influence of liquefaction on the performance of structures, however, depends on the *effects* of liquefaction. While estimation of liquefaction effects has been improved by development of empirical procedures, the uncertainty involved in predicting these effects is still extremely high. More reliable prediction of structural performance requires more accurate prediction of liquefaction effects. A significant portion of current and planned PEER research, in both the core and lifelines programs, is directed toward improved prediction of the effects of soil liquefaction. This research includes, and will eventually rely upon, the development of accurate, reliable, and practical models for soil liquefaction.

### **Contemporary Issues in Liquefaction Modeling**

The geotechnical engineering profession's understanding of the mechanics of soil liquefaction has improved greatly in recent years. The process by which excess porewater pressure increases and stiffness decreases at both low and high strain levels is well understood conceptually, although the experimental database for high strain behavior is quite limited. This improved understanding has allowed the development of constitutive models that capture important aspects of soil behavior that were not included in previous liquefaction models. Several PEER

researchers have made significant advances in this area, and continue to address contemporary issues in liquefaction modeling.

The development of models capable of predicting the effects of liquefaction requires that several issues be addressed. First, the model should be capable of accounting for phase transformation behavior. Second, the model should consider the effects of pore-pressure (and void-ratio) redistribution. Third, the model should account for the residual strength of the soil.

Fluctuations in the porewater pressure generated during laboratory tests on liquefiable soils have been observed for many years, but the phenomenon responsible for their occurrence has become well understood only relatively recently. In the early stages of cyclic loading, whether in the laboratory or in the field, liquefiable soils exhibit contractive behavior that causes porewater pressure to increase and effective stress to decrease. At high stress ratios (ratio of shear stress to effective normal stress), however, the soil can exhibit dilative behavior. Dilative behavior leads to reduced porewater pressure and increased effective stress. The condition at which the behavior changes from contractive to dilative, i.e., the phase transformation state, occurs at a particular stress ratio; when plotted graphically in stress path space, this stress ratio is referred to as the “phase transformation line.” The dilation associated with phase transformation behavior leads to stiffening and strengthening of a liquefied soil with increasing strain level. Therefore, phase transformation behavior plays a key role in determining the level of deformations, both cyclic and permanent, that can develop in a liquefied soil deposit. Because performance is so closely related to deformations, consideration of phase transformation behavior is a crucial part of liquefaction modeling for performance-based earthquake engineering.

As excess porewater pressures develop in a liquefiable soil deposit, the resulting hydraulic gradients cause the porewater to flow from regions of high hydraulic head to regions of low hydraulic head both during and after earthquake shaking. Frequently, this flow occurs in an upward direction and can, when a sufficient volume of water moves upward fast enough, lead to the ejection of sand and formation of sand boils at the ground surface. At some sites, however, the presence of low-permeability layers of soil impedes the flow of water. In such cases, porewater pressures increase in the vicinity of these layers, often for some period of time following the end of earthquake shaking. As the porewater pressure increases, the effective stress decreases, and the soil rebounds to a higher void ratio. At the higher void ratio, the

residual strength of the soil decreases (often significantly because residual strength is sensitive to void ratio), which can lead to the type of flow sliding that has frequently been observed following earthquakes in the past. Reliable prediction of the performance of structures in areas underlain by liquefiable soil requires that this important mechanism be considered in liquefaction hazard analysis; hence, liquefaction models should be capable of accounting for this type of behavior.

When a soil has liquefied, its available shearing resistance is generally reduced to a lower residual strength. If the residual strength is lower than the shear stresses required to maintain static equilibrium, large permanent deformations (e.g., flow slides) can occur. Accurate estimation of the residual strength of liquefied soil is one of the most difficult tasks faced by geotechnical engineers. Laboratory-based approaches suffer from the difficulty of obtaining undisturbed samples — the sampling process can affect soil properties to which residual strength is very sensitive. Field-based approaches, which involve back-calculation of residual strength from flow slide case histories and correlation to commonly available soil parameters, produce residual strength estimates with very high uncertainty. Reliable prediction of the performance of liquefied soil requires models that are capable of representing the residual strength of the liquefied soil, and additional information with which to make more reliable estimates of residual strength.

### **State-of-the-Art Approaches to Liquefaction Modeling**

The development of models for liquefiable soil should account for a number of important features of the behavior of those soils, including (a) nonlinear inelastic shear stress-strain response, (b) dependence of shear and volumetric stiffness on effective confining pressure, (c) contraction of the soil skeleton during the early stages of loading, (d) dilation of the soil skeleton at large strain excursions, (e) the critical state at which shearing occurs with neither contractive nor dilative tendencies, (f) controlled accumulation of cyclic shear strain when cyclic loading is superimposed upon static stresses, and (g) post-liquefaction void-ratio redistribution (dilative and, as the liquefied soil re-consolidates, contractive). Such models should be implemented within computational frameworks that consider the coupled response of the soil skeleton and porewater, and the effect of the permeability of the soil on the rate at which volume change can occur. Furthermore, the model should be capable of being calibrated with

information that is commonly available to practicing geotechnical engineers, rather than requiring a time-consuming and expensive series of laboratory tests.

This report describes the basis of the UCSD liquefaction model, a plasticity-based model that accounts for important characteristics of liquefiable soil response, and that can be relatively easily calibrated. Validation of the model by comparison of its predictions vs observed behavior in laboratory element tests, physical model tests, and observed field behavior is described. The model has been implemented into PEER's OpenSees computational platform and is being used to analyze the performance of soil-foundation-structure systems.

### **Research Needs and Future Directions**

Current liquefaction research needs can be broken into three main categories — investigation of liquefaction behavior, development of predictive tools, and collection of field data. These three categories are closely related, and an integrated program of research in all three should move forward. Among the most important of these fundamental research needs is characterization of post-liquefaction stress-strain behavior (shear-volume interaction, role of permeability, and permeability variation). This work will lead to advances in the prediction of delayed flow slides, which have been observed in numerous earthquakes and are not addressed by current liquefaction hazard evaluation procedures. This above needs should be addressed by laboratory (element) testing and model (centrifuge) testing on a variety of potentially liquefiable soils so that the soil characteristics that influence post-liquefaction stress-strain behavior can be identified.

Improved procedures for estimation of residual strength are needed, and the relationship between residual strength, steady state strength, and quasi-steady state strength must be clarified and defined with respect to performance-based earthquake engineering. Ongoing research is addressing the problem of steady state strength and residual strength, but integration with other ongoing experimental research involving quasi-steady state behavior is needed.

The PEER OpenSees computational platform is a valuable simulation tool for soil and soil-structure interaction problems. The “open”-available-to-all philosophy, and the broad range of structural and geotechnical contributions will make this a unique simulation environment. Planned Internet and parallel-processing (distributed computing) capabilities will further extend and facilitate use by all interested parties. The emphasis placed by PEER on calibration of

available OpenSees soil models is among the main strengths (and distinguishing elements) from the geotechnical engineering point of view.

## **Conclusions**

Geotechnical engineers have been studying soil liquefaction intensely since its effects were so dramatically revealed in the 1964 Niigata and Alaska earthquakes. The profession has developed reasonable procedures for evaluating the susceptibility of soils to liquefaction and for evaluating the level of loading required to initiate liquefaction.

Most liquefaction research to date has focused on the evaluation of liquefaction potential, i.e., on the behavior of the soil up to the point of initial liquefaction. Accurate prediction of the performance of structures founded on or near liquefiable soils requires the capability of modeling the most important aspects of the behavior of liquefiable soil both up to and, particularly, after the initiation of liquefaction. Additional experimental work, involving both soil element and model testing, is needed to elucidate the response of liquefiable soils over a wide range of stress and strain conditions.

Because the behavior of liquefiable soils is complex, and because performance-based earthquake engineering seeks to predict a virtually continuous range of performance levels, the development and validation of numerical models of liquefiable soil is necessary. These models should be capable of representing the most important aspects of the behavior of liquefiable soils, i.e., they should realistically model nonlinear inelastic behavior, phase transformation behavior, quasi-steady state and steady state behavior, and porewater pressure redistribution/dissipation. To be useful, these models should be of a form that can be calibrated using the type of information that is commonly available to geotechnical engineers. The models should be validated by comparing their predictions with the results of laboratory element and model tests, and with full-scale behavior from well-documented case histories.

The existence of numerical models with these capabilities will benefit the development of performance-based earthquake engineering in several ways. They will, when implemented into an analytical platform such as OpenSees, allow direct analysis of soil-foundation-structure interaction involving liquefiable soils. They will also be useful, through sensitivity and uncertainty analyses, for identification of the parameters that most strongly influence performance. Such efforts can be used to identify the required parameters, and even the

optimum mathematical form, for simplified, empirical (regression-based) performance prediction relationships. These models can also be used to guide the development of performance-based design procedures for liquefaction hazard mitigation by soil improvement.

PEER has taken a number of steps necessary to develop improved procedures and tools for evaluating performance at liquefiable soil sites, and is continuing work in that direction. Continuation and completion of this work will eventually result in more accurate, reliable, and cost-effective procedures for evaluating and mitigating the effects of soil liquefaction on the performance of structures.

## **ACKNOWLEDGMENTS**

This work was supported in part by the Pacific Earthquake Engineering Research Center through the Earthquake Engineering Research Centers Program of the National Science Foundation under Award number EEC-9701568. Their financial support is gratefully acknowledged.

In addition, the authors would like to thank PEER researchers working in the area of liquefaction modeling, including Pedro Arduino, Yannis Dafalias, Bruce Kutter, Juan Pestana, and Raymond Seed, who contributed thoughtful and stimulating discussions during formal and informal meetings. Important PEER case history research has been overseen by J. P. Bardet and Jon Bray. UC Berkeley graduate student Ann Marie Kammerer was a model of collaborative cooperation, and the PEER liquefaction research program has benefited from the results of her laboratory testing. The authors owe a particular debt of gratitude to Dr. Zhao Hui Yang of UC San Diego, who made significant contributions to chapters 5 and 6 of this report.

## **ABSTRACT**

The first widespread observations of damage attributed to liquefaction were made in the 1964 Niigata, Japan, and 1964 Alaska earthquakes. In numerous earthquakes since, liquefaction has been deemed responsible for significant damage to buildings and bridges. Liquefaction has been studied extensively over the past 35 years, and substantial advances have been made in understanding the development and effects of this phenomenon. These advances have led to a series of practical procedures for evaluating the potential for occurrence and for estimating its effects. These procedures, however, are almost entirely empirical in nature and, as such, are difficult to apply to the problem of performance prediction for individual structures.

The Pacific Earthquake Engineering Research (PEER) Center is committed to the development of methods and procedures for performance-based earthquake engineering (PBEE). The use of PBEE requires the ability to predict a nearly continuous spectrum of performance states for individual structures. This requirement implies the need for tools and procedures for evaluation of the entire process of liquefaction — from initiation to effects. Recent advances in the understanding of liquefaction-related phenomena offer the promise of improved analytical predictions of the initiation and effects of soil liquefaction. The purpose of this synthesis report is to summarize current procedures for practical prediction of liquefaction behavior, to describe recent advances in the understanding of liquefaction behavior, and to describe the incorporation of this improved understanding into new solutions for detailed modeling of soil liquefaction. The focus of this report, however, is on performance, and the reader should expect that aspects of liquefaction that relate to the performance of buildings, bridges, and lifelines will be emphasized. Well-known and widely used empirical tools and procedures for evaluation of liquefaction hazards will be reviewed relatively briefly, with more detailed discussions devoted to emerging knowledge about the mechanics of liquefiable soil behavior, and methods for incorporating those mechanics into improved models for performance prediction.

# CONTENTS

<b>EXECUTIVE SUMMARY .....</b>	<b>iii</b>
<b>ACKNOWLEDGMENTS .....</b>	<b>xi</b>
<b>ABSTRACT .....</b>	<b>xiii</b>
<b>TABLE OF CONTENTS .....</b>	<b>xv</b>
<b>LIST OF FIGURES .....</b>	<b>xix</b>
<b>LIST OF RESEARCH CAPSULES.....</b>	<b>xxv</b>
<b>PREFACE.....</b>	<b>xxvii</b>
<b>1 INTRODUCTION .....</b>	<b>1</b>
<b>2 FUNDAMENTALS OF SOIL LIQUEFACTION.....</b>	<b>3</b>
2.1 Introduction .....	3
2.2 Terminology .....	4
2.3 Examples of Soil Liquefaction .....	5
2.3.1 Field Case Histories.....	6
2.3.2 Laboratory Element Testing.....	22
2.3.3 Laboratory Model Test Results .....	37
2.4 Hazard Evaluation .....	40
2.4.1 Liquefaction Susceptibility.....	40
2.4.2 Initiation of Liquefaction.....	43
2.4.3 Effects of Liquefaction .....	54
2.5 Summary.....	65
<b>3 PERFORMANCE-BASED EARTHQUAKE ENGINEERING .....</b>	<b>67</b>
3.1 Introduction .....	67
3.2 Performance States .....	67
3.3 PBEE Framework .....	68
3.4 Geotechnical Considerations in Performance Prediction .....	70
3.4.1 Free-Field Response .....	71
3.4.2 Soil-Structure Interaction .....	72
3.5 Summary.....	74
<b>4 CONTEMPORARY ISSUES IN LIQUEFACTION MODELING.....</b>	<b>77</b>
4.1 Introduction .....	77
4.2 Liquefaction Susceptibility.....	77
4.3 Initiation of Liquefaction.....	78
4.4 Effects of Liquefaction .....	82
4.4.1 Phase Transformation Behavior .....	82
4.4.2 Pore-Pressure Redistribution .....	87
4.4.3 Residual Strength.....	90
4.5 Summary.....	93

<b>5</b>	<b>STATE-OF-THE-ART APPROACHES TO LIQUEFACTION MODELING .....</b>	<b>95</b>
5.1	Introduction .....	95
5.2	Desirable Features in a Liquefaction Soil Model .....	96
5.2.1	Practical Calibration Procedure .....	97
5.3	Liquefaction Models .....	98
5.3.1	Available Liquefaction Models .....	98
5.3.2	UCSD Model Description .....	100
5.3.3	Model Calibration .....	103
5.4	Model Performance .....	107
5.4.1	Simulation of UC Berkeley Laboratory Sample Tests .....	108
5.4.2	Simulation of UC Davis Centrifuge Test .....	111
5.4.3	Simulation of RPI (VELACS) Centrifuge Test, and Permeability Effects .....	112
5.4.4	Permeability Variation Effects .....	116
5.4.5	Simulation of RPI Centrifuge Embankment Tests .....	117
5.4.6	Simulation of Field Data .....	120
5.5	Recent UC Davis Contributions .....	123
5.5.1	State-Dependent Dilatancy .....	124
5.5.2	Stress-Induced Anisotropy during Loading/Unloading .....	126
5.5.3	Inherent (Material) Anisotropy .....	127
5.6	New Trends in Modeling of Soil Mechanics Behavior and Liquefaction .....	127
5.7	Implementation Issues .....	130
5.7.1	Model Calibration .....	130
5.7.2	Uncertainty .....	131
5.7.3	Discussion .....	131
5.8	Summary .....	132
<b>6</b>	<b>RESEARCH NEEDS AND FUTURE DIRECTIONS .....</b>	<b>133</b>
6.1	Introduction .....	133
6.2	Research Needs .....	133
6.2.1	Investigation of Liquefaction Behavior .....	134
6.2.2	Development of Predictive Tools .....	134
6.2.3	Collection of Field Data .....	135
6.3	OpenSees .....	135
6.3.1	Available Geotechnical Capabilities .....	136
6.3.2	Validation .....	137
6.3.3	Further Development .....	140
6.4	Interactive Website .....	141
6.4.1	Website Available Functionality .....	141
6.4.2	Presentation of Results .....	142
6.5	Summary .....	145
<b>7</b>	<b>SUMMARY AND CONCLUSIONS .....</b>	<b>147</b>
7.1	Effects of Liquefaction on Performance .....	147
7.2	Contemporary Issues .....	148

7.3	PEER Accomplishments.....	149
7.4	Conclusions.....	150
<b>REFERENCES.....</b>		<b>153</b>

## LIST OF FIGURES

Fig. 2.1	Kawagishi-cho apartment buildings in Niigata, Japan: (left) tilting due to bearing capacity failure; (right) close-up of shallow foundation exposed by failure.....	8
Fig. 2.2	Failure of Showa River Bridge in Niigata, Japan, due to lateral spreading .....	9
Fig. 2.3	Pile damage due to lateral spreading beneath the NHK building in Niigata, Japan .....	10
Fig. 2.4	Instrumentation layout and subsurface conditions at Wildlife array site (after Youd and Holzer, 1994) .....	11
Fig. 2.5	Sand boil at Wildlife array (courtesy of Earthquake Engineering Research Center, University of California, Berkeley) .....	12
Fig. 2.6	Measured ground surface acceleration and porewater pressures at Wildlife array site (after Zeghal and Elgamal, 1994) .....	13
Fig. 2.7	Average stress-strain and stress path curves at Wildlife array site .....	14
Fig. 2.8	Lateral spreading along Sandholdt Road (left), and at Monterey Bay Aquarium Research Institute (right) at Moss Landing (courtesy of Earthquake Engineering Research Center, University of California, Berkeley).....	15
Fig. 2.9	Location of inclinometers near Monterey Bay Aquarium Research Institute at Moss Landing (after Boulanger et al., 1997).....	16
Fig. 2.10	Lateral movement of inclinometer SI-5 at Moss Landing (after Boulanger et al., 1997) .....	17
Fig. 2.11	Location of Port Island vertical array .....	18
Fig. 2.12	Soil profile and accelerometer locations at Port Island vertical array (after Elgamal et al., 1996).....	19
Fig. 2.13	Recorded accelerograms at Port Island vertical array (after Elgamal et al., 1996) .....	20
Fig. 2.14	Computed average stress-strain behavior at Port Island array (after Elgamal et al., 1996) .....	21

Fig. 2.15	Stress conditions on cyclic triaxial test specimen (a) before cyclic loading and (b) during cyclic loading. Shaded region indicates orientation of plane of maximum shear stress.....	23
Fig. 2.16	Stress and strain conditions in cyclic simple shear test.....	25
Fig. 2.17	Three basic types of response observed by Castro (1969) in static triaxial tests: A — liquefaction, B — limited liquefaction, and C — dilation .....	28
Fig. 2.18	Flow liquefaction in isotropically consolidated triaxial test.....	29
Fig. 2.19	Flow liquefaction in anisotropically consolidated triaxial tests .....	30
Fig. 2.20	Schematic illustration of phase transformation line .....	32
Fig. 2.21	Schematic of constitutive model response showing the octahedral stress $\tau$ , the effective confining pressure $p$ , and the octahedral strain $\gamma$ relationship (after Parra, 1996).....	33
Fig. 2.22	Cyclic mobility with phase transformation behavior in a cyclic simple shear test .....	34
Fig. 2.23	Cyclic mobility with phase transformation behavior in a cyclic simple shear test with non-zero initial shear stress.....	36
Fig. 2.24	Stress-strain and excess-pore-pressure histories during an undrained, anisotropically consolidated cyclic triaxial test of Nevada Sand at $D_r=40\%$ (Arulmoli et al., 1992) .....	37
Fig. 2.25	Lateral spreading deformations indicated by vertical layers of colored sand, as observed in PWRI shaking table tests .....	38
Fig. 2.26	Geotechnical centrifuge at UC Davis. Note laminar box in centrifuge bucket for testing models under seismic loading conditions .....	38
Fig. 2.27	Schematic illustration of steady-state line with conditions of susceptibility to flow liquefaction.....	42
Fig. 2.28	Number of equivalent cycles of loading for liquefaction potential evaluation .....	44
Fig. 2.29	Relationship between cyclic resistance ratio and $(N_l)_{60}$ for $M_w = 7.5$ earthquakes .....	45
Fig. 2.30	Magnitude scaling factors.....	45
Fig. 2.31	Probability of liquefaction contours of Liao et al. (1988) (after Seed et al., 2001) ...	47

Fig. 2.32	Probability of liquefaction contours of Youd and Noble (1997) (after Seed et al., 2001).....	48
Fig. 2.33	Probability of liquefaction contours of Toprak et al. (1999) (after Seed et al., 2001).....	49
Fig. 2.34	Probability of liquefaction contours of Juang and Jiang (2000).....	50
Fig. 2.35	Relationship between SPT resistance and Arias intensity required to trigger liquefaction (after Kayen and Mitchell, 1997) .....	53
Fig. 2.36	Time history of ground surface acceleration from Niigata, Japan. Note dramatic change in frequency content after initiation of liquefaction at 6 – 7 sec.....	55
Fig. 2.37	Coastal flooding due to liquefaction-induced subsidence in Gölcük (from Izmit Collection, Earthquake Engineering Research Center, University of California, Berkeley).....	56
Fig. 2.38	Structural failure due to liquefaction-induced settlement of isolated footing at Port of Taichung (from Izmit Collection, Earthquake Engineering Research Center, University of California, Berkeley) .....	56
Fig. 2.39	Schematic illustration of different types of response of liquefiable soils (after Yoshimine and Ishihara, 1998).....	58
Fig. 2.40	Examples of the effects of lateral spreading on bridges and wharf structures: (a) Nishinomiya bridge, (b) Port of Kobe wharf .....	60
Fig. 2.41	Liquefaction-induced bearing capacity failure in Adapazari, Turkey (from Izmit Collection, Earthquake Engineering Research Center, University of California, Berkeley).....	64
Fig. 2.42	Damage to Monterey Bay Aquarium Research Institute following 1989 Loma Prieta earthquake .....	64
Fig. 2.43	Pile damage due to lateral spreading in Kobe, Japan (from Izmit Collection, Earthquake Engineering Research Center, University of California, Berkeley).....	65
Fig. 4.1	Schematic illustration of apparatus and results of shaking table tests on saturated sand with silt layer (after Kokusho, 1999) .....	88
Fig. 5.1	Measured and numerically simulated shear behavior of Fuji River Sand (Ishihara, 1985; Iai, 1991).....	99

Fig. 5.2	Stress-strain and excess-pore-pressure histories during an undrained, anisotropically consolidated cyclic triaxial test of Nevada Sand at $D_r=40\%$ (Arulmoli et al., 1992) .....	99
Fig. 5.3	Computed simulation of undrained torsional shear-test response (Tateishi et al., 1995).....	100
Fig. 5.4	Conical yield surface in principal stress space and deviatoric plane (after Prevost, 1985; Lacy, 1986; Parra, 1996; and Yang, 2000).....	101
Fig. 5.5	Piecewise linear representation of soil nonlinear shear stress-strain response ( $\tau_f$ = model peak shear strength) .....	102
Fig. 5.6	Schematic of constitutive model response showing the octahedral stress $\tau$ , the effective confining pressure $p$ , and the octahedral strain $\gamma$ relationships (Parra, 1996; Yang, 2000) .....	103
Fig. 5.7	Experimental and computed (UCSD model) stress-strain curves for an isotropically consolidated, drained monotonic triaxial loading test (VELACS Test No. 40-100, Arulmoli et al., 1992; $\tau_{oct}$ and $\gamma_{oct}$ are octahedral quantities).....	104
Fig. 5.8	Experimental and computed (UCSD model) results of an isotropically consolidated, undrained monotonic triaxial loading test (VELACS Test No. 40-04, Arulmoli et al., 1992; PWP is porewater pressure).....	105
Fig. 5.9	Experimental and computed (UCSD model) results of an anisotropically consolidated, undrained cyclic triaxial loading test (VELACS Test No. 40-58, Arulmoli et al., 1992) .....	106
Fig. 5.10a	NS 11 experimental (left) and computed (right, UCSD model) response of dense Nevada sand (Kammerer et al., 2000) .....	109
Fig. 5.10b	NS 8 experimental (left) and computed (right, UCSD model) response of dense Nevada sand (Kammerer et al., 2000) .....	110
Fig. 5.11	UC Davis centrifuge model configuration and numerical model simulation (Balakrishnan et al., 1997; Yang, 2000).....	111
Fig. 5.12	Recorded and computed excess pore-pressure time histories along the soil profile (Yang, 2000) .....	112
Fig. 5.13	Recorded and computed surface lateral displacement time histories (Yang, 2000).....	112

Fig. 5.14	Lateral displacement histories in uniform soil profile with different permeability coefficients (Yang and Elgamal, 2001).....	114
Fig. 5.15	Excess pore-pressure histories in uniform soil profile with different permeability coefficients (Yang and Elgamal, 2001).....	115
Fig. 5.16	Excess pore-pressure profile and deformed mesh for clean sand profile with a silt- <i>k</i> interlayer (deformations are not to scale and are exaggerated for clarity, Yang and Elgamal, 2001) .....	117
Fig. 5.17	Centrifuge model setup (Adalier et al., 1998, PPT is pore-pressure transducer, ACC is accelerometer, LVDT is linear variable differential transducer).....	118
Fig. 5.18	Computed deformed configuration (benchmark with no remediation and sheet-pile enclosure, Parra, 1996).....	119
Fig. 5.19a	Computed shear stress-strain histories (no remediation, Parra, 1996) .....	119
Fig. 5.19b	Computed shear stress-strain histories (sheet-pile enclosure, Parra, 1996) .....	120
Fig. 5.20	Wildlife Refuge computed NS shear stress-strain and effective stress path during the Superstition Hills 1987 Earthquake (Zeghal et al., 1996).....	121
Fig. 5.21	Port Island shear stress histories estimated from acceleration histories and corresponding constitutive model prediction (Elgamal et al., 1996; Zeghal et al., 1996) .....	122
Fig. 5.22	Port Island recorded and computed accelerations at surface, 16m and 32m depth, and computed excess pore-pressure ratio at 8m depth (Elgamal et al., 1996; Zeghal et al., 1996).....	123
Fig. 5.23a	Variation in dilatancy with material state (data from Verdugo and Ishihara, 1996): Undrained response with different densities (after Li and Dafalias, 2000) ..	124
Fig. 5.23b	Variation in dilatancy with material state (data from Verdugo and Ishihara, 1996): Undrained response with the same density under different confinements (after Li and Dafalias, 2000).....	125
Fig. 5.24	Illustration of the dilative shear response: (a) stress path; (b) stress-strain response (after Li and Dafalias, 2000).....	126
Fig. 6.1	Schematic of a generic template for soil plasticity model generation (Professor Boris Jeremic, UC Davis).....	137
Fig. 6.2	Two-dimensional modeling of Humboldt Bay, Middle Channel Bridge using OpenSees (UC San Diego) .....	138

Fig. 6.3	Three-dimensional modeling of soil-pile interaction using OpenSees (UC Davis).....	139
Fig. 6.4	2D simulation of transmitting boundary effects using OpenSees (U. Washington) .....	140
Fig. 6.5	Sample profiles of maximum, minimum, and final computed results ( <a href="http://cyclic.ucsd.edu">http://cyclic.ucsd.edu</a> ) .....	143
Fig. 6.6	Sample computed acceleration, lateral displacement and excess pore-pressure histories at 1m depth ( <a href="http://cyclic.ucsd.edu">http://cyclic.ucsd.edu</a> ).....	144
Fig. 6.7	Sample computed shear stress-strain and stress path at 1.5m depth ( <a href="http://cyclic.ucsd.edu">http://cyclic.ucsd.edu</a> ) .....	144

## LIST OF RESEARCH CAPSULES

PEER Lifelines Research Program — Probabilistic Assessment of Liquefaction Potential.....	79
PEER Lifelines Research Program — Liquefaction Site Investigation .....	80
PEER Core Research Program — Liquefaction Testing .....	83
PEER Lifelines Research Program — Lateral Spreading Prediction.....	85
PEER Core Research Program — Residual-Strength Testing.....	91

## PREFACE

The Pacific Earthquake Engineering Research Center (PEER) is an Earthquake Engineering Research Center administered under the National Science Foundation Engineering Research Centers Program. The mission of PEER is to develop and disseminate technology for design and construction of buildings and infrastructure to meet the diverse seismic performance needs of owners and society. Current approaches to seismic design are indirect in their use of information on earthquakes, system response to earthquakes, and owner and societal needs. These current approaches produce buildings and infrastructure whose performance is highly variable, and may not meet the needs of owners and society. The PEER program aims to develop a performance-based earthquake engineering approach that can be used to produce systems of predictable and appropriate seismic performance.

To accomplish its mission, PEER has organized a program built around research, education, and technology transfer. The research program merges engineering seismology, structural and geotechnical engineering, and socio-economic considerations in coordinated studies to develop fundamental information and enabling technologies that are evaluated and refined using test beds. Primary emphases of the research program at this time are on older existing concrete buildings, bridges, and highways. The education program promotes engineering awareness in the general public and trains undergraduate and graduate students to conduct research and to implement research findings developed in the PEER program. The technology transfer program involves practicing earthquake professionals, government agencies, and specific industry sectors in PEER programs to promote implementation of appropriate new technologies. Technology transfer is enhanced through a formal outreach program.

PEER has commissioned a series of synthesis reports with a goal being to summarize information relevant to PEER's research program. These reports are intended to reflect progress in many, but not all, of the research areas in which PEER is active. Furthermore, the synthesis reports are geared toward informed earthquake engineering professionals who are well versed in the fundamentals of earthquake engineering, but are not necessarily experts in the various fields covered by the reports. Indeed, one of the primary goals of the reports is to foster cross-discipline collaboration by summarizing the relevant knowledge in the various fields. A related purpose of the reports is to identify where knowledge is well developed and, conversely, where

significant gaps exist. This information will help form the basis to establish future research initiatives within PEER.

# 1 Introduction

The performance of structures such as buildings and bridges during earthquakes is strongly influenced by the performance of the soils that support them. Local soil conditions can influence structural performance in two primary ways: by influencing the ground motions that excite the structure and by imposing additional deformations on the structure through ground failure.

The first widespread observations of damage attributed to liquefaction were made in the 1964 Niigata, Japan, and 1964 Alaska earthquakes. In numerous earthquakes since, significant damage to buildings and bridges has been caused by liquefaction. Liquefaction has been studied extensively over the past 35 years, and substantial advances have been made in understanding the development and effects of this phenomenon. These advances have led to a series of practical procedures for evaluating the potential for occurrence and for estimating its effects. These procedures, however, are almost entirely empirical in nature and, as such, are difficult to apply to the problem of performance prediction for individual structures.

The Pacific Earthquake Engineering Research (PEER) Center is dedicated to the development of methods and procedures for performance-based earthquake engineering (PBEE). The use of PBEE requires the ability to predict a nearly continuous spectrum of performance states for individual structures. This requirement implies the need for tools and procedures for evaluation of the entire process of liquefaction, from initiation to effects. Recent advances in the understanding of liquefaction-related phenomena offer the promise of improved analytical predictions of the initiation and effects of soil liquefaction.

The purpose of this synthesis report is to summarize current procedures for practical prediction of liquefaction behavior, to describe recent advances in the understanding of liquefaction behavior, and to describe the incorporation of this improved understanding into new solutions for detailed modeling of soil liquefaction. The focus of this report, however, is on performance, and therefore emphasis is on aspects of liquefaction that relate to the performance

of buildings, bridges, and lifelines. Well-known and widely used empirical tools and procedures for evaluation of liquefaction hazards will be reviewed relatively briefly with more detailed discussions devoted to emerging knowledge about the mechanics of liquefiable soil behavior, and methods for incorporating those mechanics into improved models for performance prediction.

The report is organized into eight chapters. Following the Introduction in Chapter 1, Chapter 2 presents a brief review of the fundamentals of soil liquefaction and practical procedures for liquefaction hazard evaluation. Chapter 3 describes performance-based earthquake engineering and the geotechnical factors that influence performance. Chapter 4 identifies and discusses the most pressing contemporary issues in liquefaction modeling. Current state-of-the-art approaches to liquefaction modeling are described in Chapter 5; the performance of four liquefaction models recently developed by PEER researchers is compared and contrasted. Chapter 6 discusses future directions for the development and verification of liquefaction models and additional research needs. Finally, Chapter 7 presents a series of conclusions.

## 2 Fundamentals of Soil Liquefaction

### 2.1 INTRODUCTION

Soil liquefaction is a complex phenomenon that numerous researchers have investigated in its various aspects. The historical development of procedures for evaluation of liquefaction hazards has been characterized by some measure of controversy, most of which is now recognized as resulting from differences in perspective and terminology rather than disagreement about the actual nature of liquefaction.

This chapter presents a review of the fundamental aspects of soil liquefaction, and of the procedures commonly used to evaluate liquefaction hazards. The emphasis of the chapter is on performance prediction. The geotechnical engineering profession's understanding of liquefaction has developed to the point where reasonably reliable procedures for evaluation of liquefaction potential are now available. These procedures, though empirical in nature, have been shown in numerous earthquakes to do a good job of identifying sites at which liquefaction can be expected. Geotechnical engineers are seldom "surprised" when liquefaction occurs at an investigated site where it had not been expected, but they are much more likely to find sites where liquefaction was predicted and did not occur. This situation reflects both the uncertainty/variability inherent in geotechnical engineering practice and the conservatism built into current empirical liquefaction evaluation procedures.

To date, procedures for evaluation of liquefaction hazards have concentrated on the question of liquefaction potential, i.e., whether or not liquefaction will occur. The influence of liquefaction on the performance of structures, however, depends on the *effects* of liquefaction. While some empirical procedures have been developed for estimation of liquefaction effects, the extremely high uncertainty involved in such prediction must be reduced to achieve more reliable performance evaluations. For this reason, a significant part of the research conducted by PEER,

both in its core and lifelines programs, is directed toward improved prediction of the effects of soil liquefaction.

## 2.2 TERMINOLOGY

The investigation of liquefaction phenomena has been marked historically by the inconsistent use of terminology to describe various physical phenomena. In recent years, it has become recognized that much of the historical confusion and controversy regarding liquefaction resulted from terminology. In some cases, one word (e.g., “liquefaction”) was used to describe different physical phenomena. In other cases, one physical phenomenon was described by different terms. The purpose of this section is to explicitly define several terms that will be used throughout this report. The terms of primary interest are

1. *Liquefaction* — a term used to describe phenomena in which the generation of excess porewater pressure lead to significant softening and/or weakening of a soil deposit. The term covers a number of different physical phenomena, such as flow liquefaction and cyclic mobility, that are specifically defined below.
2. *Flow liquefaction* — a phenomenon that occurs when liquefaction is triggered in a soil whose residual strength is lower than that needed to maintain static equilibrium (i.e., static driving stresses exceed residual strength). Flow liquefaction occurs only in loose soils with low residual strengths. It can produce extremely large deformations (e.g., flow slides); the deformations, however, are actually driven by the static shear stresses. Cases of flow liquefaction are relatively rare in practice but can cause tremendous damage.
3. *Cyclic mobility* — a phenomenon in which cyclic shear stresses induce excess porewater pressure in a soil whose residual strength is greater than that required to maintain static equilibrium. The phenomenon of cyclic mobility is often manifested in the field in the form of lateral spreading, a process in which incremental permanent deformations build up in the presence of a static stress field during the period of earthquake shaking. These deformations, which can occur in relatively dense as well as loose soils, can range from small to quite large. The excess porewater pressure produced by cyclic mobility can, when they cause void-ratio redistribution in the vicinity of impermeable layers, lead to flow liquefaction that can occur after earthquake shaking.
4. *Pore-pressure ratio,  $r_u$*  — the ratio of excess porewater pressure to initial effective stress, generally expressed as a percentage. The pore-pressure ratio is generally zero at the beginning of cyclic loading (in the field and in laboratory tests); when it reaches a value of 100%, the effective stress is zero.
5. *Initial liquefaction* — a condition in which the effective stress in the soil at least momentarily reaches a value of zero (pore-pressure ratio,  $r_u = 100\%$ ). The stiffness of the soil is typically very low (or zero) at the point of initial liquefaction, but tendencies

for dilation can cause the shear strength to be greater than zero when monotonic strains develop.

6. *Phase transformation* — a process in which the volume change behavior of a liquefiable soil changes from contractive to dilative. Both loose and dense soils can exhibit phase transformation, showing contractive behavior at low stress ratios (ratio of shear stress to effective normal stress) and dilative behavior at high stress ratios. Phase transformation behavior becomes important as initial liquefaction is approached and after it has occurred. Phase transformation plays a strong role in determining the level of permanent deformation that develops in an earth structure subjected to liquefaction.
7. *Liquefaction curves* — the graphical representation of laboratory test results, performed in the early days of liquefaction hazard evaluation, in which liquefaction resistance was evaluated by cyclic loading of triaxial or simple shear test specimens. The graphical representation of liquefaction curves showed the relationship between cyclic stress ratio and the number of cycles to initial liquefaction.
8. *Steady state strength* — the shear strength of a soil flowing continuously under constant shear stress and constant effective confining pressure at constant volume and constant velocity (Castro and Poulos, 1977; Poulos, 1981).
9. *Residual strength* — the shear strength that can be mobilized by an element of soil when strained monotonically to very large strains. The residual strength is often determined by back-calculation of flow slide case histories that may be influenced by partial drainage, pore-pressure redistribution, and void-ratio redistribution — therefore, it may differ from the steady-state strength.

The reader may note that the authors have associated lateral deformation effects with mechanisms, i.e., flow slides are associated with flow liquefaction and lateral spreads are associated with cyclic mobility. Having been involved in field reconnaissance investigations of a number of major earthquakes, the authors are well aware that it is often difficult, if not impossible, to distinguish between flow slides and lateral spreads in the field. In fact, it may not be terribly important to distinguish between them from the standpoint of their effects on structural performance. Nevertheless, the focus of this report is on the modeling of liquefaction phenomena and it is therefore important to account for the mechanisms of the phenomena that are being modeled.

### **2.3 EXAMPLES OF SOIL LIQUEFACTION**

Liquefaction phenomena have been observed in the field, and have also been recreated in laboratory element tests and model tests. The following sections present examples of both flow

liquefaction and cyclic mobility as observed in each of these settings. The examples illustrate various aspects of the effects of liquefaction on performance, and of the basic mechanics of soil liquefaction.

### **2.3.1 Field Case Histories**

Liquefaction phenomena have been observed in many historical earthquakes. The most striking observations, however, remain those from the 1964 Niigata, Japan, earthquake. This earthquake produced numerous examples of liquefaction in low-lying areas of Niigata, particularly along the Shinano River. The widespread liquefaction observed in Niigata, combined with the substantial liquefaction observed in the 1964 Good Friday, Alaska, earthquake, led to the recognition of soil liquefaction as an important seismic hazard.

The study of case histories produces tremendous benefits in terms of understanding the conditions under which liquefaction can occur, and the effects that it can have on structures and facilities. While liquefaction has been observed at many sites in many earthquakes, there are few instances in which all of the information that a geotechnical engineer would need for a detailed case history analysis is actually available. The following sections provide brief reviews of some of the most important and most useful case histories of soil liquefaction. These and other case histories have helped provide a firm basis for the empirical methods of liquefaction hazard evaluation that are commonly used in contemporary geotechnical engineering practice. However, detailed analysis of these case histories has provided important insight into the mechanics of soil liquefaction, which is essential for the development of improved methods for performance prediction.

**(a) Niigata, Japan (1964)**

The city of Niigata is located on the estuary of the Agano and Shinano rivers. This geological environment produced loosely deposited sands with a shallow water table under the low-lying areas of the city. The ground surface in these areas is relatively flat — slopes of less than a couple degrees are common. Much of the riverbank area is lined with flexible sheet pile retaining structures.

During the Niigata earthquake ( $M=7.5$ ) on June 16, 1964, widespread liquefaction was observed in the low-lying areas. This liquefaction was accompanied by foundation failure, failure of retaining structures, and substantial lateral spreading, particularly in areas near the Shinano River. Careful interpretation of aerial photographs taken before and after the earthquake (Hamada, 1992) has indicated that lateral displacements of up to 8 m occurred in Niigata. The sheet pile walls along the river proved unable to resist the increased lateral pressures imposed upon them by the liquefied soil, and moved toward the river. The soil behind the walls followed, producing large lateral displacements that typically extended some 300 m back from the river. Many structures, such as bridges, buildings, and buried pipelines, were severely damaged by these movements.

Liquefaction-induced damage to buildings and bridges was extensive. A series of apartment buildings at Kawagishi-cho have become famous as symbols of the potential effects of soil liquefaction. These buildings were supported on shallow, grid-type foundations. When liquefaction occurred, the strength of the underlying soils was reduced from its initial value, which produced adequate bearing capacity to support the buildings, to the residual strength of the liquefied soil. Because the residual strength was lower than the shear stress imposed on the soil by the weights of the buildings, bearing capacity failures occurred (Figure 2.1). These failures were of the flow liquefaction variety, and produced very large deformations. It is important to note, however, that the structures themselves suffered very little damage — they essentially settled and rotated as rigid bodies under the loss of bearing capacity. Several of the apartment buildings were later jacked back to a vertical position and underpinned with new foundations; in even the most severely displaced buildings, structural deflections were so small that doors and windows still opened, thereby allowing residents to retrieve many of their belongings. The extent to which the good structural performance was caused by an excessively conservative design (a notion supported by the lack of damage even to structures that rotated

some 60°) or by the modification of foundation input motion due to liquefaction is not clear. This case does show, however, the critical importance of evaluating both geotechnical and structural factors when evaluating overall performance.



**Fig. 2.1 Kawagishi-cho apartment buildings in Niigata, Japan: (left) tilting due to bearing capacity failure; (right) close-up of shallow foundation exposed by failure.**

Many structures near the Shinano River were supported on pile foundations. The Showa Bridge, for example, was constructed of a series of simply supported spans resting on pile-supported bridge piers. A typical pier within the river was supported by a single row of N 25-m-long piles that extended through the loose soils of the riverbed and into underlying denser soils. The piles were connected by a common pile cap that supported bridge piers of up to about 9 m in height. Liquefaction was observed in approximately the upper 10 m of the riverbed soils, which sloped toward the center of the river. When liquefaction occurred, lateral spreading caused the shallow riverbed soils to move toward the centerline of the river. The spreading soil imposed pressures on the pile foundations that caused them to deflect toward the center of the river. The combination of lateral displacement and rotation of the pile heads produced lateral displacements of the bridge supports that were large enough to allow several of the simply supported spans to fall into the river (Figure 2.2).



**Fig. 2.2 Failure of Showa River bridge in Niigata, Japan, due to lateral spreading.**

Liquefaction also caused lateral spreading in the vicinity of the NHK building in Niigata (Hamada, 1992). This four-story reinforced concrete building was supported on 11-m-long piles connected by pile caps that extended to approximately 2 m in depth. The reinforced concrete piles extended through a profile consisting of silty sands that were loose to depths of about 10 m and medium dense to dense at greater depths. The groundwater table was at a depth of about 5 m. During the earthquake, the soil in the vicinity of the NHK building spread laterally by 1 – 2 m. The building, however, suffered negligible damage and was used continuously for many years after the earthquake. Nearly 20 years after the earthquake, excavation beneath the building, as part of the construction of upgraded foundations for an increase in the height of the building, revealed that the piles had been extensively damaged (Figure 2.3) during the Niigata earthquake. The soil deformations produced by lateral spreading caused flexural failure of the piles at the top and bottom of the liquefiable layer. Excavation of the piles confirmed the location and nature of the damage. The NHK building provides a case history of extensive lateral spreading and foundation failure with generally acceptable overall performance.

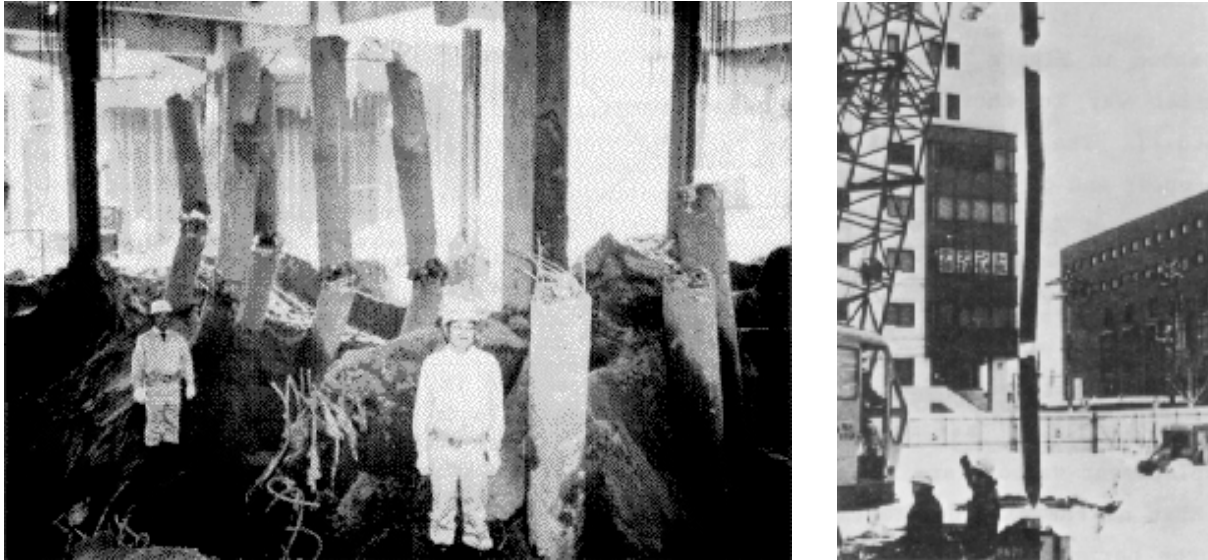


**Fig. 2.3 Pile damage due to lateral spreading beneath the NHK building in Niigata, Japan.**

These three case histories — the Kawagishi-cho apartment buildings, the Showa bridge, and the NHK building — illustrate different ways in which soil liquefaction can affect the performance of structures. In the case of the Kawagishi-cho apartment buildings, the earthquake triggered flow liquefaction that was manifested in the form of a bearing capacity failure: the strength of the liquefied soil was simply insufficient to support the weights of the buildings. Large displacements of the buildings were therefore driven by gravity and resulted in performance that would be considered as “failure” by almost any definition, even though the structural elements of the buildings were virtually undamaged. The Showa bridge was subjected to much smaller soil movements; in this case, the strength of the soil was never reduced below the point at which static stresses would produce failure. The cumulative movements of the laterally spreading soil, however, could not be resisted by the relatively slender pile foundations and led to excessive movements of the bridge supports and collapse of several bridge spans. The Showa bridge certainly failed, but the structure itself (the portion above the pile caps) performed as its designers would have expected. This failure resulted from the inability of the foundation to resist the deformations of the surrounding soil. In the case of the NHK building, pile foundations were also subjected to excessive lateral spreading deformations, and the piles failed structurally. The design of the building was such, however, that its performance was much

better than that of the Showa River bridge — good enough, in fact, that the extent of the pile damage was not recognized until many years after the earthquake.

**(b) Wildlife Refuge, California (1987)**

In order to obtain quantitative information of the in situ liquefaction behavior of saturated sands, the USGS selected and instrumented the Wildlife Refuge, a liquefaction-prone area of the Imperial Valley in southern California. Liquefaction had been documented at this site in a previous moderate earthquake (the April 26, 1981, Westmoreland earthquake, M5.9) and the site is in one of the most seismically active areas in California. The site itself is relatively flat, but a free slope existed at a distance of approximately 23 m (Holzer et al., 1989).

The Wildlife site is underlain by a 2.7-m-thick layer of silt to clayey silt which is underlain by a 3.3-m-thick layer of liquefiable silty sand (Figure 2.4). The silty sand is in turn underlain by a 5-m-thick layer of stiff clay. Two triaxial force balance accelerometers were installed at the site — one at the ground surface and the other at a depth of 7.5 m. Five piezometers were installed in a 4 m radius around the deep accelerometer at depths ranging from 3 to 7 m. A sixth piezometer was installed at a depth of 12 m. A sixth piezometer was installed at a depth of 12 m.

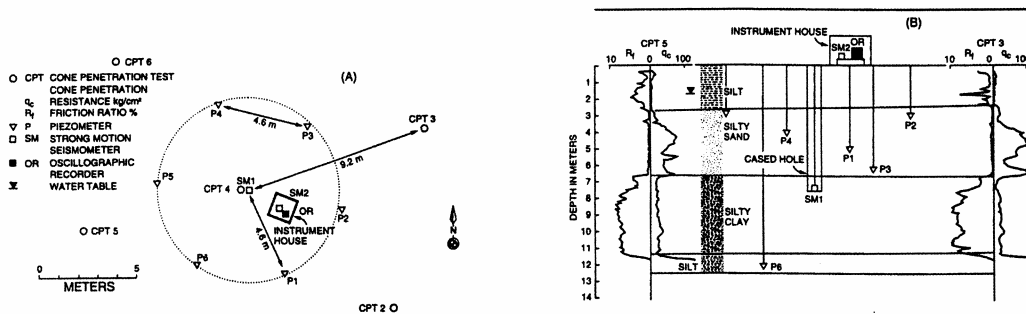


**Fig. 2.4 Instrumentation layout and subsurface conditions at Wildlife array site (after Youd and Holzer, 1994).**

The Wildlife array was triggered by two earthquakes that occurred about 12 hours apart on November 23 – 24, 1987. The first event, the Elmore Ranch (M6.2) earthquake, produced peak horizontal accelerations of 0.13g (ground surface) and 0.07g (7.5 m depth), but no

detectable change in porewater pressure (Holzer et al., 1989). The Superstition Hills (M6.6) event that followed produced peak horizontal accelerations of 0.21g (ground surface) and 0.17g (7.5 m depth); high excess porewater pressures were also recorded in this event. Subsequent examination of the site revealed sand boils within and near the site, and the opening of several ground fissures (Figure 2.5). The combination of instrumental recordings and field observations clearly showed that liquefaction occurred in the Superstition Hills event but not in the Elmore Ranch event.

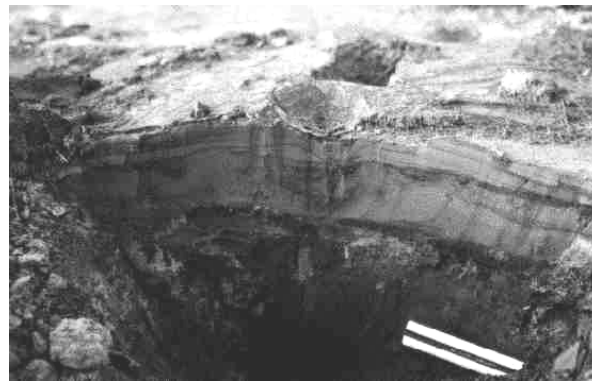


**Fig. 2.5 Sand boil at Wildlife array (courtesy of Earthquake Engineering Research Center, University of California, Berkeley).**

Subsequent analysis of the Wildlife records (Youd and Holzer, 1994; Zeghal and Elgamal, 1994) confirmed the validity of the instrumental measurements and provided important insights into the mechanics of soil liquefaction. Zeghal and Elgamal (1994) identified four stages of seismic response of the Wildlife array (Figure 2.6). In Stage 1 (0.0 – 13.7 sec), ground accelerations were relatively low (similar in amplitude, in fact, to the Elmore Ranch event) and porewater pressure buildup was small. Stage 2 (13.7 – 20.6 sec) coincided with the strongest portion of shaking, and saw a rapid increase in porewater pressure with small, nearly instantaneous drops in porewater pressure that occurred at negative peaks in the ground surface acceleration records. Stage 3 (20.6 – 40.0 sec) saw lower peak accelerations and generally longer period response at the ground surface. Porewater pressure continued to rise quickly, again with negative spikes coinciding with negative peaks in the ground surface acceleration record. In the final stage, accelerations were quite low but porewater pressure continued to increase, albeit at a slower rate than in Stages 2 and 3. A number of rapid drops in porewater

pressure were also recorded in Stage 4, and these spikes also occurred at the same time as negative spikes in the ground surface acceleration record.

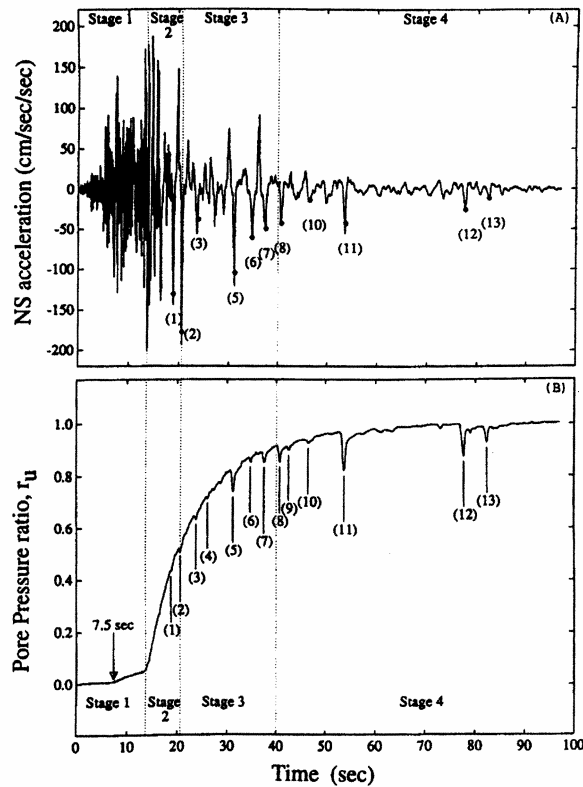


**Fig. 2.6 Measured ground surface acceleration and porewater pressures at Wildlife array site (after Zeghal and Elgamal, 1994).**

The fact that the pore-pressure ratio in the liquefied layer was only at a value of approximately 0.5 at the end of the strongest part of shaking (Stage 2) and that it continued to increase substantially in response to the relatively weak shaking that followed was viewed as anomalous by many engineers. Some speculation on the accuracy of the porewater pressure measurements, focusing principally on the question of whether the porewater pressure transducers were fully saturated, was raised (Hushmand et al., 1992a; 1992b). Subsequent detailed analysis of the acceleration and porewater pressure records (Zeghal and Elgamal, 1994) has essentially refuted that speculation.

Zeghal and Elgamal (1994) used the two accelerometer recordings to compute time histories of average shear stress and average shear strain (these quantities were spatially averaged over the 7.5 m vertical distance between the two accelerometers). Along with the porewater pressure measurements, these quantities allowed the construction of average stress-

strain and stress path curves (Figure 2.7). The stress-strain curves showed relatively high stiffness in the initial part of the record (Stage 1 and early Stage 2) followed by a gradual softening through the remainder of Stage 2 and Stage 3. When the negative shear strain amplitude exceeded about 0.5%, phases of both softening and hardening were observed in the stress-strain loops for individual loading cycles. This behavior was noted as being consistent with the phase transformation behavior (Ishihara, 1985) that has been observed in laboratory tests on saturated sands. The effective stress paths confirmed the fact that the liquefied sands at the Wildlife site were contractive at low stress ratios and dilative at high stress ratios — in other words, the Wildlife case history provided direct evidence of the existence of phase transformation behavior in the field. The fact that the dilative response was asymmetrical, i.e., that the pore-pressure drops were preferentially associated with movements in one direction, can be consistently explained by the presence of the free slope which introduced a small static shear stress acting in the direction of that slope.

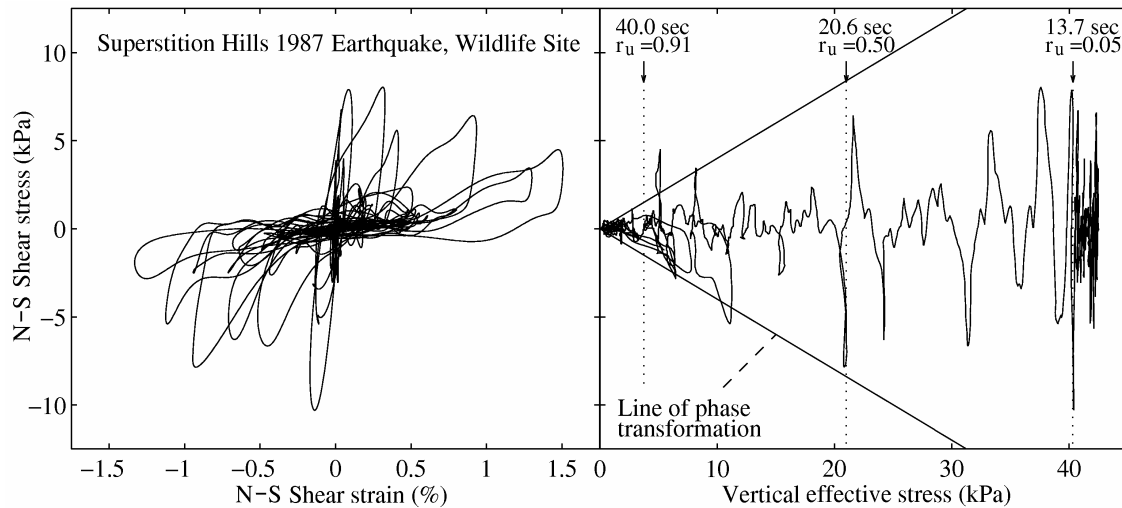


**Fig. 2.7 Average stress-strain and stress path curves at Wildlife array site.**

While the Wildlife site case history does not provide direct evidence of the effects of liquefaction on the performance of structures, it is extremely important in confirming the existence and importance of aspects of liquefiable soil behavior (namely, phase transformation) that had previously been observed in the laboratory. Because the hardening response associated with excursions into the dilative regime controls the development of permanent strain (hence, of permanent deformations in the field), recognition of its existence and development of models

capable of predicting its effects are critical to evaluating the performance of structures founded on liquefiable soils.

**(c) Moss Landing, California (1989)**

The 1989 Loma Prieta earthquake caused liquefaction-related deformations along nearly the entire length of the Moss Landing spit, a 150 – 300-m-wide shoreline spit on Monterey Bay in California. Extensive lateral spreading caused significant damage to roads and structures (Figure 2.8). Five sites on Moss Landing spit were investigated by Boulanger et al. (1997); of these, the lateral spreading observed along Sandholdt Road in the vicinity of the Monterey Bay Aquarium Research Institute (MBARI) are of particular interest due to the presence of three inclinometers installed at the site (Figure 2.9). The inclinometers allowed observation of the pattern of lateral displacements that occurred below, as well as at, the ground surface.



**Fig. 2.8 Lateral spreading along Sandholdt Road (left), and at Monterey Bay Aquarium Research Institute (right) at Moss Landing (courtesy of Earthquake Engineering Research Center, University of California, Berkeley).**

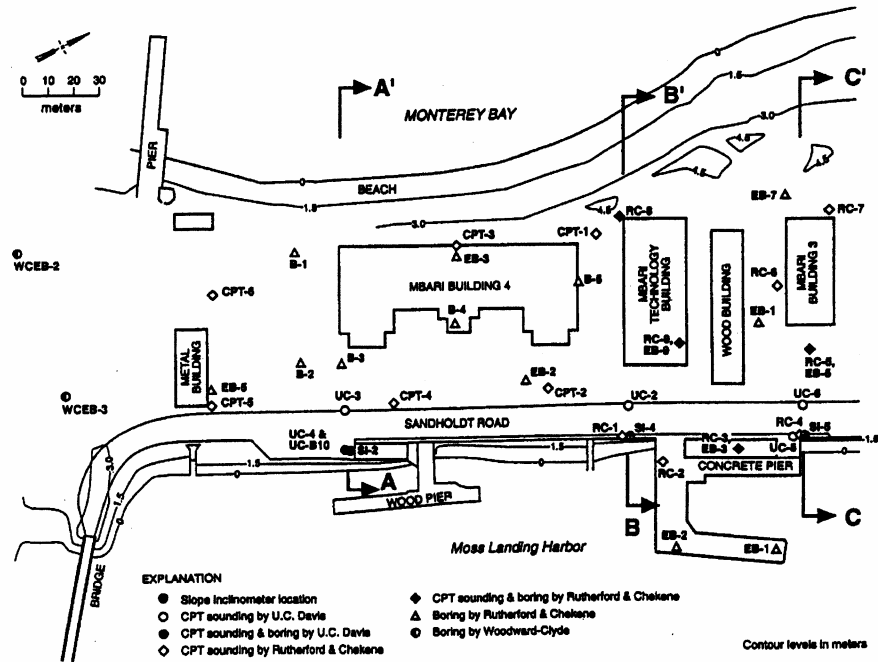


Fig. 2.9 Location of inclinometers near Monterey Bay Aquarium Research Institute at Moss Landing (after Boulanger et al., 1997).

Inclinometer SI-5, located on the east side of Sandholdt Road across from MBARI Building 3, showed that the edge of the road displaced laterally toward the harbor by about 25 cm (Figure 2.10). At the location of the inclinometer, the site conditions consisted of 8 m of loose saturated sand underlain by 4 m of silty clay underlain in turn by denser sands and stiffer clays. About 16 cm of the lateral displacement occurred between depths of 4 – 6 m where a locally decreased CPT tip resistance was measured following the earthquake. The other two inclinometers were in somewhat more complex soil conditions, but also recorded significant (7 to 27 cm) lateral displacements toward the harbor.

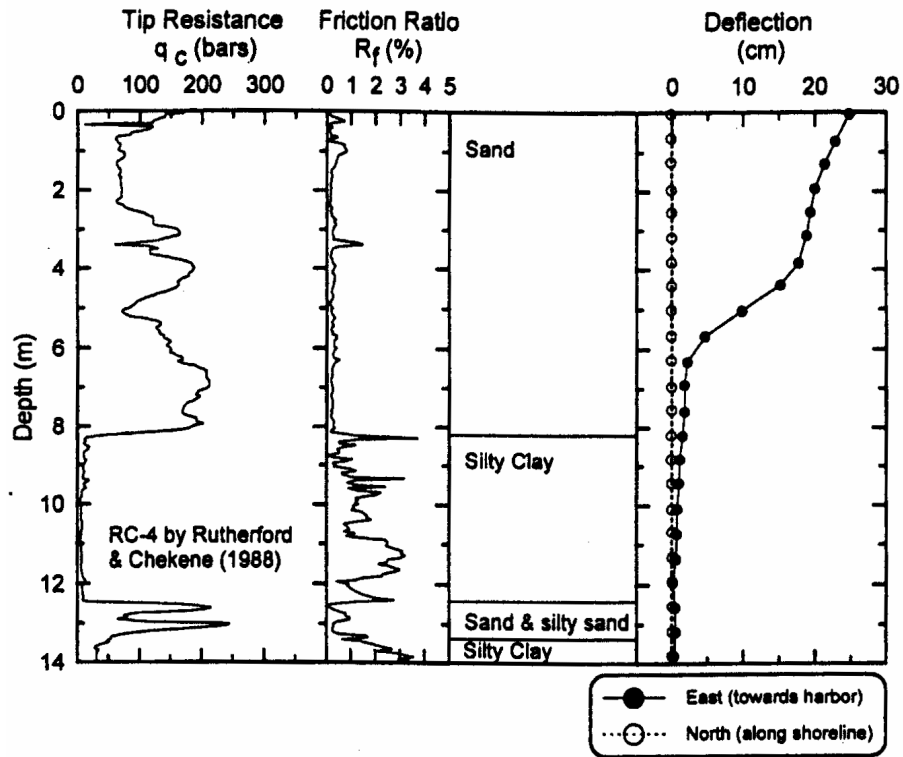


Fig. 2.10 Lateral movement of inclinometer SI-5 at Moss Landing (after Boulanger et al., 1997).

The site was subjected to strong ground motion in the Loma Prieta earthquake. While no ground motion instruments were located at the site, nearby instruments and ground motion simulations suggest that the peak horizontal acceleration at the site was approximately 0.25g. No structures were located in the vicinity of Inclinometer SI-5 at the time of the Loma Prieta earthquake; settlements of 5 – 8 cm were observed nearby. Interpretation of the deformation patterns using a Newmark-type analysis indicated that the “equivalent residual shear strength” (about 8 kPa based on back-calculation) was much lower than the residual shear strength expected for a soil of the measured CPT tip resistance. This indicated that the strains induced in the in situ soil were not sufficient to mobilize the full residual strength of the soil.

The Moss Landing case history provides valuable data on the subsurface response of a liquefied soil deposit with significant initial shear stress. Because a reliable model for liquefaction and lateral spreading should predict subsurface as well as surface displacements, the Moss Landing case history is useful for evaluation of such models.

**(d) Port Island, Japan (1995)**

The 1995 Hyogoken-Nambu earthquake caused widespread liquefaction in Kobe, Japan, particularly in reclaimed areas such as Port Island. On Port Island, the effects of liquefaction on earthquake ground motions were recorded by a vertical array (Figure 2.11) that consisted of four accelerometers extending from the ground surface to a depth of 83 m.

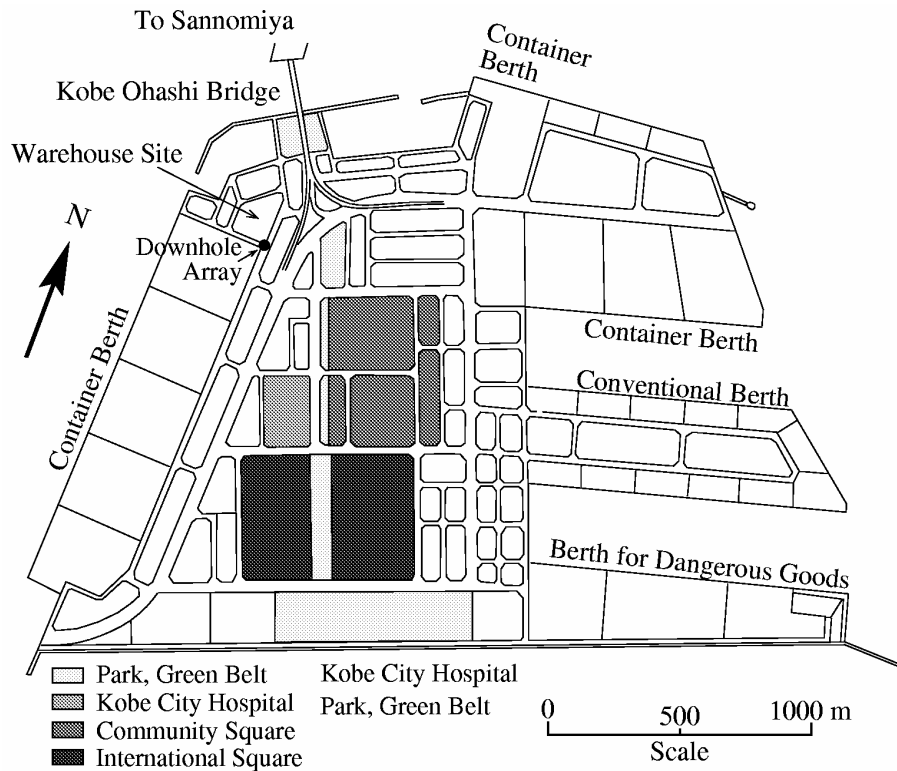


**Fig. 2.11 Location of Port Island vertical array.**

The soil profile at the Port Island vertical array and the locations of the accelerometers are shown in Figure 2.12. The site was underlain by approximately 18 m of loose decomposed granite fill which was placed without compaction below the water table (the depth of which was 4 m); an 8-m-thick alluvial clay layer, a 34-m-thick layer of medium dense sand, and sand and gravel interlayered with clay, 21 m of diluvial clay, and a sequence of very dense sand with gravel and clay interlayers that extended beyond a depth of 82 m. The four accelerometers were located at depths of 0 m, 16 m, 32 m, and 83 m.

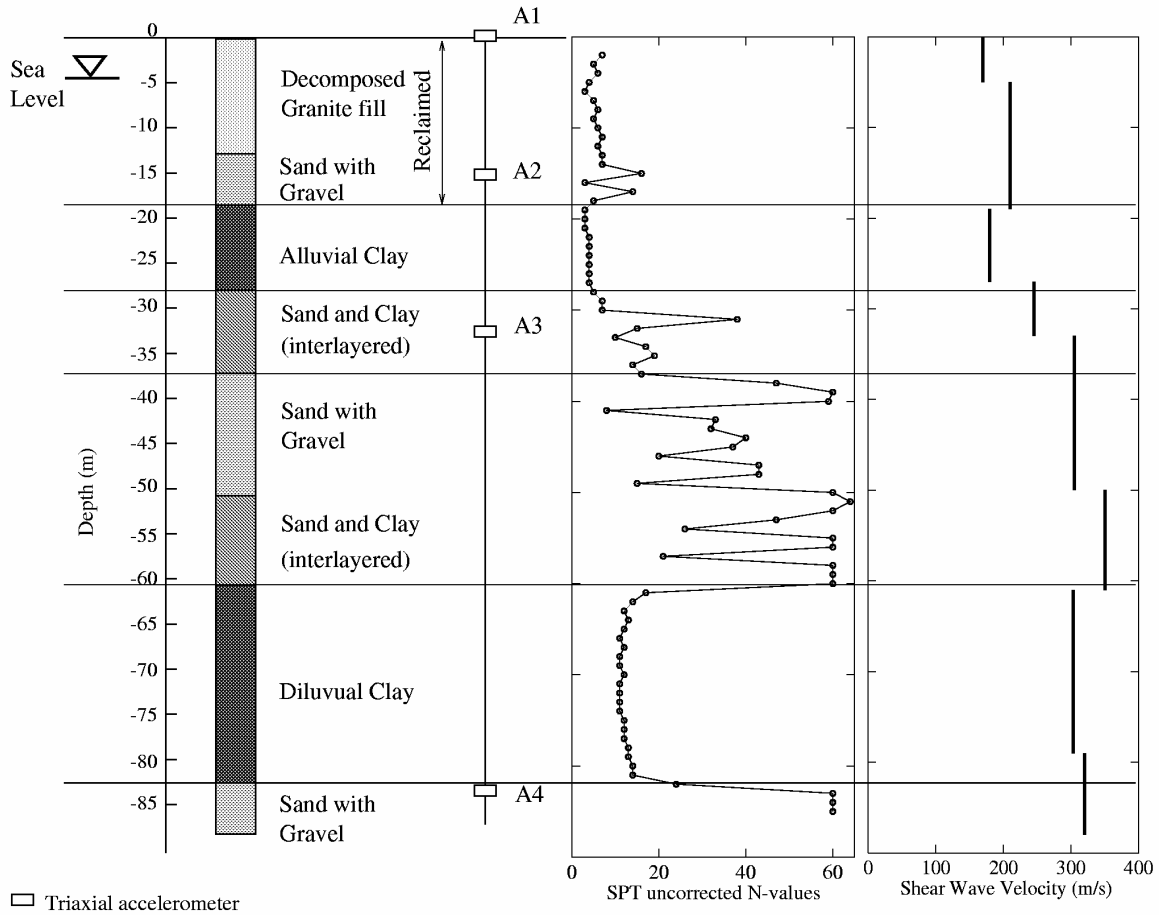


**Fig. 2.12 Soil profile and accelerometer locations at Port Island vertical array (after Elgamal et al., 1996).**

Port Island was subjected to very strong shaking in the Hyogoken-Nambu earthquake. Peak recorded horizontal accelerations in the lowest accelerometer (83 m, embedded in very dense sand and gravel) were approximately 0.6 g. As shown in Figure 2.13, however, the amplitude and frequency content of the recorded accelerations changed markedly with depth. Elgamal et al. (1996) divided the acceleration records into three stages: Stage 1 (0 – 4 sec), which consisted of the low-amplitude, initial portion of the ground motion, Stage 2 (4 – 7 sec), which corresponded to the strongest part of the motion, and Stage 3 (7 – 40 sec). During which the ground surface accelerations were considerably lower than the accelerations measured at greater depths. Shear stresses and shear strains were computed from the measured accelerograms; pore-pressure measurements were not available at the site. Because pairs of accelerograms are required to compute average time histories of shear stress and shear strain, the

four accelerometers produced three histories (at depths of 8.0 m, 24.0 m, and 57.5 m of shear stress and shear strain.

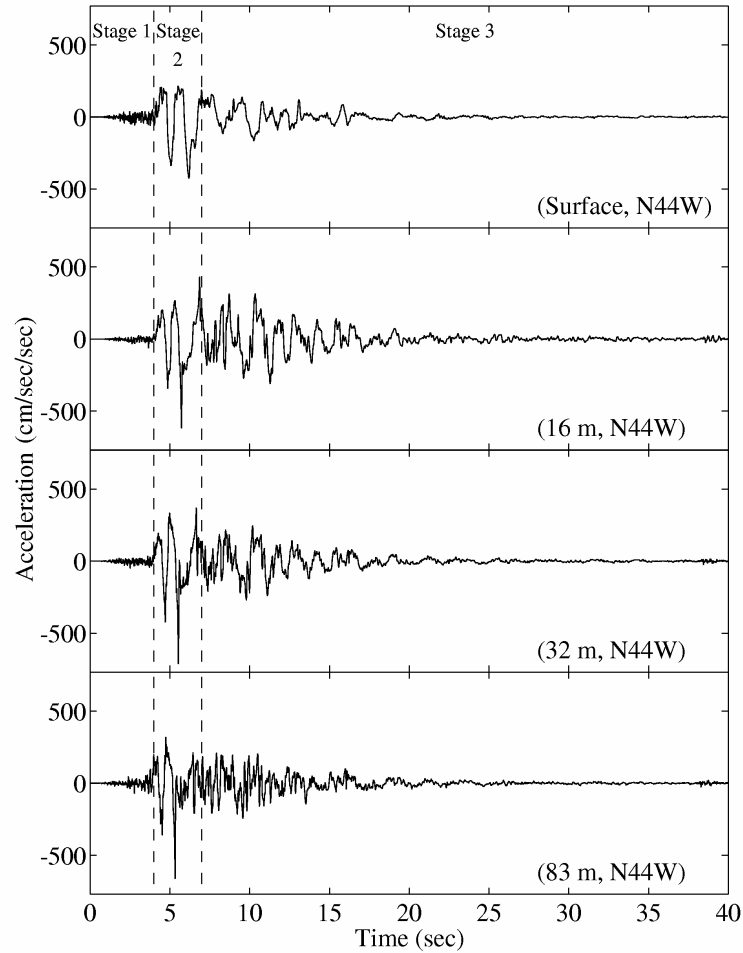


**Fig. 2.13 Recorded accelerograms at Port Island vertical array (after Elgamal et al., 1996).**

Two very different patterns of response were observed in the computed stress-strain behavior. At depths below the third accelerometer (32 m), the soil exhibited nearly linear (constant stiffness) behavior. At shallower depths, however, the computed stress-strain behavior showed (a) a reduction in stiffness with no significant loss of strength at a depth of 24 m, and (b) a dramatic loss of both stiffness and strength at a depth of 8 m (Figure 2.14). These reductions took place during Stage 2 and are responsible for the reduced acceleration amplitudes and lengthened period of vibration observed in Stage 3 of the ground surface motion.

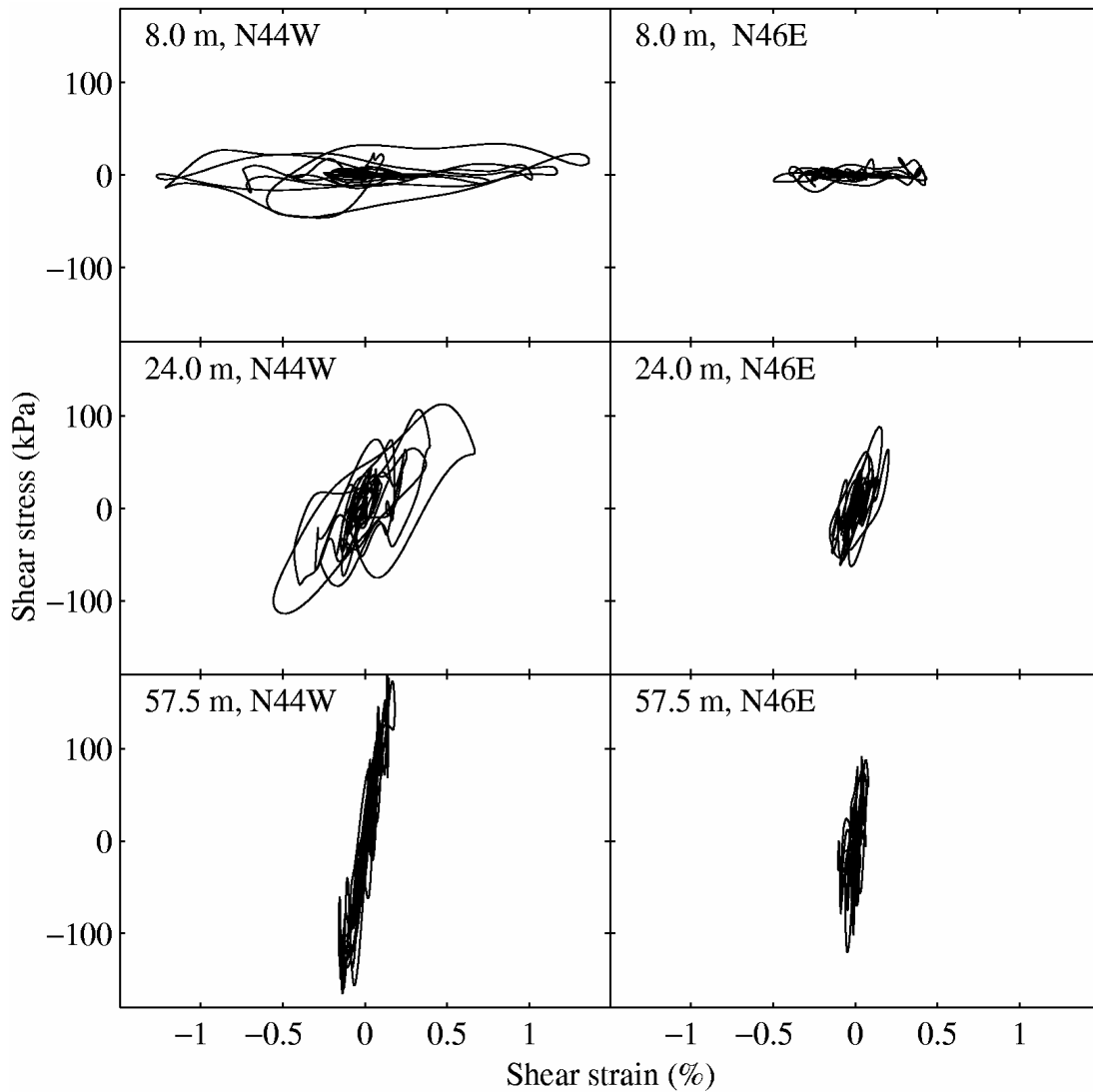


**Fig. 2.14** Computed average stress-strain behavior at Port Island array (after Elgamal et al., 1996).

The analysis of the recorded motions at the Port Island array suggest that liquefaction of the loose saturated decomposed granite fill occurred. Excess porewater pressures began to build in Stage 2 and likely continued into Stage 3. By the end of Stage 2, pore pressures had increased enough, at least in some portion of the loose soil, to prevent the transmission of high-frequency components of the underlying ground motion to the surface. Because high-acceleration levels are associated with higher frequencies, the ground surface acceleration amplitude decreased in Stage 3. The longer period of the Stage 3 ground surface motion, however, still allowed large

strains to develop. Of note is the apparent absence of dilation-induced acceleration spikes (and accompanying pore-pressure drops).

### **2.3.2 Laboratory Element Testing**

Laboratory element tests are tests performed on relatively small, uniform test specimens subjected to cyclic loading using a device that ensures that uniform stresses and strains are maintained within the specimen. Element tests commonly used for liquefaction studies include cyclic triaxial tests and cyclic simple shear tests. Laboratory element tests seek to replicate the stress and strain conditions that can exist in a single element of soil within a soil deposit. They are particularly useful for studying the basic behavior of soils under carefully controlled conditions.

Early liquefaction research relied almost exclusively on laboratory testing for characterization of the liquefaction resistance of actual soil deposits. This emphasis has diminished greatly in the past 20 years because (a) undisturbed samples of liquefiable soils are extremely difficult to obtain, (b) the complex structural, chemical, biological, and thermal conditions that exist in situ are virtually impossible to replicate in reconstituted laboratory test specimens, and (c) practical procedures for correlation of liquefaction resistance to in situ test results have been developed. Nevertheless, laboratory tests can provide important insights into the mechanics of soil liquefaction, and the behavior of liquefied soil.

#### ***(a) Laboratory Testing Equipment***

An optimum apparatus for laboratory testing of liquefaction behavior would have several important capabilities. It would allow the testing of both undisturbed and reconstituted soil specimens. It would allow reconstituted specimens to be constructed with uniform density and a fabric representative of that of the in situ soil. The apparatus would ensure that both stress and strain conditions are uniform throughout the specimen. It would allow the accurate measurement of low shear stresses and the small strains that they produce. It would also allow the accurate measurement of large shear stresses, and the development of large, uniform shear stresses. Finally, it would allow both cyclic and monotonic loading to be applied to the soil specimen.

Unfortunately, no individual testing apparatus has all of these capabilities. The most commonly used testing devices have most of these capabilities, but none has all of them. As a result, it is often necessary to use different testing apparatuses to investigate different aspects of liquefiable soil behavior. This situation can complicate the comparison of results, and the interpretation of the mechanical behavior of liquefiable soils. Some of the prominent features of the testing apparatuses most commonly used for investigation of the response of liquefiable soils are briefly reviewed in the following sections.

### ***Cyclic Triaxial Test***

The cyclic triaxial test is typically performed using conventional triaxial testing equipment that has been modified to allow application of a cyclic deviator stress (Figure 2.15). The cyclic deviator stress is usually applied harmonically at periods of 1 to 60 sec. Test specimens are consolidated isotropically (occasionally anisotropically) and subjected to a series of cycles of constant amplitude loading. The deviator stress, axial strain, and porewater pressure are recorded during the test; test results are most commonly expressed in terms of stress-strain loops, stress paths, and compilations of numbers of cycles to initial liquefaction (i.e., pore-pressure ratio,  $r_u = 1.0$ ) or, in the event that initial liquefaction is not reached, to some limiting axial strain (e.g., 3%).

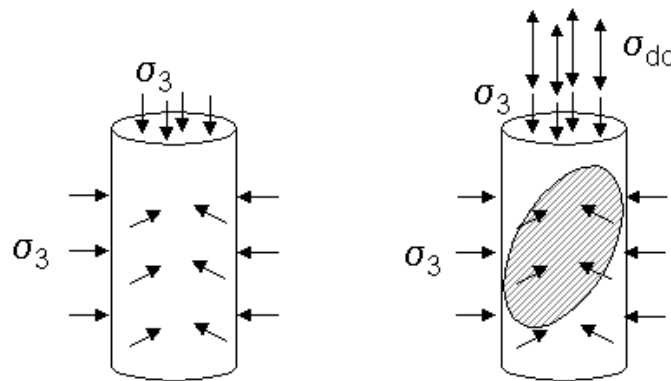


**Fig. 2.15** Stress conditions on cyclic triaxial test specimen (a) before cyclic loading and (b) during cyclic loading. Shaded region indicates orientation of plane of maximum shear stress.

The cyclic triaxial test allows specimens to be tested under relatively uniform stress and strain conditions, at least at low strain levels. This test has historically been the most commonly used for measuring liquefaction behavior in the laboratory, so a considerable amount of data exists. The limitations of the cyclic triaxial test, however, influence its use for measuring liquefaction behavior, most significantly in the following ways:

1. *In a triaxial test specimen, shear stresses do not exist on horizontal planes.* In the conventional cyclic triaxial test, maximum shear stresses are imposed on planes oriented at  $45^\circ$  to the horizontal. Because most of the energy in earthquake ground motions at shallow depths is in the form of vertically propagating SH-waves, shear stresses in the field act primarily in the horizontal direction. Therefore, the cyclic triaxial test does not impose shear stresses on the planes upon which they are imposed in the field. For soils with inherent or induced anisotropy, the response in the cyclic triaxial test may be different than that which would occur in the field.
2. *Principal stress axis rotation is not realistic in the cyclic triaxial test.* In the field, the propagation of vertical SH-waves produces continuous rotation of principal stress axes. In the cyclic triaxial test, the principal stress axes remain unchanged until a stress reversal occurs; then they rotate instantaneously by  $90^\circ$ .
3. *Mean stress and shear stress are not applied independently.* In the conventional cyclic triaxial test, the cell pressure is held constant while the deviator stress is changed. As a result, the mean stress acting on the specimen changes during cyclic loading. At level ground sites in the field, the mean stress remains constant when subjected to vertically propagating shear waves. Cyclic triaxial testing can be performed by cycling the deviator and confining stresses simultaneously to maintain constant mean stress, but it is not common to do so.
4. *Stresses and strains become non-uniform.* At strain levels above 15% – 20%, changes in the shape of a cyclic triaxial specimen prevent accurate determination of the stresses and strains associated with its response. The problem can be alleviated to some degree by the use of lubricated ends, but even these measures increase the uniform range to axial strain levels of perhaps 25% or so. Important

properties of liquefiable soils, particularly the residual strength, may not be fully mobilized at these strain levels.

5. *Bedding errors can prevent the accurate measurement of small strain behavior.* Bedding errors occur with conventional strain instrumentation (external measurement of axial strain). Alternative instrumentation schemes, such as those that measure deformations across the central third of the test specimen, can alleviate this problem.

### ***Cyclic Simple Shear Test***

Like the cyclic triaxial test, the cyclic simple shear test is a modified version of a test commonly used to measure shear strength and stress-strain behavior under static loading conditions (Figure 2.16). In the cyclic simple shear test, a specimen is placed within a container that allows no lateral strain, and then subjected to a static vertical stress. Horizontal shear stresses are then applied to the specimen. As in the cyclic triaxial test, the shear stresses are typically harmonic with constant amplitude, and are applied at periods of 1 to 60 sec.

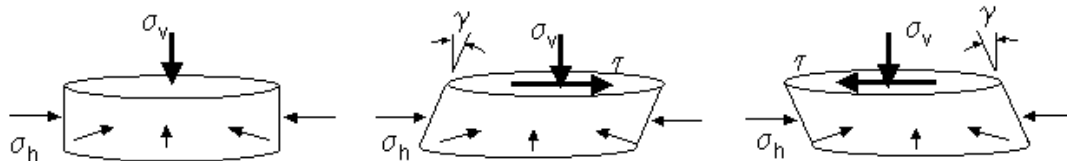


**Fig. 2.16 Stress and strain conditions in cyclic simple shear test.**

The cyclic simple shear test has a few advantages over the cyclic triaxial test. Because it applies cyclic shear stresses on horizontal planes and permits continuous rotation of principal stress axes, it replicates field loading conditions much more accurately than the cyclic triaxial test. The cyclic simple shear test also has some limitations for liquefaction testing, however, which include

1. *Lack of complementary shear stresses on the vertical sides of the specimen.* Because shear stresses are applied only horizontally and the devices make no

provisions for applying complementary shear stresses on the sides of the test specimen, the internal stress distribution is non-uniform. The degree of non-uniformity is most pronounced near the sides (and corners) of the test specimen. Previous research (Kovacs and Salamone, 1982) has shown that minimum test specimen aspect ratios of approximately 8:1 (width:thickness) are required to make the effects of non-uniformity insignificant. Most cyclic simple shear devices have aspect ratios on the order of 3:1.

2. *Unknown stress state.* Because a zero-displacement boundary condition is imposed upon the lateral boundaries of the test specimen, the lateral stress is not known. As a result, the actual stress state within the test specimen is not known. Some simple shear devices have been instrumented to measure lateral stresses (e.g., Budhu, 1985), but the accuracy of the stress state inferred from those measurements is not clear.
3. *Low strain behavior not measured accurately.* Because of friction in the loading systems of conventional cyclic simple shear devices, the magnitudes of small shear stresses transmitted to the test specimen cannot be accurately measured. This prevents the determination of low-strain properties from conventional cyclic simple shear testing. PEER researcher Mladen Vucetic has designed an innovative double specimen direct simple shear device (Doroudian and Vucetic, 1985) that does allow measurement of small strain soil properties.
4. *Constrained, unidirectional loading.* In a conventional cyclic simple shear apparatus, unidirectional loading is applied to the specimen in a predetermined direction. In the cyclic triaxial test, shearing can occur in an infinite number of directions. Because earthquake shaking produces three-dimensional ground motions which induce three-dimensional cyclic shear stresses in the soil, conventional simple shear apparatuses may not reflect the range of response that can be exhibited by the soil. PEER researchers Ross Boulanger and Ray Seed developed a bidirectional simple shear device to evaluate the effects of bidirectional loading on liquefaction resistance.
5. Stress concentrations, and potential for arching in the corners of cyclic simple shear test specimens limit the range of uniform shear strains to levels of perhaps

15% to 20%. Important properties of liquefiable soils, particularly the residual or steady-state strength may not be fully mobilized at these strain levels. PEER researchers have developed a new testing device, the ring simple shear device, that allows very large strains to be achieved (Section 4.4.3a).

**(b) *Laboratory Test Results***

Though rarely used for characterization of soil liquefaction resistance in current practice, laboratory tests have played a crucial role in the development of contemporary procedures for evaluation of liquefaction hazards. Indeed, the geotechnical engineering profession's understanding of the basic mechanics of liquefaction stems almost exclusively from the results of many detailed laboratory testing programs.

Early laboratory tests were conducted for the primary purpose of characterizing liquefaction resistance. In the late 1960s, Castro (1969) performed an extensive series of static triaxial tests on sands spanning a wide range of relative densities. Castro observed three primary types of response (Figure 2.17). Very loose specimens (Curves A in Figure 2.17) exhibited a distinct peak shearing resistance at relatively low strains, followed by a period of rapid straining with increasing porewater pressures. Eventually, these very loose specimens strained with constant effective confining pressure and constant shearing resistance — Castro referred to this process as liquefaction. Dense test specimens (Curves C in Figure 2.17) showed a brief period of increasing porewater pressure followed by continuous dilation; the shearing resistance of the dense specimens increased monotonically with no peak value at low strains — Castro referred to this behavior as dilation. Test specimens of intermediate density (Curves B in Figure 2.17) showed an initial period of increasing porewater pressure and a peak shearing resistance at low strain followed by a period of reduced post-peak shearing resistance and nearly constant effective confining pressure. This was followed, at substantial strain levels, by a period of dilation and increasing shearing resistance. Castro referred to this behavior as limited liquefaction. The point at which the effective stress path for the intermediate density specimen (Curve B) exhibits neither contractive nor dilative behavior, i.e., the point at which the mean effective stress is momentarily constant (marked with an “X” in Figure 2.17), is referred to as the

quasi-steady state and the available shearing resistance at that point is called the quasi-steady-state strength.

In the 1960s and early 1970s, liquefaction resistance was characterized in terms of the normalized shear stress amplitude required to produce initial liquefaction in a given number of loading cycles. Because the development of excess porewater pressure was of primary interest, relatively little attention was paid to stress-strain and stress path behavior during the process of liquefaction, and virtually no attention was paid to these aspects of soil behavior after the occurrence of initial liquefaction. As the geotechnical engineering profession moves toward improved predictions of performance, these aspects of the behavior of liquefiable soils become quite critical.

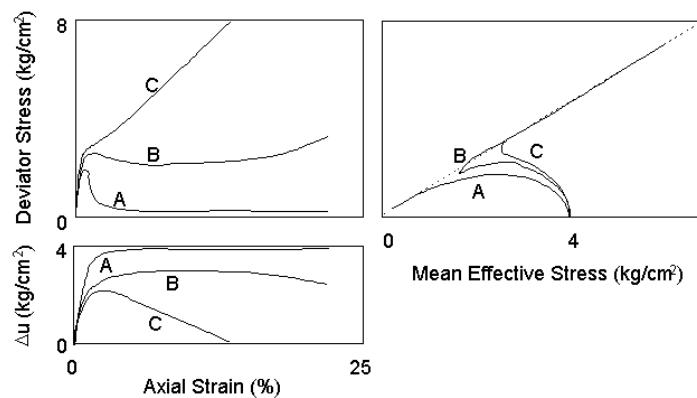


**Fig. 2.17 Three basic types of response observed by Castro (1969) in static triaxial tests: A — liquefaction, B — limited liquefaction, and C — dilation.**

### ***Flow Liquefaction***

Flow liquefaction occurs when static shear stresses exceed the residual strength of the soil. In the field, these static shear stresses are the stresses required to maintain static equilibrium. They may result from the presence of a slope, a retaining wall, or from the loads imposed on the soil by a foundation. In both the field and laboratory, flow liquefaction can be produced by both static and cyclic loading. Flow liquefaction tests in the laboratory are typically performed under stress- controlled loading conditions.

Figure 2.18 shows the stress-strain and stress path behavior of an isotropically consolidated element of soil undergoing flow liquefaction when subjected to stress-controlled monotonic loading. The figure shows that excess pore pressure increases as the deviator stress

increases. At a relatively small strain of level, however, the deviator stress reaches a peak value. At this point, the excess pore pressure is still relatively low ( $r_u = 0.5$ ). After the deviator stress reaches its peak value, the strain rate and the porewater pressure increase rapidly. Flow liquefaction can be said to have initiated at the point where the deviator stress reached its maximum value. At this point, the structure of the soil skeleton breaks down so that the available strength becomes equal to the residual strength. Because the deviator stress is greater than the residual strength, the testing specimen cannot maintain static equilibrium and, therefore, undergoes flow liquefaction.

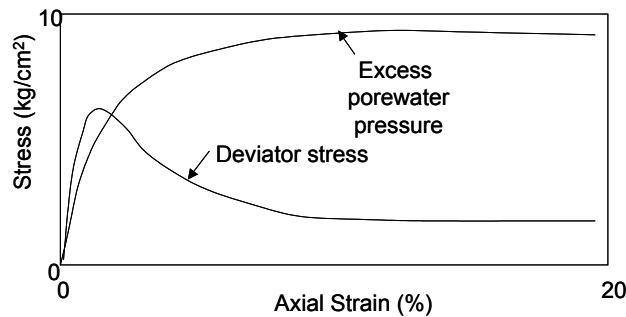


**Fig. 2.18 Flow liquefaction in isotropically consolidated triaxial test.**

Laboratory testing programs have shown that flow liquefaction is initiated when the effective stress ratio reaches a critical value. The locus of points with this critical stress ratio, when plotted in stress path space, defines the flow liquefaction surface. When the effective stress path of an element of soil that is susceptible to flow liquefaction reaches the flow liquefaction surface, whether by static or cyclic loading, flow liquefaction will occur. As the structure of the soil skeleton breaks down, the excess pore pressure rises quickly and the specimen strains rapidly due to the difference between the static shear stress and the residual strength. It is important to note, however, that the pore-pressure ratio can be well below unity at the initiation of flow liquefaction. The pore-pressure ratio increases, often substantially, following the initiation of flow liquefaction and reaches a maximum value when the soil reaches the steady state of deformation. Except for the case of extremely loose soils, the pore-pressure ratio does not reach a value of unity.

Figure 2.19 shows the stress-strain and stress path behavior of three very loose anisotropically consolidated triaxial specimens subjected to monotonic loading. In each of these cases, the initial shear stress exceeds the residual strength of the soil. The application of relatively small undrained increases in deviator stress are sufficient to trigger flow liquefaction; the strain at which the soil skeleton breaks down is very small. Nevertheless, the low residual strength causes the specimen to build up additional pore pressure and strain rapidly after flow liquefaction was triggered. Again, the level of pore pressure at the point of initiation of flow liquefaction is low. The large and rapid straining is driven by the difference between the static shear stress and the residual strength, which can be large even when the undrained triggering load is small.

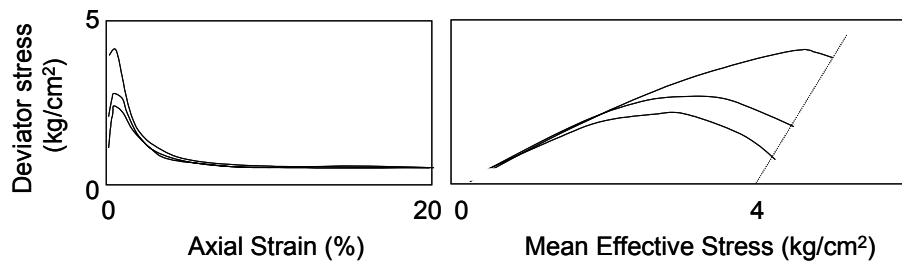


**Fig. 2.19 Flow liquefaction in anisotropically consolidated triaxial tests.**

Flow liquefaction can typically occur only in soils that are very loose and at sufficiently high confining pressures to make them highly contractive, and that exist under significant initial shear stress. Because such conditions are not commonly encountered in the field, occurrences of flow liquefaction are relatively rare.

### ***Cyclic Mobility***

If the static shear stresses are lower than the residual strength, flow liquefaction cannot occur under undrained conditions. The application of cyclic shear stress, however, can still lead to the development of excess pore pressure. Initial liquefaction ( $r_u = 100\%$ ) and associated deformations remain among the main causes of damage during earthquakes (Seed et al. 1990; Bardet et al. 1995; Sitar 1995; Japanese Geotechnical Society 1996; Ansal et al. 1999). Indeed,

dramatic unbounded (flow failure) deformations due to liquefaction in dams and other structures (Seed et al. 1975, 1989; Davis and Bardet 1996) have highlighted the significance of this problem in earthquake engineering research. However, liquefaction more frequently results in limited but objectionable levels of deformation (Bartlett and Youd 1995; Youd et al., 1999). This pattern of response has been well documented in the pioneering work of Seed and Lee (1966), and Castro (1969). In such situations, the deformation process may be characterized mainly as cyclic straining with limited amplitudes (Seed, 1979), commonly known as cyclic mobility (Castro and Poulos, 1977) or cyclic liquefaction (Casagrande, 1975).

A valuable comprehensive survey of experimental research (triaxial, shear, and shake-table tests), documenting the significance of cyclic mobility during liquefaction was compiled by Seed (1979). Based on this survey, clean sands with a relative density  $D_r$  of 45% or more, appear to exhibit the mechanism of limited strain cyclic mobility during liquefaction. At and above  $D_r = 45\%$ , the tendency for soil-skeleton dilation at large shear strain excursions rapidly reduces porewater pressure, allowing for significant regain in soil stiffness and strength that can eventually arrest further deformation.

For many years, laboratory tests on liquefiable soils focused on the generation of excess porewater pressure from the beginning of loading to the point of initial liquefaction (i.e., the point at which  $r_u = 100\%$ ). The mechanics of the liquefaction process, particularly the fluctuations in excess porewater pressure that occur as initial liquefaction was reached and after it had occurred, were not investigated in detail. Because of increased attention to the mechanics of the liquefaction process, the geotechnical engineering profession's understanding of cyclic mobility has increased dramatically in recent years, particularly in several aspects of the behavior of liquefiable soils that have long been observed, but not understood, in the laboratory. Because of this, it is now possible to model important aspects of cyclic mobility and thereby predict its effects on the performance of structures.

Laboratory testing programs have shown that both loose and dense soils exhibit contractive behavior at relatively low stress ratios ( $\eta = q/p'$ ). At higher stress ratios, however, the behavior becomes dilative. Careful interpretation of laboratory tests has shown (Ishihara, 1985) that the transition from contractive to dilative behavior occurs at a particular stress ratio, which has been called the constant volume stress ratio,  $\eta_{cv}$ . When plotted in stress path space

(Figure 2.20), the boundary between contractive and dilative behavior is referred to as the phase transformation line.

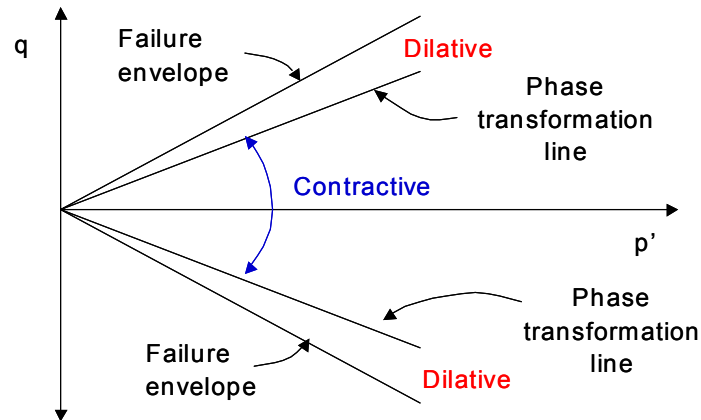


**Fig. 2.20 Schematic illustration of phase transformation line.**

Under undrained cyclic loading conditions, the tendency for a saturated, cohesionless soil to exhibit contractive behavior (Phase 0-1 in Figure 2.21), leads to the development of excess pore pressure and reduction in effective confining pressure (Lambe and Whitman, 1969). As the shear strain increases and the stress path approaches the phase transformation envelope (Ishihara, 1985; Vaid and Thomas, 1995; Vaid and Sivathayalan, 1999; Iai, 1991, 1998; Dobry and Abdoun, 1998; Kramer and Arduino, 1999), the contractive tendency changes to a dilative tendency that increases effective confining pressure (Vaid and Thomas, 1995; Vaid and Sivathayalan, 1999). This dilative tendency allows the soil to resist increased levels of shear stress — the stress path moves upward along the failure envelope, e.g., Phase 2-3 in Figure 2.21). For the purpose of liquefaction-induced shear deformations, medium-dense clean granular soils are found to exhibit this type of response (Elgamal et al., 1998). During a dilative phase (Phase 2-3 in Figure 2.21), the increased confinement may generate significant shear stiffness and strength in the soil, which progressively prevents further shear deformation. Further discussion of this behavior, including all subsequent phases, is presented in Section 5.3.2(c).

Dilation can result in significant increases in shear stress and mean effective confining stress). This increase will be limited (Casagrande, 1936; 1975) by

1. Fluid avitation: If soil response is essentially undrained (fluid migration is relatively slow), the tendency for dilation can eventually drop pore pressure to the minimum value

of  $-1.0$  atmospheric pressure (i.e., cavitation). Cavitation will prevent the effective confining pressure from further increase (Iai, 1998).

2. Critical void-ratio or constant volume soil response: If the soil is partially or fully drained (relatively rapid flow of pore fluid), dilation-induced expansion of the soil skeleton will occur. To this end, the soil will eventually reach a critical void-ratio or “constant volume state,” whereupon further shear deformation continues to develop without additional volume change. At this state, the effective confining pressure, and hence the shearing resistance, will remain constant.

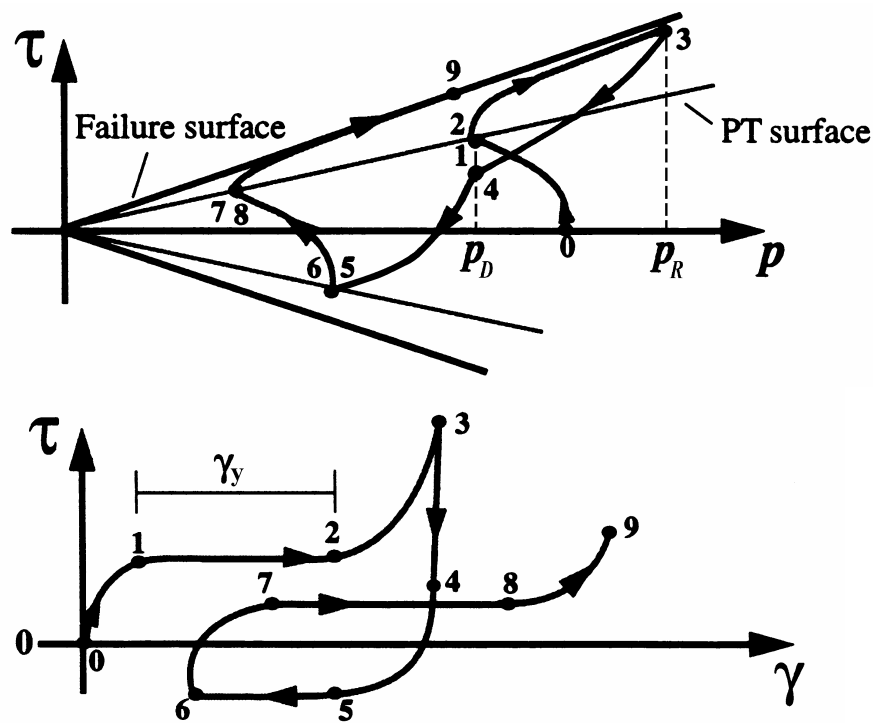
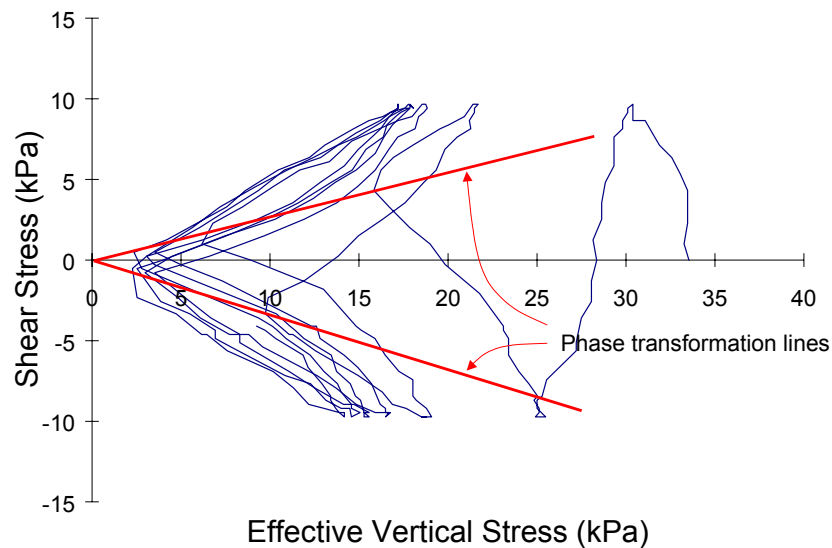


Fig. 2.21 Schematic of constitutive model response showing the octahedral stress  $\tau$ , the effective confining pressure  $p$ , and the octahedral strain  $\gamma$  relationship (after Parra, 1996).

Cyclic mobility with phase transformation behavior is easily observed in laboratory element tests. Figure 2.22 shows the results of a cyclic simple shear test on a medium dense clean sand specimen subjected to symmetric (zero static shear stress) harmonic loading. Each of the early loading cycles causes the excess pore pressure to increase; as a result, the effective stress path moves monotonically to the left. Because the cyclic shear stress amplitude remains

constant while the mean effective stress decreases, the stress ratio (ratio of shear stress to effective vertical stress) tends to increase as the test proceeds. Eventually, the stress ratio reaches and exceeds the constant volume stress ratio, which corresponds to the phase transformation line in stress path space. When the stress ratio exceeds the constant volume stress ratio, the specimen begins to dilate. Dilation causes the effective stress to increase and the pore pressure to decrease; therefore, the effective stress path moves to the right. Upon a stress reversal, the specimen again becomes contractive until the phase transformation line is crossed during loading in the opposite direction. Eventually, the effective stress path converges to a nearly constant shape with periods of contractive and dilative behavior occurring within each loading cycle.



**Fig. 2.22** Cyclic mobility with phase transformation behavior in a cyclic simple shear test.

After many cycles of loading, the effective stress may drop to values of nearly zero twice within each loading cycle. When the effective stress reaches such low values, the stiffness of the soil specimen is low. However, the specimen immediately dilates until the stress is reversed. As dilation occurs, however, the increasing effective stress leads to increased stiffness. This leads to the S-shaped stress-strain curves commonly observed following initial liquefaction. The tendency for dilation and increased stiffness that accompanies it limits the strain amplitudes that can develop following initial liquefaction. These aspects of the behavior of liquefiable soils

have important implications for the development of permanent deformations in the field. Because permanent soil deformations have a direct and important effect on structural performance, modeling of this aspect of liquefiable soil behavior is vital for the development of PBEE. Unfortunately, relatively little experimental data focusing on post-liquefaction behavior are currently available.

More recent observations continue to corroborate the concept of phase transformation and cyclic mobility. A large body of laboratory experiments (e.g., Ishihara, 1985; Arulmoli, 1992; Boulanger and Seed, 1995), shake-table, and centrifuge tests (Dobry, et al., 1995; Taboada, 1995; Dobry and Abdoun, 1998; Fiegel and Kutter, 1992; Kutter and Balakrishnan, 1998; Balakrishnan and Kutter, 1999) all point to the same pattern of deformation (clean sands and non-plastic silts). In these experimental observations (compiled by Elgamal et al., 1998), clean uniform cohesionless soils with a reported  $D_r$  of as low as 37% may accumulate large liquefaction-induced cyclic shear strains, but do not exhibit flow-type failures (in laboratory samples, shaking-table, and centrifuge tests). For instance, the Imperial County, Wildlife Refuge earthquake-induced liquefaction case history (Holzer et al., 1987; Youd and Holzer, 1994), also demonstrates clear signs of this response mechanism (Elgamal and Zeghal, 1992; Zeghal and Elgamal, 1994). In a recent full-scale lateral pile-soil interaction experiment conducted in liquefied soil (Ashford and Rollins, 1999), much of the above response characteristics were observed and documented.

Under sloping ground conditions, cyclic shear stresses are superimposed upon non-zero static shear stresses. The resulting loading is non-symmetric, which causes permanent strain to accumulate in one direction. Figure 2.23 shows the results of a cyclic simple shear test with non-symmetric, loading. In the early cycles of loading, excess pore pressure builds up and effective stress decreases. Eventually, the effective stress path reaches the phase transformation line and the soil exhibits both contractive and dilative behavior in each cycle. The non-symmetric nature of the loading causes permanent shear strains to accumulate in one direction. Each successive loading cycle produces an increment of permanent strain. The level of permanent strain is limited, however, by the dilation that takes place when the stress path crosses the phase transformation line. The rate at which stiffness increases during dilation following initial liquefaction will control the development of lateral spreading displacements; however, very little experimental data on this aspect of liquefiable soil behavior are currently available.

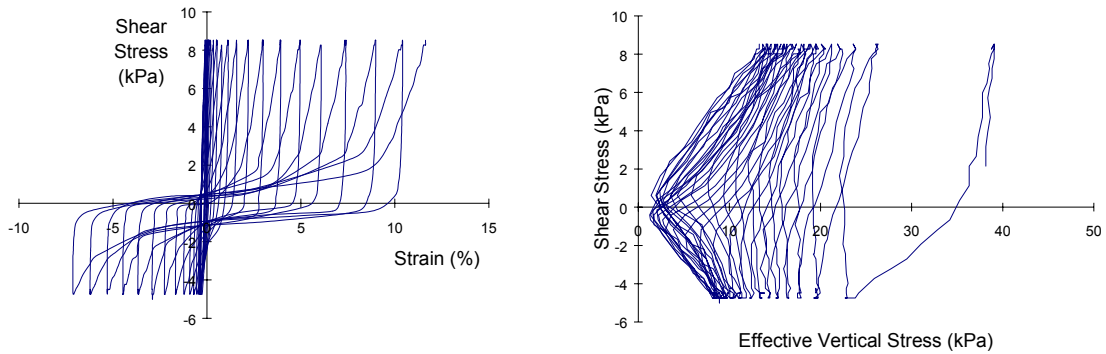


**Fig. 2.23** Cyclic mobility with phase transformation behavior in a cyclic simple shear test with non-zero initial shear stress.

For the important situations of lateral spreading (Dobry et al., 1995; Dobry and Abdoun, 1998; Kutter and Balakrishnan, 1998; Balakrishnan and Kutter, 1999) or biased strain accumulation due to an acting superposed static (locked-in) shear stress, the tendency for soil dilation may continue to play a dominant role. This is clearly seen from the results of a triaxial test (Figure 2.24), where a superposed static shear stress causes the strain to occur in a biased (downslope) direction, on a cycle-by-cycle basis (Arulmoli et al., 1992). Inspection of Figure 2.24 shows that a net finite increment of permanent (downslope) shear strain occurs in each cycle. The magnitude of such increments determines the total accumulated permanent deformation.

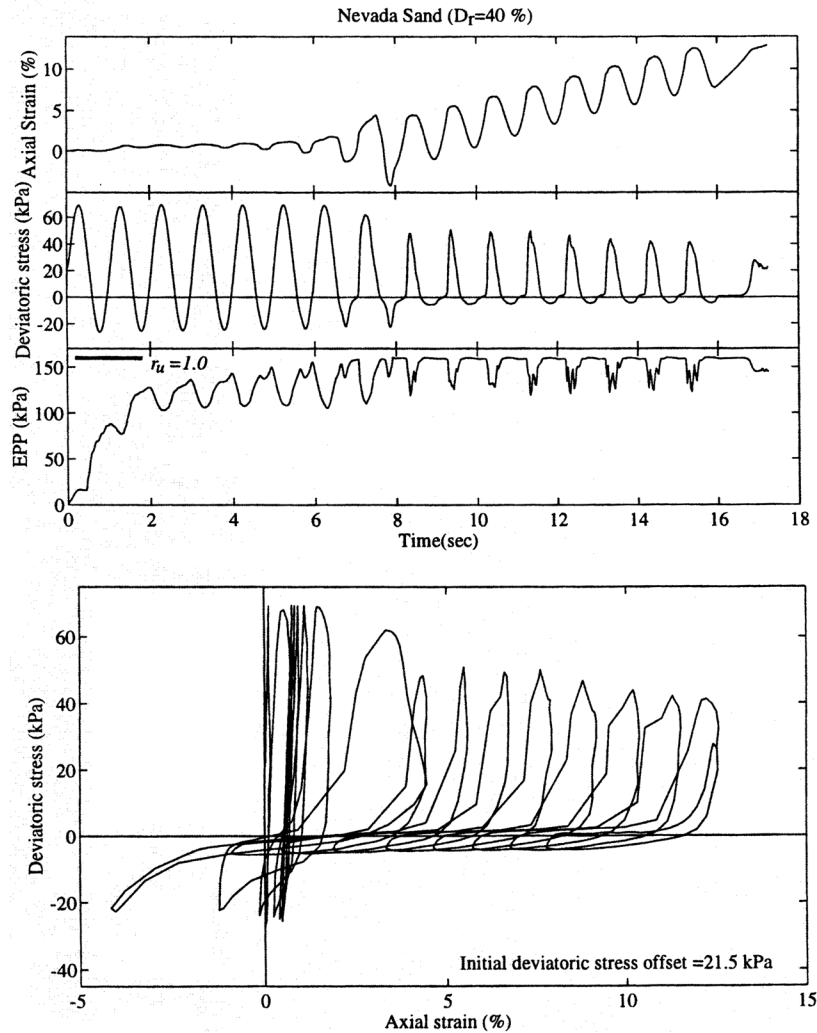
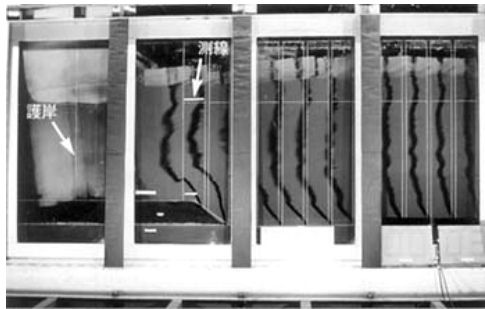


Fig. 2.24 Stress-strain and excess-pore-pressure histories during an undrained, anisotropically consolidated cyclic triaxial test of Nevada Sand at  $D_r=40\%$  (Arulmoli et al. 1992).

### 2.3.3 Laboratory Model Test Results

Model tests are commonly used to measure soil response. By constructing scale models of soil deposits with and without structures, the response of actual physical problems in the field can be simulated. For earthquake engineering purposes, geotechnical models are usually well instrumented and then tested using shaking tables or centrifuge devices. Shaking tables offer the advantage of testing larger models, but centrifuge devices are capable of modeling in situ stresses more accurately.

Shaking tables are available in many different sizes, from those capable of testing models with dimensions of tens of centimeters to those capable of testing models several meters in height. The shaking table at the Public Works Research Institute (PWRI) in Japan, for example, has a base that measures 7.6 m by 7.6 m. This shaking table has been used for testing large specimens of saturated soil, such as that for which lateral spreading deformations are shown in Figure 2.25. Within PEER, shaking tables are in operation at Berkeley, Irvine, San Diego, and Washington.



**Fig. 2.25 Lateral spreading deformations indicated by vertical layers of colored sand, as observed in PWRI shaking table tests.**

Centrifuge devices are also available in different sizes, ranging from small drum centrifuges with radii less than 1 m to large centrifuges with radii of several meters. Within PEER, small centrifuges are located at Caltech and Davis, and a very large geotechnical centrifuge is available at Davis (Figure 2.26).

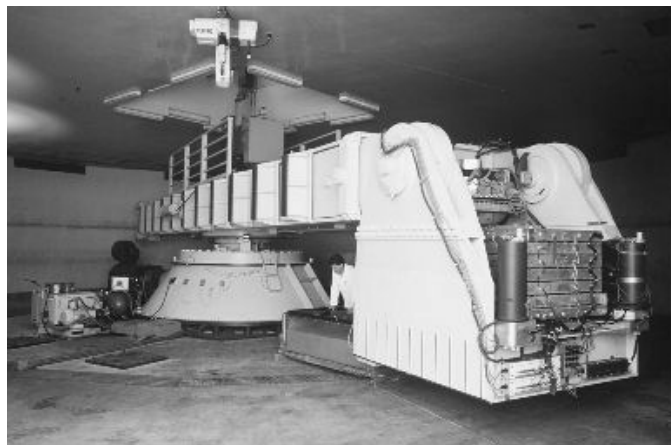


**Fig. 2.26 Geotechnical centrifuge at UC Davis. Note laminar box in centrifuge bucket for testing models under seismic loading conditions.**

In concept, both flow liquefaction and cyclic mobility can be produced in model tests. The generation of flow liquefaction in model tests, however, has proven to be difficult. To date, flow liquefaction has not been produced in uniform models on shaking tables. Because the limited size of shaking tables results in low effective confining pressures, the sands of which the models are comprised tend to exhibit dilative behavior. Flow liquefaction has been observed in shaking table tests when stratified soil models have been used. Kokusho (1999) constructed model slopes of uniform sand with and without seams of silt on a small shaking table. The models were tested by shaking them parallel to the strike of the slope, i.e., such that no inertial forces were produced in the downslope direction. When uniform models were tested under a given level of input motion, limited downslope displacements were observed. However, when the stratified models were tested, limited displacements were observed during shaking but the redistribution and the accumulation of porewater pressure immediately below the silt seams led to rapid flow sliding that occurred after shaking had ended. Similar results have recently been observed in centrifuge tests performed at UC Davis (Boulanger and Kutter, personal communication, 2000).

For sands and silts, the assumption of undrained excess pore pressure ( $u_e$ ) buildup is usually employed for liquefaction susceptibility/triggering analyses (NRC, 1985; Seed and Idriss, 1982; Kramer, 1996; Youd et al., 2001). However, the influence of permeability on liquefaction and associated deformations is being clearly manifested in the results of centrifuge testing investigations (e.g., Tan and Scott, 1985; Arulanandan and Scott, 1993, Kimura et al., 1998). In such dynamically induced liquefaction studies, scaling laws dictate that prototype permeability be simulated through the use of a higher viscosity pore fluid. In a recent series of centrifuge experiments to study liquefaction behind a quay wall, Lee et al. (2000) employed three pore fluids with different viscosity values (in three separate tests). It was found that higher fluid viscosity (or lower soil permeability) caused higher buildup and slower dissipation of excess pore pressure. Consequently, larger movements of the quay wall occurred in the lower permeability cases (deformations increased by as much as 2 times).

Because it does not require very loose soil conditions or very high confining pressure, cyclic mobility can be produced much more easily than flow liquefaction in model tests.

Numerous observations of cyclic mobility in shaking table and centrifuge tests, including its manifestation in the form of lateral spreading, can be found in the literature.

## **2.4 HAZARD EVALUATION**

Evaluation of liquefaction hazards involves three primary steps. First, the susceptibility of the soil to liquefaction must be evaluated. If the soil is determined to be not susceptible to liquefaction, liquefaction hazards do not exist and the liquefaction hazard evaluation is complete. If the soil is susceptible to liquefaction, however, the liquefaction hazard evaluation moves to the second step — evaluation of the potential for initiation of liquefaction. This step involves comparison of the level of loading produced by the earthquake with the liquefaction resistance of the soil. If the resistance is greater than the loading, liquefaction will not be initiated and the liquefaction hazard evaluation can be considered complete. If the level of loading is greater than the liquefaction resistance, however, liquefaction will be initiated. If liquefaction is initiated, the liquefaction hazard evaluation must move to the third stage, the evaluation of the effects of liquefaction. If the effects are sufficiently severe, the engineer and owner may consider improvement of the site, or alternative sites for the proposed development.

Liquefaction hazard evaluation to date has focused primarily on the first two steps in this process — liquefaction susceptibility and the initiation of liquefaction. The performance of structures, however, depends ultimately on the effects of liquefaction, a subject for which much less data are available. In fact, the generation of additional laboratory data on post-liquefaction stress-strain behavior (both shear and volumetric) is a critical research need in geotechnical earthquake engineering.

### **2.4.1 Liquefaction Susceptibility**

In order for liquefaction to occur, the soil must be susceptible to liquefaction. There are several criteria by which the susceptibility of individual soils to liquefaction can be judged.

Historical observations of liquefaction in past earthquakes can provide an indication of liquefaction susceptibility in future earthquakes. At a number of sites, repeated instances of

liquefaction have been observed in different earthquakes. Therefore, observed field evidence is a good indicator of liquefaction susceptibility.

Geologic conditions can also provide a good indication of liquefaction susceptibility. Liquefaction susceptibility is strongly influenced by soil composition, specifically by factors such as grain size distribution and particle shape. Uniformly graded soils and soils with rounded particle shapes are most susceptible to liquefaction. Consequently, geologic processes that sort soils into deposits of uniform gradation with rounded particles will tend to produce soil deposits with high susceptibility to liquefaction. For many years, only sands were considered to be susceptible to liquefaction. It is now recognized, however, that liquefaction can occur over a broader range of soil types. Liquefaction of gravels and non-plastic silts has been observed in several earthquakes, though the database of these observations is small compared to that of clean and silty sands.

Clays are not susceptible to liquefaction, although some can exhibit strain-softening behavior similar to that of liquefiable soils. The so-called “Chinese criteria” are used to identify clayey soils that are susceptible to significant strength loss (all of the following conditions must be met):

Clay fraction (finer than 0.005 mm)	≤ 15%
Liquid limit, LL	< 35%
Natural water content	≥ 0.90 LL
Liquidity index	≤ 0.75

Some sandy soils include clayey fines. Ishihara and Koseki (1989) showed that plastic fines tend to inhibit pore-pressure generation and suggested that the plasticity index, PI, of the fines be used to determine a factor

$$F = \max [1.0, 1.0 + 0.022(\text{PI} - 10)]$$

by which the computed factor of safety against liquefaction should be multiplied to account for plastic fines.

Liquefaction susceptibility is also strongly influenced by soil state. The “state” of an element of soil is defined by its density and effective stress. Castro (1969) showed that soils

with low density under high effective stress consistently exhibited highly contractive behavior (with flow liquefaction) under monotonic loading (see Curves A in Figure 2.17), that soils with high density under low effective stress consistently exhibited dilative behavior under monotonic loading (Curves C in Figure 2.17), and that soils of intermediate density and/or intermediate effective stresses exhibited limited liquefaction (Curves B in Figure 2.17). Building upon the critical void-ratio concept first identified by Casagrande (1936), Castro postulated that a given soil sheared to large strain levels under undrained conditions would eventually reach a steady-state condition, and that the steady-state stress conditions would be a function of void ratio alone. By plotting the steady-state effective confining pressure as a function of void ratio, Castro defined a steady-state line that marked the boundary between (contractive) states susceptible to flow liquefaction and (dilative) states not susceptible to flow liquefaction (Figure 2.27).

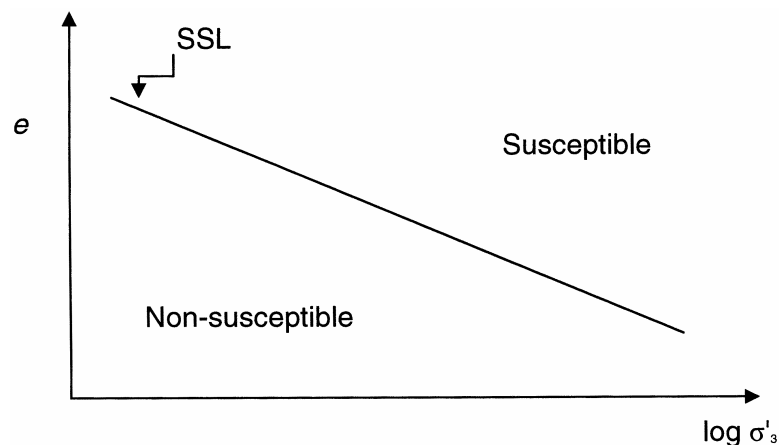


**Fig. 2.27 Schematic illustration of steady-state line with conditions of susceptibility to flow liquefaction.**

For frictional materials such as most liquefiable soils, the existence of a unique relationship between density and steady-state effective confining pressure implies a unique relationship between density and steady-state shear strength. Castro observed such a relationship in triaxial compression tests. Subsequent triaxial testing (e.g., Vaid and Chern, 1985; Vaid et al., 1990; Verdugo and Ishihara, 1996; Reimer and Seed, 1997) suggests that the relationship between steady-state strength and density may not be unique; instead, it may be a function of stress path (with extensional stress paths producing lower steady-state strengths than compressional stress paths) and soil fabric. These conclusions, however, are actually based on observations of the quasi-steady-state strength, which is mobilized at considerably lower strain

levels than the steady-state strength. However, the limited strain capabilities of the testing devices used to develop these conclusions does not ensure that true steady-state conditions were reached or measured. The distinction between the quasi-steady state and the steady state is an important one, for both theoretical and practical reasons.

## **2.4.2 Initiation of Liquefaction**

Liquefaction can be initiated by earthquakes, by non-seismic loading such as low amplitude vibrations produced by train traffic, or by static loads such as those that might be caused by rapid drawdown. Several approaches for evaluation of the potential for earthquake-induced initiation of liquefaction have been proposed. The following sections provide a brief review of the most prominent of these approaches and an introduction to a new method for probabilistic evaluation of liquefaction potential.

### ***(a) Cyclic Stress Approach***

The most well-documented and commonly used procedure for evaluation of liquefaction potential is referred to as the cyclic stress approach. In the cyclic stress approach, both the loading imposed on the soil by the earthquake and the resistance of the soil to liquefaction are characterized in terms of cyclic shear stresses. By characterizing both loading and resistance in common terms, they can be directly compared to determine the potential for liquefaction.

#### ***Characterization of Loading***

For the purposes of liquefaction evaluation, loading is typically characterized in terms of the cyclic stress ratio,  $CSR$ , which is defined as the ratio of the equivalent cyclic shear stress,  $\tau_{cyc}$ , to the initial vertical effective stress,  $\sigma'_{vo}$ .

$$CSR = \frac{\tau_{cyc}}{\sigma'_{vo}} \quad (2.1)$$

The equivalent cyclic shear stress is generally taken as being equal to 65% of the peak cyclic shear stress, a value arrived at by comparing rates of porewater pressure generation caused by transient earthquake shear stress histories with rates caused by uniform harmonic shear stress histories (Seed et al., 1975). The factor was intended to allow comparison of a transient shear stress history from an earthquake of magnitude,  $M$ , with that of  $N$  cycles of harmonic motion of amplitude  $0.65\tau_{\max}$  where  $N$  is an equivalent number of cycles of harmonic motion. If  $N$  is obtained from Figure 2.28, the porewater pressures generated by the transient and harmonic shear stress histories should be approximately the same. In a procedure commonly referred to as the “simplified method,” the peak cyclic shear stress is estimated from the peak ground surface acceleration and a depth reduction factor,  $r_d$ , which represents the average rate at which peak shear stress attenuates with depth. In the simplified method, therefore, the cyclic stress ratio is defined as

$$CSR = 0.65 \frac{a_{\max}}{g} \frac{\sigma_v}{\sigma_{v0}} r_d \quad (2.2)$$

where  $a_{\max}$  is the peak ground surface acceleration that would be expected to occur in the absence of liquefaction, i.e., the value of  $a_{\max}$  predicted by a SHAKE-type of analysis in which excess pore-pressure generation is not considered (Youd et al., 2001). It should be noted that this value of  $a_{\max}$  may differ from the actual value of  $a_{\max}$  that would occur at the surface of a liquefiable soil profile. The simplified method is very commonly used in geotechnical engineering practice.

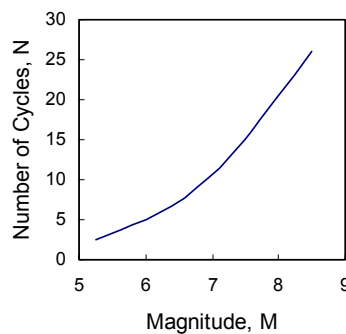


**Fig. 2.28 Number of equivalent cycles of loading for liquefaction potential evaluation.**

## Characterization of Resistance

Liquefaction resistance is also typically expressed in terms of a cyclic stress ratio commonly referred to as the cyclic resistance ratio, CRR. The cyclic resistance ratio is defined as the cyclic stress ratio that just causes initial liquefaction. In practice, the cyclic resistance ratio is typically determined as a function of two parameters: penetration resistance and earthquake magnitude.

As indicated previously, early procedures for evaluation of liquefaction potential determined liquefaction resistance from the results of laboratory tests. Subsequent investigations showed that laboratory test results were significantly influenced by a number of factors, such as soil fabric, that could not be reliably replicated in laboratory test specimens. As a result, it is now most common to relate cyclic resistance ratio to corrected Standard Penetration Test resistance, i.e.,  $(N_1)_{60}$ . Youd et al. (2001) recently proposed a graphical relationship between CRR and  $(N_1)_{60}$  (Figure 2.29). This graphical relationship is appropriate for M7.5 earthquakes — correction factors for other earthquake magnitudes, which account for the correlation between magnitude and number of equivalent cycles, have been proposed by various researchers (Figure 2.30). Youd et al. (2001) recommended the use of magnitude scaling factors in the range between the curves of Idriss and Andrus and Stokoe (1997) (Figure 2.30).

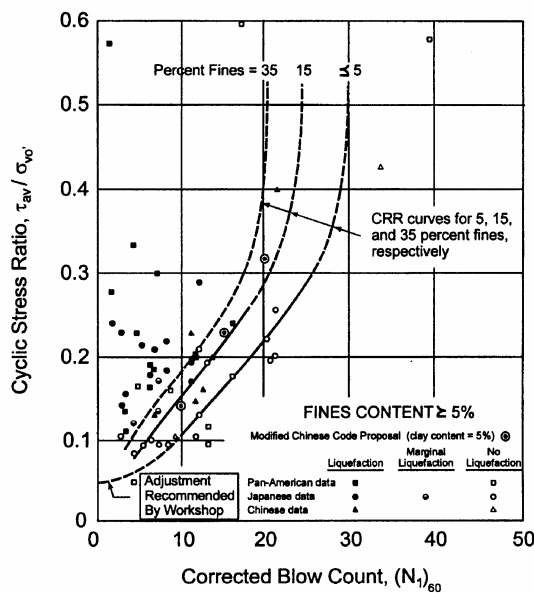


Fig. 2.29 Relationship between cyclic resistance ratio and  $(N_1)_{60}$  for  $M_w = 7.5$  earthquakes.

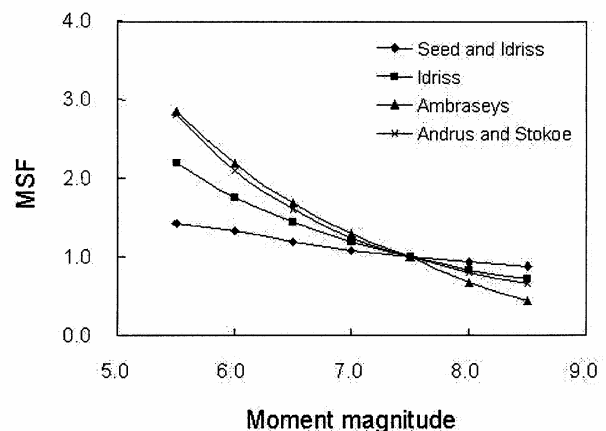


Fig. 2.30 Magnitude scaling factors.

Liquefaction resistance can also be determined by correlation to the results of other in situ tests such as CPT and shear wave velocity tests. Because this report is primarily concerned with modeling of liquefaction, these additional empirical approaches will not be reviewed in detail. The techniques are presented in concise form in Youd et al. (2001), which also provides references to more detailed descriptions.

### ***Evaluation of Liquefaction Potential***

The potential for initiation of liquefaction in a particular earthquake is usually expressed in terms of a factor of safety against liquefaction. The factor of safety is defined in the usual way — as a ratio of capacity to demand. In the case of liquefaction, the factor of safety can be expressed as

$$FS = \frac{CRR}{CSR} \quad (2.3)$$

Factor-of-safety values less than one indicate that initial liquefaction is likely. It should be noted that this factor of safety does not distinguish between flow liquefaction and cyclic mobility, and provides no information on post-liquefaction behavior. Because it is based on case history data where liquefaction is evidenced by ground surface disruptions such as sand boils, cracks, ground oscillation, etc., it provides an indication of the likelihood of such effects at the site of interest.

### ***Probability of Liquefaction***

In recognition of the considerable degree of uncertainty in evaluation of both the loading (denominator) and resistance (numerator) terms of the factor-of-safety expression, procedures for estimating the probability of liquefaction have been developed. The various procedures differ in the databases on which they are based, the extent to which different variables are treated deterministically or probabilistically, and the method of analysis/regression used.

Liao et al. (1988) applied a binary regression technique to a database of 278 case histories of liquefaction/non-liquefaction to develop expressions for the probability of liquefaction for local models (in which loading was characterized by a local measure such as

PGA) and source models (in which source parameters such as magnitude and distance were used to characterize loading). Analyses were performed for clean sand (<12% fines) and clean/silty sand databases. The magnitude scaling factor and depth reduction factor,  $r_d$ , were treated deterministically. For the local model with clean sand data, the following expression was developed to estimate the probability of liquefaction:

$$P_L = \frac{1}{1 + \exp(-16.447 - 6.4603 \ln(CSRN) + 0.39760(N_1)_{60})} \quad (2.4)$$

Figure 2.31 shows contours of the probability of liquefaction for Equation 2.4; the uncertainty in the liquefaction hazard evaluation can be seen to be quite high. The uncertainty in the model developed for silty sands was even higher.

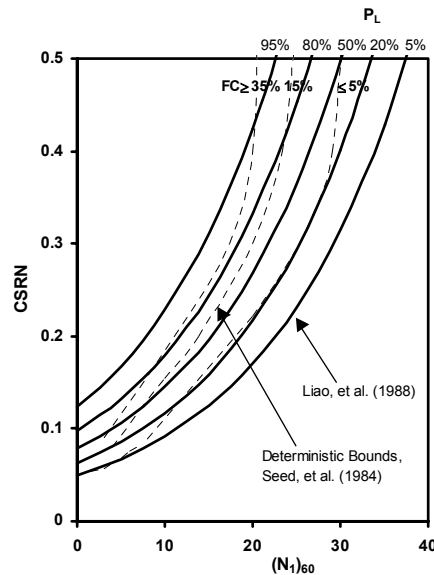


**Fig. 2.31 Probability of liquefaction contours of Liao et al (1988) (after Seed et al., 2001).**

Youd and Noble (1997) used a database that included case histories that occurred after the Liao et al. (1988) relationship had been developed and deleted data used by Liao et al. (1988) that was judged to be of questionable quality. The effects of fines content were considered deterministically, and maximum likelihood estimation was used to evaluate liquefaction

probabilities. As seen in Figure 2.32, the uncertainty in liquefaction hazard evaluation is quite high.

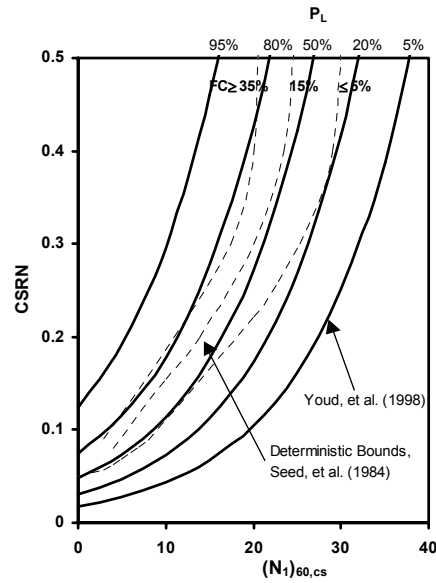


**Fig. 2.32 Probability of liquefaction contours of Youd and Noble (1997) (after Seed et al., 2001).**

Liao and Lum (1998) used procedures similar to those of Liao et al. (1988) to analyze 182 clean sand (<12% fines) cases from the Liao and Whitman (1986) database with magnitude as a variable in the regression. This approach allows elimination of the magnitude scaling factor from the expression for probability of liquefaction. Two alternative forms of a probability of liquefaction expression, with and without logarithmic linearization of the magnitude term, were proposed with no indication of preference for one or the other; the one without the logarithmic transformation is

$$P_L = \frac{1}{1 + \exp(-5.2175 - 5.9831 \ln(CSR) + 0.39166(N_1)_{60} - 1.3745M)} \quad (2.5)$$

This expression had goodness-of-fit statistics that were comparable to those of Liao et al. (1988). Liao and Lum (1998) also tested a series of MSF expressions to determine their consistency with the database used in their analyses; the results showed that the MSF of Seed and Idriss (1982) provided the best statistical agreement but that none of the proposed MSF expressions produced poor agreement.

Toprak et al. (1999) used SPT and CPT data at 25 natural soil sites in the Monterey and San Francisco Bay regions to develop SPT- and CPT-based procedures for estimation of liquefaction probability. To minimize variability, all data was obtained by the same personnel using the same equipment. This database was supplemented with data from four other earthquakes of similar magnitude collected by the USGS, and then with the Noble and Youd (1998) database (for a total of 440 cases). Using the Idriss MSF expression, Toprak et al. (1999) proposed the equation

$$\text{Logit}(P_L) = \ln[P_L/(1-P_L)] = 10.4459 - 0.2295 (N_1)_{60cs} + 4.0573 \ln(\text{CSR}/\text{MSF}) \quad (2.6)$$

Using CPT data from Loma Prieta sites, Toprak et al. (1999) proposed use of the equation

$$\text{Logit}(P_L) = \ln[P_L/(1-P_L)] = 11.6896 - 0.0567 (q_{c1N})_{cs} + 4.0817 \ln(\text{CSR}) \quad (2.7)$$

but recommended that it be used with caution until the CPT database is supplemented with case histories from other earthquakes. The results of the SPT model, illustrated in Figure 2.33, show a considerable degree of uncertainty.

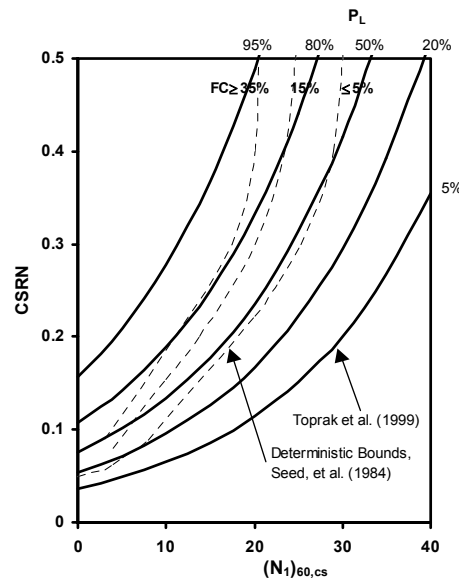
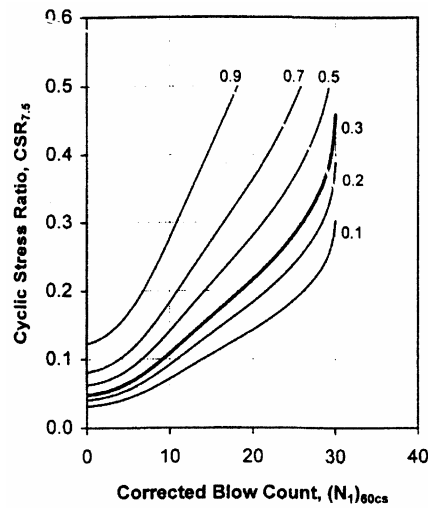


Fig. 2.33 Probability of liquefaction contours of Toprak et al. (1999) (after Seed et al., 2001).

Juang et al. (1999) developed a reliability-based method for evaluating liquefaction potential and later (Juang et al., 2000a) expressed its results in the form of a “mapping function” between probability of liquefaction and factor of safety against liquefaction. Chen and Juang (2000) used 233 SPT-based case histories to express the mapping function as

$$P_L = \frac{1}{1 + \left(\frac{FS}{0.77}\right)^{3.25}} \quad (2.8)$$

where  $FS$  is as defined in Equation 2.3. Juang and Jiang (2000) combined Equation 2.8 with the cyclic resistance ratio obtained from Figure 2.29 to produce the liquefaction probability curves shown in Figure 2.34.



**Fig. 2.34 Probability of liquefaction contours of Juang and Jiang (2000).**

Each of the previously described procedures for estimation of the probability of liquefaction is based on empirical observations of liquefaction/non-liquefaction during actual earthquakes. The loading is based on cyclic shear stresses, which are estimated from peak accelerations with an assumption of how acceleration amplitude varies with depth below the ground surface. Because strong motion records are seldom available at the sites of these

liquefaction observations, and because site response varies significantly from one site to another, significant uncertainty exists in the loading parameters. The resistance is based on correlation with SPT (or, in the case of Toprak et al. (1999), also CPT) resistance. Because SPT data from these case histories is limited, spatially variable, and obtained using a wide variety of testing procedures that have been shown to influence measured SPT resistances, there is a considerable degree of uncertainty in the resistance parameters. Hence, it is not surprising to see that all of these procedures show a large degree of uncertainty in estimates of the probability of liquefaction. Improved probabilistic analysis procedures have recently been developed by PEER researchers (Section 4.3).

**(b) *Cyclic Strain Approach***

Because liquefaction is caused by the generation of excess porewater pressure, and excess porewater pressure generation is caused by the tendency of individual soil particles to move into a denser configuration, liquefaction should be strongly influenced by the level of strain induced in the soil. In fact, detailed laboratory investigations (e.g., Dobry and Ladd, 1980) have shown that the rate at which pore pressure is generated in saturated sand is largely controlled by cyclic shear strain amplitude; the sensitivity of pore pressure to factors such as soil fabric and prior strain history (which strongly influence the relationship between porewater pressure and cyclic stress amplitude) is very low.

When cyclic shear stresses are applied to an element of soil, they produce cyclic shear strains. When the stresses are very low, the strains may develop through elastic distortion of the soil skeleton, i.e., without slip between individual soil particles. Under such conditions, the soil exhibits no tendency for volume change and hence generates no excess porewater pressure under undrained conditions. There is, therefore, a threshold shear strain (Drnevich and Richart, 1970; Dobry and Ladd, 1980; Dobry et al., 1982) below which no porewater pressure will develop; this shear strain is on the order of 0.01% for typical liquefiable soils at relatively shallow depths.

In the cyclic strain approach, both loading and resistance are described in terms of cyclic shear strains. The cyclic strains induced in the soil by earthquake loading are typically predicted by site response analysis — this is probably the greatest weakness of the cyclic strain approach, since cyclic strains are much more difficult to predict accurately than cyclic stresses. Procedures

are available for converting a transient time history of shear strain to a given number of cycles of uniform strain amplitude (Dobry et al, 1982). Liquefaction resistance is obtained from the results of strain-controlled tests and expressed as the cyclic strain amplitude required to cause liquefaction in the number of cycles of loading that corresponds to the magnitude of the earthquake. By comparing the cyclic strain amplitude produced by the earthquake with the cyclic strain amplitude required to cause liquefaction, the likelihood of liquefaction can be determined.

The cyclic strain approach has an advantage over the cyclic stress approach in that pore-pressure generation is more closely related to cyclic strains than cyclic stresses. However, cyclic strain amplitudes cannot be predicted as accurately as cyclic stress amplitudes, and equipment for cyclic strain-controlled testing is less readily available than equipment for cyclic stress-controlled testing. Primarily due to these reasons, the cyclic strain approach is less commonly used than cyclic stress approach in engineering practice.

**(c) Energy Approach**

While methods based on cyclic stresses or cyclic strains have seen widespread use in geotechnical engineering practice, each has significant limitations. One measure that reflects both cyclic stress and strain amplitudes is dissipated energy. Nemat-Nasser and Shokooh (1979) developed a relatively simple theory that related soil densification (drained conditions) and pore-pressure generation (undrained conditions) to dissipated energy. Others have since attempted to characterize the relationship between excess pore pressure and dissipated energy experimentally.

Kayen and Mitchell (1997) noted that Arias intensity is equal to the total energy absorbed by a population of simple oscillators spaced evenly in frequency, and proposed that liquefaction potential could be evaluated using Arias intensity. Arias intensity (two-component) can be computed from two orthogonal accelerograms as

$$I_h = \frac{\pi}{2g} \left[ \int_0^{t_o} a_x^2(t) dt + \int_0^{t_o} a_y^2(t) dt \right] \quad (2.9)$$

where  $t_0$  is strong motion duration or estimated as a function of source parameters from an attenuation relationship. Liquefaction resistance was correlated to in situ test parameters such as  $(N_1)_{60}$  and  $q_{c1}$  by careful evaluation of liquefaction case histories (Figure 2.35). Kayen and Mitchell (1997) showed that the use of Arias intensity provided a better discrimination between cases of liquefaction and non-liquefaction than can be obtained for the cyclic stress approach. In this approach, the factor of safety against liquefaction is defined as the ratio of the Arias intensity required to cause liquefaction to the Arias intensity produced by the ground motion, i.e.,

$$FS = \frac{I_{hb}}{I_h} \quad (2.10)$$

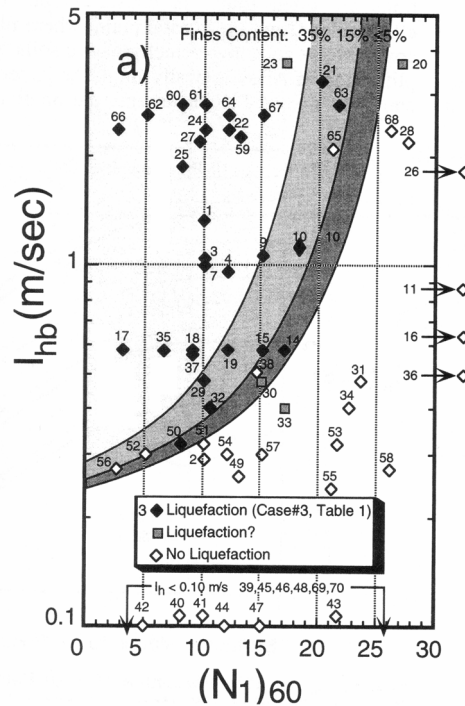


**Fig. 2.35 Relationship between SPT resistance and Arias intensity required to trigger liquefaction (after Kayen and Mitchell, 1997).**

The use of a parameter such as Arias intensity for evaluation of liquefaction potential has several useful advantages over the use of traditional quantities like cyclic stress and cyclic strain. Arias intensity reflects the amplitude, frequency content, and duration of a ground motion; other

parameters use earthquake magnitude as a proxy for frequency content and duration, and require artificial constructs such as magnitude scaling factors to do so. The close relationship between Arias intensity and energy lends itself to more direct comparison with in situ tests in which controlled/measured amounts of work/energy are obtained.

### **2.4.3 Effects of Liquefaction**

Liquefaction can affect the performance of buildings and bridges in a number of different ways. Liquefaction phenomena can alter ground motions in terms of amplitude, frequency content, and duration. Liquefaction can also lead to ground failure, either through flow liquefaction or lateral spreading.

#### ***(a) Effects on Site Response***

The characteristics of ground surface motions are well known to be influenced by local site conditions. The thickness, stiffness, and damping characteristics of the various soil layers that underlie a particular site control the relative amplification, or de-amplification, of various components of a bedrock motion. Stiff soil deposits tend to amplify the higher-frequency components of a bedrock motion, while soft soil deposits amplify low-frequency motions. Site response of liquefiable sites is somewhat unusual in that the stiffness of a specific soil deposit can change rapidly and drastically between the beginning and end of the earthquake.

In general, the development of excess porewater pressure and consequent reduction in effective stress will lead to the softening of a liquefiable soil deposit. Therefore, a soil layer that may amplify relatively high-frequency components of the early portion of a bedrock motion will tend to amplify successively lower frequency components as the motion proceeds.

Ground motions recorded at the surface of liquefiable soil deposits showed a pronounced reduction in high-frequency amplitude and increase in low-frequency amplitude following initial liquefaction (Figure 2.36). This change in frequency content corresponds to the dramatic reduction in stiffness and strength that accompanies initial liquefaction. However, these ground motions often also display several isolated spikes of high accelerations (e.g., Figure 2.6). Viewed in accelerograms, these spikes have a distinctive concave-upward shape. Through the

pioneering analyses of Elgamal and Zeghal (1994) and others, the spikes are now known to be produced by episodes of dilation within the liquefied soil. As the soil dilates above the phase transformation line, it stiffens, thereby leading to an increasing ability to transmit higher-frequency motions with time. This leads to the constructive interference of waves traveling upward through the liquefied soil; the resulting waves have been termed de-liquefaction shock waves by Kutter and Wilson (1999).

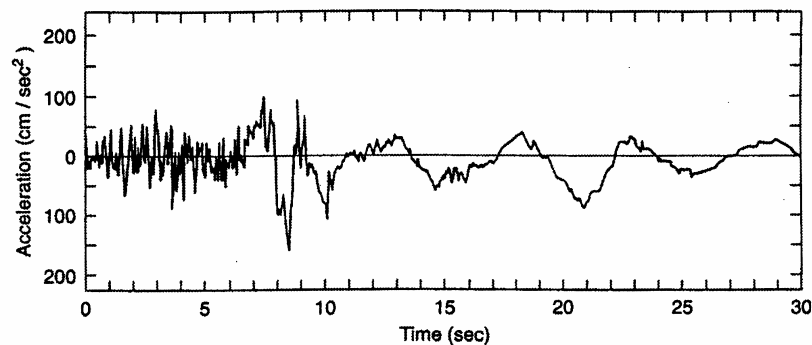


**Fig. 2.36 Time history of ground surface acceleration from Niigata, Japan. Note dramatic change in frequency content after initiation of liquefaction at 6 – 7 sec.**

Evaluation of the effects of liquefaction on structures, particularly those located on level ground where permanent horizontal displacements do not occur, requires the ability to predict the generation of excess porewater pressure with time. The extent to which excess pore pressures develop during, or even before, the strongest part of the input motion will strongly influence performance. When liquefaction occurs early in an earthquake, strong portions of the input motion may induce strong dilation pulses in the liquefied soil; these pulses may produce high accelerations with high velocities and displacements. If liquefaction occurs later in the earthquake, the stronger portion of the input motion may occur before initial liquefaction has occurred. The resulting ground motions for these two cases can be significantly different.

**(b) Settlement**

It is the tendency for contraction, i.e. for densification due to applied shear stresses, that produces liquefaction in saturated soils. The generation of excess porewater pressure, however, is a transient event. Following strong earthquake shaking, the presence of excess porewater

pressure implies the presence of hydraulic gradients that will cause the porewater to flow until hydrostatic porewater pressure conditions are once again reached. This dissipation of excess porewater pressure occurs through the process of consolidation, and is accompanied by a reduction in the volume of the soil, which is typically manifested in the form of settlement of the ground surface.

Ground surface settlement following liquefaction has been observed in numerous earthquakes. Large areas of settlement can produce regional subsidence, which can lead to submergence of low-lying coastal areas (Figure 2.37). Such conditions obviously produce poor performance of structures, even if the structure itself is not physically damaged. While regional subsidence can produce relatively uniform settlements of the area occupied by an individual structure, more localized settlement can produce significant differential settlement. Differential settlement can impose high demands on structures and lead to significant damage of structures supported on shallow foundations (Figure 2.38). Such settlement may result from the combined effects of soil densification and reduction of bearing capacity (i.e., shearing deformation of soil beneath foundation). Structural damage due to settlement can often be avoided by the use of deep foundations; piles that extend through liquefiable soils to derive their support from underlying dense/stiff soils will tend to hold the structure at its original elevation, even when settlement occurs. Though such foundations can prevent structural damage due to settlement, damage to nonstructural elements such as utility connections can occur.



**Fig. 2.37 Coastal flooding due to liquefaction-induced subsidence in Gölcük (from Izmit Collection, Earthquake Engineering Research Center, University of California, Berkeley).**



**Fig. 2.38 Structural failure due to liquefaction-induced settlement of isolated footing at Port of Taichung (from Collection, Earthquake Engineering Research Center, University of California, Berkeley).**

**(c) Flow Slides**

The development of flow liquefaction can obviously lead to devastating damage. Structures founded in areas involved in deep flow slides can be carried long distances by those slides. Estimation of the forces exerted on pile foundations by flowing soil, for example, is an important contemporary challenge in geotechnical earthquake engineering.

Flow slides can be triggered during or after strong ground shaking. If the ground motion produces high porewater pressure in an area of a slope that is critical to the maintenance of stability, flow liquefaction may be triggered during the earthquake. In some cases, however, the highest porewater pressures are generated in zones that are not critical for stability — for example, under the central portion of an earth dam. Following earthquake shaking, redistribution of excess porewater pressure will cause porewater pressure to decrease in some areas but temporarily increase in others. When the porewater pressure increases, the effective stress decreases and the void ratio increases (due to rebound). This causes the residual strength to decrease. If excess porewater pressures migrate into areas that are critical for stability, a flow slide may be triggered at some period of time after earthquake shaking has ended. The occurrence of delayed flow slides depends on hydraulic as well as dynamic soil properties, and is likely to be strongly influenced by the presence and distribution of layers and seams of fine-grained soils.

Reliable evaluation of the effects of flow liquefaction on structures requires reliable estimation of the residual strength of liquefied soil. Accurate estimation of residual strength has proven to be very challenging. Part of this challenge results from different interpretations of the term residual strength. Yoshimine and Ishihara (1998) provide a useful framework for understanding the mechanics of liquefiable soil behavior, and the different terms used to describe it, when liquefaction is produced by monotonic loading. This framework, shown in Figure 2.39, makes use of the relationship between the initial consolidation line (ICL), the phase transformation line (PTL), and the steady-state line (SSL). Because these curves may not be parallel when plotted in  $e$ - $\log p'$  space, the response of an element of soil may differ depending on void ratio. For Condition (a) in Figure 2.39, the initial point (denoted by the circle symbol) is to the left of the SSL but to the right of the PTL; consequently, that element of soil will initially exhibit contractive behavior but then dilate after reaching the PTL (triangle symbol). Because

the PTL is relatively close to the ICL, dilation begins relatively quickly — before any strain-softening behavior can occur. The dilation occurs until the element of soil reaches the SSL (square symbol). For Condition (b), the initial point (circle) is to the right of the SSL and PTL. As undrained shearing begins, the soil exhibits contractive behavior including strain-softening until the PTL is reached (triangle). The soil then dilates until it reaches the SSL (square) at which point it continues to strain while mobilizing the steady-state shear strength. The element of soil in Condition (c) is to the right of the SSL and PTL, and the SSL and PTL are virtually coincident. In this case, the soil will exhibit highly contractive behavior with strain-softening, and virtually no dilation will occur.

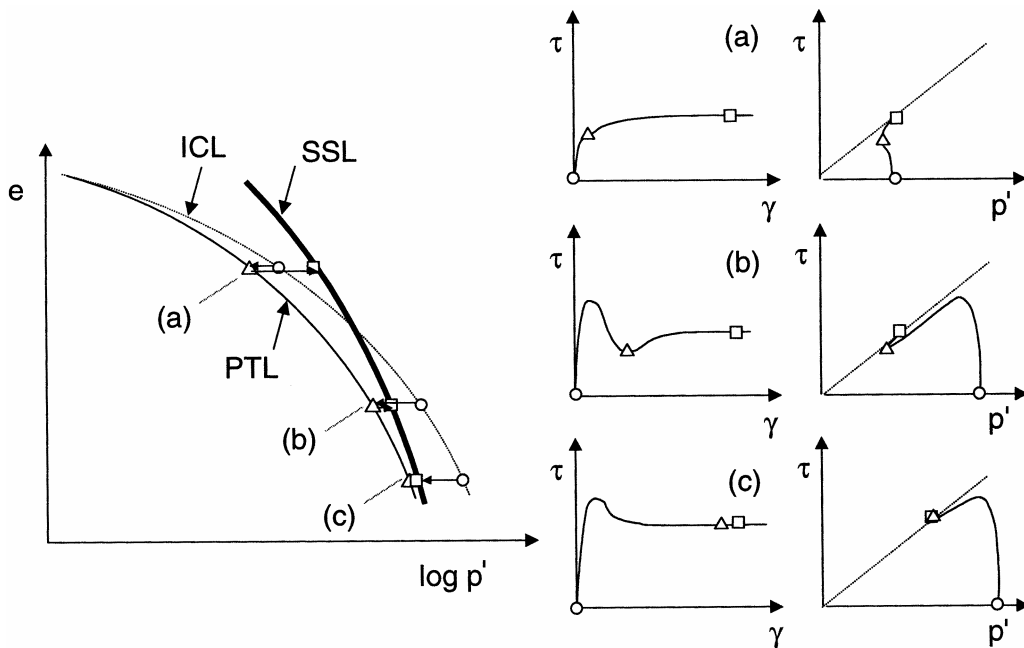


**Fig. 2.39 Schematic illustration of different types of response of liquefiable soils (after Yoshimine and Ishihara, 1998).**

The behavior of soil element (b) in Figure 2.39 bears some examination: it passes through two points at which it is neither contractive nor dilative and at which its shearing resistance is constant (the slope of the stress-strain curve is zero). The first of these points is at the PTL, at which point the soil is in the so-called quasi-steady state (Alarcon-Guzman et al., 1988; Ishihara, 1993); the second is when the soil has reached the steady state. The quasi-steady state is reached at strains that are much lower than those required to reach the steady state, but may still be quite substantial. The question then becomes, What value of the residual strength should be used in design? Is it the available strength at the quasi-steady state or at the steady

state? The answer depends on the performance criteria — if unbounded deformations associated with a full flow slide define unacceptable performance, the steady-state strength would be the most appropriate definition of residual strength; if a moderate level of deformation defines unacceptable performance, it may be more appropriate to use the strength corresponding to the quasi-steady state as the residual strength. Yoshimine and Ishihara (2000) recommend use of the quasi-steady-state strength unless, as in Condition (c) of Figure 2.39, it does not exist (i.e., it is equal to the steady-state strength).

While this framework helps provide a conceptual understanding of the mechanics of liquefiable soils under monotonic loading, its implications for cyclic loading are less clear. Under cyclic, and perhaps under static, loading conditions, the PTL is not unique in  $e\text{-log } p'$  space — it would tend to move to the left (i.e., the effective confining pressure,  $p'$ , will decrease with increasing number of cycles) during cyclic loading. Therefore the quasi-steady-state strength (the residual strength according to Yoshimine and Ishihara) will depend on the stress (and likely strain) history of the soil. These factors point toward the need to model all of these aspects of liquefiable soil behavior for reliable evaluation of the performance of liquefiable soils.

#### **(d) Lateral Spreading**

Lateral spreading occurs when earthquake-induced dynamic shear stresses temporarily exceed the yield strength of a liquefiable soil that is not susceptible to flow liquefaction. Lateral spreading is characterized by lateral deformations that occur during earthquake shaking (and end when earthquake shaking has ended). The displacements may be small or large, depending on the slope of the ground, the density of the soil, and the characteristics of the ground motion.

Lateral spreading can occur in gently sloping areas or in flat areas adjacent to free surfaces. In both cases, static shear stresses that tend to drive displacements in a downslope direction exist. As earthquake-induced stresses produce softening and yielding of the soil, the static shear stresses cause permanent strain to accumulate preferentially in one direction. Because the residual strength exceeds the static shear stress, large flow deformation that could continue after the end of earthquake shaking do not develop. It should be noted, however, that post-earthquake redistribution of porewater pressure may cause rebound that reduces the

available residual strength, particularly in the vicinity of low-permeability layers, and can lead to post-earthquake flow slides.

Lateral spreading can have a severe impact on the performance of structures. Because it occurs so frequently in waterfront areas, it has historically had a profound effect on structures such as bridges and wharves (Figure 2.40) and, consequently, a strong economic impact on transportation systems and ports.



**Fig. 2.40** Examples of the effects of lateral spreading on bridges and wharf structures: (a) Nishinomiya bridge, (b) Port of Kobe wharf.

Several approaches are available for estimation of permanent deformations associated with lateral spreading. The lateral spreading phenomenon is a complex one, and it has proven to be extremely difficult to make accurate *a priori* predictions of permanent deformations using analytical/numerical procedures alone. As a result, currently available procedures are empirically based.

Bartlett and Youd (1992) used a large database of lateral spreading case histories with multiple linear regression analysis to develop empirical equations for ground surface displacement caused by lateral spreading. The database included a series of borehole logs and a series of measured displacement vectors; Bartlett and Youd (1992) used an interpolation procedure to estimate the average soil properties at the location of each displacement vector. By evaluating the statistical significance of a large number of possible source and site parameters, Bartlett and Youd (1992) were able to identify a set of parameters that produced reasonable predictions of ground surface displacement for two types of conditions: sites with gentle,

constant slope (ground slope model) and sites with slopes of limited extent or steep banks (free-face model). Bartlett and Youd (1992) did not explicitly address uncertainty in permanent displacement prediction, but observed that 90% of the observed displacements in their database were within a factor of 2 of the values predicted by their equation. Later, Youd et al. (1999) produced revised equations for predicting ground surface displacements with both the ground slope and free-face models. The equations were revised to correct displacement errors in a portion of the original database, remove several sites judged to have been influenced by boundary effects, add case history data from additional sites and earthquakes, modify the forms of the terms that describe the effects of grain size distribution and source-site distance, and put an upper limit on the fines content value. The revised empirical equations are

Ground slope conditions:

$$\begin{aligned} \log D_H = & -17.614 + 1.581M_w - 1.518 \log R^* - 0.011R + 0.343 \log S & (2.11a) \\ & + 0.547 \log T_{15} + 3.976 \log (100-F_{15}) - 0.923 \log (D50_{15} + 0.1 \text{ mm}) \end{aligned}$$

Free-face conditions:

$$\begin{aligned} \log D_H = & -18.084 + 1.581M_w - 1.518 \log R^* - 0.011R + 0.551 \log W & (2.11b) \\ & + 0.547 \log T_{15} + 3.976 \log (100-F_{15}) - 0.923 \log (D50_{15} + 0.1 \text{ mm}) \end{aligned}$$

where

$M$  = moment magnitude

$R^*$  =  $R + 10^{(0.89M - 5.64)}$

$R$  = horizontal distance (km) from site to seismic energy source

$S$  = ground slope (%)

$W$  = free-face ratio defined as ratio of height of free face to distance from base of slope to point of interest

$T_{15}$  = cumulative thickness (m) of saturated granular soil with  $(N_1)_{60} < 15$

$F_{15}$  = average fines content of material comprising  $T_{15}$

$D50_{15}$  = average mean grain size of material comprising  $T_{15}$

The statistical fit of the revised equations to the improved database was about the same as for the original Bartlett and Youd (1992) model. The manner in which the soil profile is described in the Bartlett and Youd (1992) and Youd et al. (1999) models is of interest, particularly the parameter  $T_{15}$ . By its definition, this parameter produces a discontinuous step in permanent displacement predictions at an  $(N_1)_{60}$  value of 15. In other words, a soil layer with  $(N_1)_{60} = 16$  would be expected to produce very little permanent displacement, while a soil layer with  $(N_1)_{60} = 14$  would be expected to produce permanent displacements as large as a layer with  $(N_1)_{60} = 3$ . In reality, geotechnical engineers would expect a relatively smooth decrease in permanent displacement (all other things being equal) with increasing SPT resistance. Given the spatial variability of  $(N_1)_{60}$  and the uncertainty involved in its measurement, the existence of this discontinuous response can make application of the model difficult.

Rauch (1997) developed a procedure referred to as EPOLLS (Empirical Prediction of Liquefaction-induced Lateral Spreading), which included three complementary components that could be used with different levels of site information. Rauch used essentially the same data as Bartlett and Youd, but grouped nearby displacement vectors into individual slides and computed an average displacement and average soil properties for each slide. The number of boreholes per slide ranged from 0 to 10 with a median and mode of 2. The average permanent displacement,  $D$ , and standard deviation,  $\sigma_D$ , predicted by each of the three models are given by

$$\text{Regional:} \quad D = (D_R - 2.21)^2 + 0.149 \quad \sigma_D = 0.589D \quad (2.12a)$$

$$\text{Site:} \quad D = (D_R + D_S - 2.44)^2 + 0.111 \quad \sigma_D = 0.560D \quad (2.12b)$$

$$\text{Geotechnical:} \quad D = (D_R + D_S + D_G - 2.49)^2 + 0.124 \quad \sigma_D = 0.542D \quad (2.12c)$$

where

$$D_R = (613M_W - 13.9R_f - 2420 a_{\max} - 11.4T_d)/1000$$

$$D_S = (0.526L_{\text{slide}} + 42.3S_{\text{top}} + 31.3H_{\text{face}})/1000$$

$$D_G = (50.6Z_{\text{FSmin}} - 86.1Z_{\text{liq}})/1000$$

$$R_f = \text{shortest horizontal distance (km) to fault rupture}$$

$$M_W = \text{moment magnitude}$$

$$a_{\max} = \text{peak horizontal acceleration (g) at ground surface}$$

- $T_d$  = bracketed duration (sec)  
 $L_{slide}$  = length (m) of slide area from head to toe  
 $S_{top}$  = average slope (%) across the surface of the lateral spread  
 $H_{face}$  = height (m) of free face measured vertically from toe to crest  
 $Z_{FSmin}$  = average depth (m) to minimum factor of safety  
 $Z_{liq}$  = average depth (m) to top of liquefied layer

The regression analyses used to develop these predictive equations unexpectedly produced a negative coefficient for the peak acceleration term in the regional model; the implication of this is that the permanent displacements would decrease with increasing peak ground acceleration. Therefore, the EPOLLS model should be used very carefully for conditions other than those corresponding to the database from which it was developed, particularly for very strong ground motions.

**(e) Foundation Failure**

Liquefaction can cause the failure of foundation systems by a variety of mechanisms. Both shallow and deep foundations can be damaged by soil liquefaction.

Perhaps the most visible of these shallow foundation failure mechanisms is through the loss of bearing capacity associated with loose saturated soils with low residual strength. By this mechanism, the earthquake shaking can trigger flow liquefaction and dramatic bearing failures of the type shown in Figures 2.1 and 2.41.



**Fig. 2.41 Liquefaction-induced bearing capacity failure in Adapazari, Turkey (from Izmit Collection, Earthquake Engineering Research Center, University of California, Berkeley).**

Local failure of shallow foundations can occur through the mechanism of cyclic mobility. In a manner analogous to the accumulation of lateral spreading displacements in sloping ground, the static stresses imposed in the soil beneath a shallow foundation can cause the accumulation of permanent strain in a particular direction. Permanent strains that develop in this manner lead to settlement of the shallow foundation. Such settlement in combination with lateral spreading can be extremely damaging to structures supported on shallow foundations (Figure 2.42).



**Figure 2.42 Damage to Monterey Bay Aquarium Research Institute following 1989 Loma Prieta earthquake.**

Liquefaction can also have a significant impact on pile foundations. As described in Section 2.3.1(a), liquefaction and lateral spreading in Niigata caused failure of pile foundations beneath the NHK building (Figure 2.3) and the Showa bridge (Figure 2.2). Liquefaction-induced failure of deep foundations has been observed in many other earthquakes (e.g., Figure 2.43).



**Fig. 2.43 Pile damage due to lateral spreading in Kobe, Japan (from Izmit Collection, Earthquake Engineering Research Center, University of California, Berkeley).**

## **2.5 SUMMARY**

Liquefaction encompasses a wide range of phenomena that can strongly influence the performance of structures during earthquakes. The behavior of liquefiable soil can be seen in laboratory tests on single elements of soil, in laboratory model tests, and in full-scale field recordings of liquefiable site response. Each of these approaches to the observation of liquefiable soil behavior has its own limitations, but all have proven useful in improving the geotechnical engineering profession's understanding of soil liquefaction. All have been, and will continue to be, used to develop models for the stress-strain behavior of soils.

A number of practical procedures have been developed for evaluation of liquefaction potential. Most of these procedures are deterministic but several probabilistic approaches are available; all show considerable uncertainty in their predictions.

While procedures for evaluation of liquefaction susceptibility and liquefaction potential are well established and verified, procedures for evaluating the effects of liquefaction are less

well established. The primary effects that lead to structural damage are permanent deformation (lateral and vertical). These deformations can be produced by lateral spreading or flow sliding.

Practical, empirical procedures are available for estimation of the ground surface displacements caused by lateral spreading. These procedures have been developed by regressing a large number of potential parameters against a database of observed lateral spreading case histories and retaining the parameters that showed high statistical significance. The resulting relationships are easily used, but imply behavior that is inconsistent with some of the known characteristics of liquefiable soil.

The potential for flow sliding depends on the residual strength of a liquefied soil. Accurate estimation of residual strength has proven to be a difficult challenge, as apparent residual strengths can be produced by different physical mechanisms that occur in different strain ranges and can be sensitive to partial drainage and void redistribution.

The complexity of behavior exhibited by liquefiable soils calls for the development of constitutive models that are capable of representing the most important aspects of their behavior. Such models, when implemented into suitable numerical analysis packages, will allow prediction of the performance of structures founded on or near liquefiable soil deposits.

## **3 Performance-Based Earthquake Engineering**

### **3.1 INTRODUCTION**

PBEE deals with the design, evaluation, and construction of engineered facilities whose performance under both typical and extreme loading responds to the diverse needs and objectives of its owners and users, and of society in general. The implementation of PBEE in practice requires the capability of predicting different levels of performance with sufficient reliability to allow owners and their agents to make decisions based on life-cycle cost considerations rather than solely on construction costs. This chapter describes the basic concepts of PBEE and the effects of soil liquefaction on the performance of civil structures such as buildings and bridges.

### **3.2 PERFORMANCE STATES**

Earthquake-resistant design has historically been carried out using essentially a single performance criterion — that of “life safety.” In other words, structures and facilities have been considered to have performed satisfactorily if they do not directly contribute to loss of life. This life safety performance criterion can be thought of as a socio-economic performance state, i.e., a performance state that describes a performance goal very clearly in social or economic terms. The life-safety performance state is less clear, however, in engineering terms. For most civil structures such as buildings and bridges, it translates to a goal of collapse prevention. Because most loss of life in such structures is caused by structural collapse, the elimination of collapse will generally eliminate loss of life.

Recent earthquakes in the U.S., Japan, and Taiwan have shown that the total economic costs of earthquakes, which go beyond the direct costs of replacing and/or repairing damaged structures to include damage to the contents of structures and economic losses from interruption of business activities, can far exceed expectations. Owners and operators of civil structures and facilities are therefore motivated to consider investing in the achievement of seismic resistance that exceeds the assurance of life safety. The owner of a building may, for example, consider spending more money to assure no structural damage or no interruption of business activities. The owner of an important bridge may desire a performance state corresponding to, say, a maximum closure time of three days; for a bridge that can be bypassed easily by alternative routes, a lower performance state (e.g., closure for three months) may be more appropriate. By comparing the cost of improved seismic resistance with the costs and probabilities of various levels of unsatisfactory performance, rational and objective design and/or hazard remediation decisions can be made.

Ideally, PBEE will develop to a point where a continuous spectrum of socio-economic performance states, each corresponding to some identifiable engineering performance state, can be considered. Because PBEE is in its early stages of development, however, near-term implementations are likely to involve only a small number of performance states.

### **3.3 PBEE FRAMEWORK**

Making quantitative predictions of the performance of structures in earthquakes requires the understanding and integration of a variety of seismological, geotechnical, structural, and socio-economic factors. Therefore, the development of PBEE requires the close cooperation and collaboration of seismologists, geotechnical engineers, structural engineers, economists, and social scientists. It also requires the participation of researchers and practitioners, of designers and constructors, and of owners and regulators.

Earthquake professionals have long recognized the numerous sources of uncertainty inherent in performance prediction. The quantitative characteristics of bedrock motions are uncertain, their modification by geotechnical conditions and soil-structure interaction is uncertain, the response of the structure and its engineering performance is uncertain, and the costs associated with a given level of engineering performance are uncertain.

As a result, PBEE is best carried out within a probabilistic framework. This allows the various sources of uncertainty to be identified, quantified, and objectively considered in a performance evaluation. PEER has developed a probabilistic framework for PBEE that can be expressed in the following equation:

$$\lambda(DV) = \iint G(DV | DM) dG(DM | IM) d\lambda(IM) \quad (3.1)$$

where  $\lambda(DV)$  = mean annual rate of exceedance of  $DV$ ,

$DV$  = decision variable(s) — number of lives lost, dollar cost of repair, or other socio-economic measure of performance (scalar or vector),

$DM$  = damage measure — interstory drift, permanent displacement, crack width, or other engineering measure of performance (scalar or vector), and

$IM$  = intensity measure — quantitative description of ground shaking intensity (scalar or vector)

In this equation,  $G(DV|DM)$  is the probability that the (socio-economic) decision variable(s) exceed given values of the (engineering) damage measures.

Equation 3.1 produces an estimate of the mean annual rate of exceeding some (socio-economic) decision variable(s). Its meaning and use are most easily understood by considering each of its constituent elements, working from right to left.

The quantity,  $\lambda(IM)$ , is the mean annual rate of exceeding an intensity measure,  $IM$ . If we assume that peak rock outcrop acceleration is a useful measure of ground motion, then  $\lambda(PGA)$  describes the mean annual rate at which different  $PGA$  values can be expected to be exceeded. A plot of  $\lambda(PGA)$  vs.  $PGA$  comprises the familiar seismic hazard curve, which is a typical result of a probabilistic seismic hazard analysis. In this form,  $\lambda(IM)$  reflects uncertainties in earthquake size, location, mechanism, and attenuation behavior.

Once the intensity measure is quantified, the next step becomes prediction of performance in engineering terms. The quantity  $dG(DM|IM)$  describes the level of damage associated with a given level of ground motion intensity. To illustrate the influence of

geotechnical factors on performance, it is helpful to break this term down further, i.e., to consider

$$dG(DM | IM) = \iint dG(DM | FM)dG(FM | FF)dG(FF | IM) \quad (3.2)$$

where, again working from right to left,  $dG(FF|IM)$  is the incremental probability of exceeding some free-field soil motion given the rock outcrop motion,  $IM$ ;  $dG(FM|FF)$  is the incremental probability of exceeding some foundation input motion given a particular level of free-field motion; and  $dG(DM|FM)$  is the incremental probability of exceeding an engineering damage measure given some level of foundation input motion. The evaluation of  $dG(FF|IM)$  typically involves performance of a site response analysis. Evaluating  $dG(FM|FF)$  requires a soil-structure interaction analysis, and  $dG(DM|FM)$  requires a structural response analysis.

Finally, the term  $G(DV|DM)$  describes the probability of exceeding some socio-economic decision variable for a given damage measure level. Evaluation of these probabilities may involve detailed economic analysis of seismic damage repair, and of business interruption.

Selection of the actual quantities that comprise  $DV$ ,  $DM$ , and  $IM$  are important for minimizing the eventual uncertainty in  $DV$ . The quantities used to describe  $DV$  must be of a form that can be implemented directly into a decision analysis. The quantities that comprise  $DM$  should be strongly correlated to  $DV$ , i.e., the variance of the distribution  $G(DV|DM)$  should be as low as possible. Finally, the quantities used to describe  $IM$  should have a direct relationship to  $DM$  (the variance of  $dG(DM|IM)$  should be low). Research on the identification of optimum parameter(s) for  $IM$ ,  $DM$ , and  $DV$  is currently under way within the PEER Core Research Program.

### 3.4 GEOTECHNICAL CONSIDERATIONS IN PERFORMANCE PREDICTION

As indicated in Equation 3.2, geotechnical aspects of the prediction of structural performance can be crudely broken into two primary tasks — prediction of free-field response and prediction of soil-structure interaction behavior. Accurate prediction of free-field response is an important part of virtually every performance prediction; soil-structure interaction effects are not

significant for all combinations of geotechnical/structural conditions but can be critical for many important structures.

Integrated evaluation of performance using a method of analysis which treats the geotechnical and structural aspects of a particular problem with equal levels of rigor has long been desired. Models, most commonly implemented in the framework of finite element analysis, are available for geotechnical problems and for structural problems. To date, however, no numerical model for rigorous, integrated analysis of complete soil/structural systems is available. PEER's OpenSees analytical platform, currently under development, will provide earthquake engineers with such a tool.

### **3.4.1 Free-Field Response**

The free-field behavior of a soil deposit is the behavior that would occur in the absence of structures. Free-field behavior can be classified into two types — dynamic response and ground failure. These two types of behavior are distinguished by the development of significant permanent deformations. Ground failure problems involve significant permanent deformations driven by the dynamic stresses induced in the soil by earthquake shaking, and in some cases by changes in soil properties induced by earthquake shaking. Dynamic response problems involve the modification (amplification or de-amplification) of bedrock motions by soil deposits where significant permanent deformations do not occur.

#### **(a) Site Response**

The extent to which a soil deposit will modify the characteristics of the motion of the bedrock below depends on the geometry, stiffness, and damping characteristics of the soil deposit and on the characteristics of the bedrock motion. All soil deposits will amplify certain components of a bedrock motion, and de-amplify others. In general, stiff and/or shallow soil deposits will tend to amplify the higher-frequency components of a bedrock motion; soft and/or deep soil deposits will tend to amplify the lower frequency components. The overall effect of the soil deposit will depend on how closely the fundamental frequency of the soil deposit matches the predominant frequencies of the bedrock motion. When the fundamental frequency (or characteristic site

period) of the soil deposit matches the predominant frequency (or predominant period) of the input motion, strong amplification can occur, particularly when the soil damping is low. Strongly amplified ground motions will induce large forces in structures and lead to poorer performance than would occur in the absence of amplification. Accurate prediction of performance, therefore, requires accurate evaluation of the free-field response of a soil deposit.

### **(b) *Ground Failure***

Ground failure involves the development of significant permanent strains in soil deposits; such strains may be produced by intermittent exceedance of the shear strength of the soil or by earthquake-induced reduction of the available strength of the soil. Ground failure may occur in the free field or in the vicinity of structures. The masses of soil involved in ground failures are usually so large that the presence or absence of a structure may have little effect on the extent to which they occur.

Ground failure can have severe impacts on the performance of structures. Structures located on unstable soil, for example, may be fully capable of resisting the inertial loads induced within them by earthquake shaking, but may be unable to resist the deformations imposed upon them by the movement of one or more supports.

### **3.4.2 Soil-Structure Interaction**

The dynamic response of many structures is influenced by their interaction with the soil that supports them. In these cases, the response of the soil influences the response of the structure and vice versa. Because the soil and the structure are in contact through the foundation, this process is often referred to as soil-foundation-structure interaction (SFSI). SFSI is generally most significant for cases where relatively stiff structures are supported on relatively soft soil conditions. When soft or flexible structures are founded on stiff soils, SFSI effects may be negligible.

There are two primary aspects to SFSI, each of which may or may not be important for a particular case. A complete evaluation of SFSI would involve evaluation of both; ideally, this would be done simultaneously. In certain cases, however, only one of the two need be analyzed,

so methods for their individual consideration have been developed. In other cases, the two effects are evaluated separately and the results combined; this is frequently referred to as a decoupled approach. In this approach, the two effects are evaluated separately and their effects combined. For linear problems, i.e., problems in which both the soil and the structure are assumed to exhibit linear behavior, the results of the decoupled approach can be shown to be equivalent to those of a coupled analysis.

**(a) *Kinematic Soil-Structure Interaction***

The stiffness of a foundation may prevent it from deforming in the same manner as the soil it is in contact with would deform if the foundation was not present. Because of this, the motion of the foundation will not be identical to the free-field motion that would occur in its absence. The motion of the soil will, however, impose stresses on the foundation. The portion of SFSI that results solely from the stiffness (neglecting the mass) of the foundation is referred to as kinematic soil-structure interaction.

Kinematic soil-structure interaction has two effects that can influence the performance of structures. First, it can influence the motion that is transmitted to the structure — the motion at the top of the foundation (at the base of the structure) may have a different amplitude and frequency content than the free-field motion. Kinematic soil-structure interaction may also induce different modes of foundation motion. For example, it may cause rocking as well as translational motion of the base of a structure when the free-field motion would consist of only translatory motion. Second, the forces induced in the foundation by movement of the surrounding soil may be so large as to damage the foundation and, hence, degrade the performance of the structure it supports. Kinematic interaction can be significant for pile foundations in liquefiable soils, particularly at the point where the pile passes through the liquefiable soil and into a much stiffer underlying layer (e.g., Figure 2.3).

**(b) *Inertial Soil-Structure Interaction***

Inertial soil-structure interaction results from the compliance (or flexibility) of the soil surrounding the foundation. As a structure responds dynamically, it imposes forces on the

foundation that supports it. Since the soil beneath the foundation is never completely rigid, it will deform in response to the foundation loading. For a rigid foundation, six components (three translational and three rotational) of motion are possible.

Inertial soil-structure interaction has several significant effects on structural performance. First, the effective natural period of a soil-structure system is longer than the fixed-base natural period of the structure alone. Second, the effective damping ratio of the soil-structure system is higher than that of the structure due to the existence of radiation damping (in addition to hysteretic damping). Third, the forces induced within the structure itself (i.e., due to dynamic distortion of the structure) can be reduced by the occurrence of inertial soil-structure interaction. Finally, the occurrence of inertial soil-structure interaction can increase total displacements, particularly for tall, slender structures for which rocking is important.

Because inertial soil-structure interaction depends on the relative stiffness of the soil and the structure, its evaluation for cases involving liquefiable soils is both important and challenging. Because of phase transformation effects, the stiffness of a liquefiable soil layer can change rapidly and dramatically. Reliable prediction of the performance of structures founded on liquefiable soils, therefore, requires accurate modeling of the influence of liquefaction on both free-field and soil-structure interaction behavior.

A detailed description of SFSI and its effects on the performance of structures is presented in a companion report (Pestana and Martin, 2001).

### **3.5 SUMMARY**

Soil liquefaction clearly can influence the performance of structures in many different and complicated ways. Within the framework of performance-based earthquake engineering adopted by PEER, prediction of the effects of liquefaction on the performance of structures requires the capability to predict the effects of liquefaction on site response, SFSI, and ground failure potential. Furthermore, the uncertainty in those predictions must be characterized.

The reliability of any structural performance prediction will depend on the uncertainties of the data and models upon which that prediction is based. Improvements in this reliability can be achieved by improvements in the models themselves, and in the data used as input to the models. With respect to soil liquefaction problems, this indicates a need to identify *IM* values

that correlate well to liquefaction behavior and to develop models that accurately represent phenomena such as phase transformation and residual strength, which strongly influence performance.

## **4 Contemporary Issues in Liquefaction Modeling**

### **4.1 INTRODUCTION**

Over the past 40 years, tremendous advances have been made in understanding and predicting soil liquefaction. The evaluation of liquefaction hazards is often divided into three components: susceptibility, initiation, and effects. Consideration of advances with respect to each of these components can help identify the most pressing contemporary issues in liquefaction modeling. This chapter presents a brief review of the components of a typical liquefaction hazard evaluation with comments on which aspects the geotechnical engineering profession currently does well, which aspects we do not do particularly well, and what improvements are needed for the advancement of performance-based earthquake engineering.

### **4.2 LIQUEFACTION SUSCEPTIBILITY**

Geotechnical earthquake engineers are now generally able to identify the geologic conditions and types of soils that are susceptible to liquefaction with good confidence. The occurrence of liquefaction in loose clean sands has long been recognized and is well documented with field and laboratory evidence. The occurrence of liquefaction in silty sands is also well established. The occurrence of liquefaction in soils that would be classified as silts is less well established. Coarse silts appear to be fully susceptible to liquefaction and finer-grained silts do not; the borderline between the two conditions is not clear, although the plasticity of the soil is likely to play a significant role.

Liquefaction of gravelly soils has also been observed in the field but with much lower frequency than liquefaction in clean and silty sands. As a result, the conditions under which

gravelly soils are susceptible to liquefaction is not as well established as those for sandy soils. However, loose gravelly soils are encountered much less frequently than loose sandy soils, so this deficiency is not considered critical at this time.

The term “liquefaction” has also been applied to clayey soils, although the use of the term in that context is not universally accepted. It is clear that some sensitive clayey soils can exhibit strain-softening behavior that, when manifested in the field, produces instabilities that share some of the primary characteristics of liquefaction-induced flow slides. The basic mechanism that produces these instabilities in fine-grained soils, however, is much different than that which produces liquefaction of granular soils. For the purposes of this report, liquefaction will be considered to be limited to granular soils.

### **4.3 INITIATION OF LIQUEFACTION**

Soils susceptible to liquefaction do not automatically liquefy during earthquakes — they must be subjected to a ground motion of sufficient intensity to trigger liquefaction. Empirical procedures are currently available to determine the level of shaking required to trigger liquefaction in different types of soils. To date, these procedures have proven to be satisfactory for engineering practice. Geotechnical earthquake engineers are seldom surprised by the occurrence of liquefaction at a site for which the subsurface conditions and ground motions are known. Because current liquefaction evaluation procedures are relatively conservative, and because they contain no information on the uncertainty of their conclusions, it is much more common to be surprised by the non-occurrence of liquefaction at a site for which current procedures would have indicated liquefaction to be likely.

While the current degree of conservatism is not unreasonable for design purposes, and the current procedures have been widely embraced by geotechnical engineering practitioners, they do not fit easily into the framework of performance-based earthquake engineering, in which unbiased estimates of the probability of liquefaction are required. Thus, there is a pressing need for development of procedures for evaluation of new procedures for probabilistic characterization of liquefaction potential. Such a procedure has recently been developed by Seed et al. in a project sponsored by the PEER Lifelines Program (see inset).

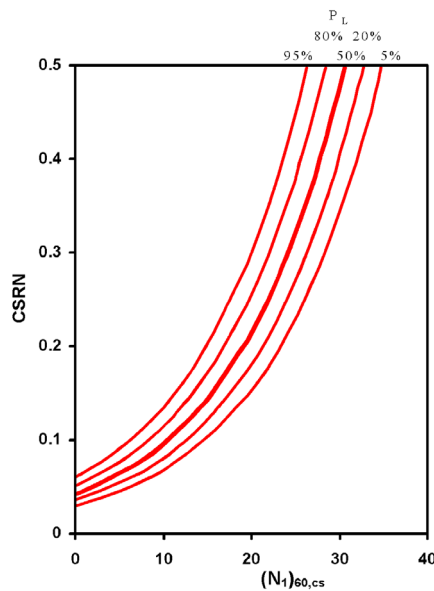
.....

## PEER Lifelines Research Program — Probabilistic Assessment of Liquefaction Potential

Consideration of liquefaction hazards within the PEER framework for performance-based earthquake engineering requires unbiased estimates of the probability of liquefaction. PEER researchers Raymond Seed and Armen Der Kiureghian of UC Berkeley, working with colleagues in Turkey, Japan, and the United States, have developed a probabilistic procedure for evaluation of liquefaction potential.

The new procedure was developed by expanding the database of field liquefaction case histories, using new information on the interpretation of SPT data, considering various factors that influence site-specific ground motions, developing improved procedures for evaluating the depth-dependency of cyclic stress ratio, and considering the quality of the data associated with each case history. A Bayesian updating procedure was used to consider numerous sources of uncertainty and identify relationships for magnitude scaling factor, fines content correction, and overburden stress correction factor that were consistent with the available data.

The results are presented in exactly the form (below) — liquefaction curves showing  $CRR$  vs.  $(N_1)_{60}$  — that geotechnical engineers are currently accustomed to working with. The only difference is that a series of curves, each corresponding to a different probability level, is presented. An expression for explicit calculation of the probability of liquefaction (as a function of  $(N_1)_{60}$ , fines content,  $CSR$ , magnitude, and effective vertical stress) is also presented.



When deterministic analyses are to be performed, the use of the curve for 20% probability of liquefaction is recommended as being consistent with the general level of conservatism inherent in previous liquefaction evaluation procedures.

These procedures represent a major improvement in current, cyclic stress-based procedures for evaluation of liquefaction potential. They are based on a largest database considered to date, they have used the most advanced case history interpretation and analysis techniques used to date, and the most rigorous probabilistic analyses that have been applied to date to liquefaction potential evaluation. The resulting bands of uncertainty are significantly reduced when compared to those of previous procedures for probabilistic liquefaction evaluation. The reduction in uncertainty achieved by this research can be seen by comparing the positions of the contours in the figure below with those of the corresponding contours from the previous probabilistic analyses shown in Figures 2.31 – 2.33.

.....

Empirically-based procedures for liquefaction, whether deterministic or probabilistic, rely on the interpretation of field case history data. This data includes documentation of liquefaction observations, subsurface site conditions, and ground motions. One of the greatest weaknesses in the current empirical database is the high variability in methods of subsurface investigation and the incomplete documentation of the procedures used to obtain subsurface data. The recent earthquakes in Turkey and Taiwan provide excellent opportunities for significant enhancement of the empirical database — not just in terms of increasing the quantity of data, but also the quality of data (see inset).

.....

### **PEER Lifelines Research Program — Liquefaction Site Investigation**

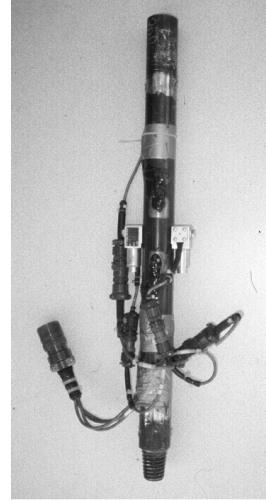
Field observations of soil liquefaction provide the best data with which to calibrate and validate procedures for liquefaction hazard evaluation. As the geotechnical earthquake engineering profession’s understanding of liquefaction has increased, understanding of the care and detail with which liquefaction case histories must be documented has also increased.

Following the 1999 Kocaeli earthquake in Turkey, the PEER Lifelines Program co-sponsored field investigations of liquefaction sites in Adapazari, Turkey. PEER researchers Jonathan Bray (UC Berkeley) and Jonathan Stewart (UCLA) worked with Turkish and other American colleagues to perform subsurface investigations at a number of sites where liquefaction-induced damage to buildings, electrical substations, and other facilities was observed. The primary goal of this work is to develop well-documented case histories of building performance at sites undergoing severe ground failure to advance our understanding of these phenomena and enhance our ability to numerically simulate the associated physical processes. A parallel goal is to provide a

comprehensive record of observed building and ground performance data in Adapazari so that the lessons learned from specific case histories can be generalized.



**Drilling equipment in operation in Adapazari**



**Instrumented segment of drilling rod for continuous measurement of SPT energy**

In Adapazari, PEER researchers are performing SPT and seismic CPT tests at numerous sites. The tests are being conducted using state-of-the-art procedures; documentation of the test procedures as well as test results are available on a webpage that can be accessed through the PEER website.

.....

Liquefaction potential can also be evaluated using a variety of different measures of liquefaction resistance, e.g., SPT resistance, CPT resistance, and shear wave velocity. The empirical nature of the various liquefaction evaluation procedures, combined with the relatively small amounts of data upon which some of the procedures are based, produces situations where different procedures can produce conflicting assessments of liquefaction potential.

Also, current procedures for evaluation of liquefaction potential are based on the cyclic stress approach in which loading and resistance are characterized in terms of cyclic shear stress amplitudes. The effects of frequency content and duration are represented, by proxy, by earthquake magnitude. While this approach has been satisfactory for past practice, there is evidence that cyclic shear stress amplitude is not the best parameter for characterization of liquefaction potential. This suggests that fundamentally improved procedures could be developed; the recent proposition of Arias intensity as an alternative parameter for evaluation of

liquefaction potential (Kayen and Mitchell, 1997) is promising for implementation into performance-based earthquake engineering and deserves further exploration.

#### **4.4 EFFECTS OF LIQUEFACTION**

The performance of structures located in areas with liquefaction-susceptible soil conditions depends on the effects of liquefaction. While the geotechnical engineering profession's ability to evaluate liquefaction susceptibility and the initiation of liquefaction are relatively well-advanced, *a priori* prediction of the effects of liquefaction remains a much more challenging problem.

To advance the profession's capabilities for predicting the effects of soil liquefaction on the performance of structures, several important issues must be addressed. Geotechnical aspects of performance, for surface structures such as buildings, bridges, dams, and embankments, but also for buried structures such as pipelines and foundations, are closely related to the development of permanent deformations. Therefore, improvements in predicting the permanent deformations of liquefiable soils are required for the advancement of performance-based earthquake engineering. These permanent deformations are sensitive to phase transformation behavior and to the residual strength of liquefied soil.

##### **4.4.1 Phase Transformation Behavior**

As previously discussed in detail, the identification of phase transformation behavior has helped improve the geotechnical engineering profession's understanding of the mechanics of soil liquefaction. By explicitly identifying the conditions under which soil exhibits contractive and dilative behavior, constitutive models that incorporate phase transformation behavior can be developed. These models can then be implemented within various numerical analyses to determine the effects of phase transformation behavior on the behavior of soil deposits.

**(a) *Effects on Site Response***

The stiffness of an element of liquefiable soil changes continuously throughout an earthquake. In general, excess porewater pressure builds up during the early stages of the earthquake and effective stresses decrease. As the effective stresses are reduced, the stiffness of the soil is also reduced. As a result, high shear stresses produced by higher-frequency components of a ground motion cannot be transmitted through the softening layer. At the ground surface, acceleration amplitudes tend to decrease and the frequency content of the surface motion tends toward lower frequencies. Equivalent linear site response analyses, which are far and away the most commonly used in practice, cannot account for this softening over the duration of the earthquake. Nonlinear, effective stress-based site response analysis programs such as DESRA and TESS can model the buildup of porewater pressure, but they assume that it increases monotonically. While analyses of the type performed by DESRA and TESS are a step above equivalent linear analyses, the relatively simple cyclic nonlinear soil model they employ do not allow phase transformation effects to be considered. They are capable of modeling many of the most important aspects of liquefaction up to the point of initial liquefaction, but cannot accurately represent the behavior of the soil after initial liquefaction.

The significance of post-liquefaction site response, in terms of its effects on the performance of structures and foundations, has not been carefully investigated to date. Such an investigation would require an integrated program of numerical analysis, model testing, and identification and investigation of pertinent case histories.

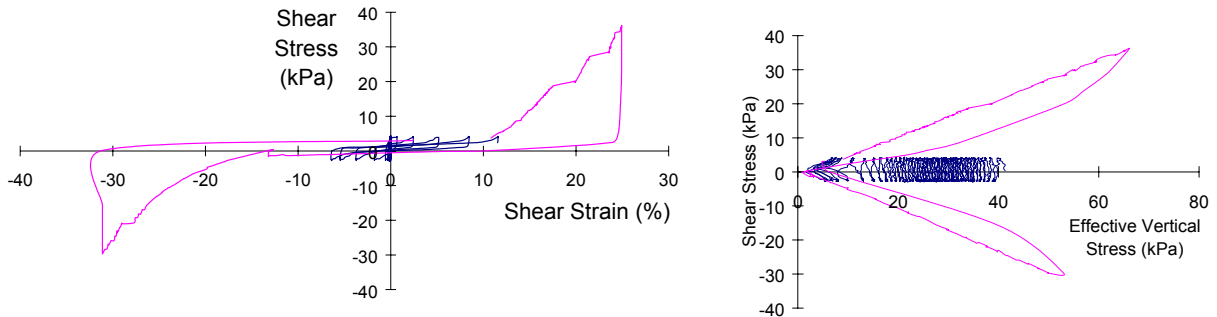
.....

**PEER Core Research Program — Liquefaction Testing**

To better develop additional data on the behavior of sands following initial liquefaction, PEER researchers Raymond Seed and Juan Pestana have overseen an extensive direct simple shear testing program at UC Berkeley. Using the Berkeley bidirectional simple shear apparatus, research assistant Anne Kammerer has investigated the post-liquefaction stress-strain and stress path behavior of liquefied soils.

The tests have focused on the response of the soil after initial liquefaction. Tests have been performed under stress-controlled loading with constant shear stress amplitude. Loading has continued with the application of numerous cycles of loading after initial liquefaction has been reached. The results provide badly needed data on the manner in

which the soil dilates and the rate at which it stiffens in shear. In some of these tests, cyclic loading was stopped with zero shear stress and then followed by monotonic loading to relatively large strains (below).



These tests show that, although the post-liquefaction stiffness of the soil is very low when shear stresses are low, the application of greater shear stresses leads to dilation and significant stiffening. In the figure shown above, the stiffening continues with no sign of abatement to shear strains of some 30%, which represents the limit of the testing apparatus.

This testing program is continuing under the auspices of the PEER Core Research Program. Test results are posted to a website that can be accessed through the home page of the PEER website.

.....

**(b) *Effects on Ground Failure***

Ground failure, as indicated previously, refers to situations in which permanent deformations develop in the soil. These deformations can be divided into two categories — lateral permanent deformations and vertical permanent deformations. Permanent lateral deformations can result from flow slides and from lateral spreading. Permanent vertical deformation refers to the settlement that results from reconsolidation of liquefied or partially liquefied soil.

Phase transformation behavior has a significant, if not controlling, influence on some of the most important aspects of liquefaction-induced ground failure. Lateral spreading is by far the most common form of liquefaction-induced ground failure; flow sliding can also occur but does so much less commonly than lateral spreading.

Estimation of the permanent deformations caused by lateral spreading is an important and challenging problem in contemporary geotechnical earthquake engineering. Current procedures for estimation of lateral spreading displacements are purely empirical. They are based on the results of regression analyses that identified the parameters that lateral spreading displacements were statistically significant for and determined the coefficients of a regression equation that maximized the coefficient of determination ( $R^2$ ). Neither the form of the equation or the coefficients were constrained by the physics of the lateral spreading problem. It would seem that improved results could likely be obtained by developing a regression equation that reflects the basic mechanics of lateral spreading and that, if this was done, one would have an equation that was more likely to be consistent with new lateral spreading data than the current, purely regression-based equation.

.....

**PEER Lifelines Research Program — Lateral Spreading Prediction**

To develop a probabilistic procedure for estimation of ground surface displacements due to lateral spreading, PEER researcher J. P. Bardet is developing a GIS-based database of lateral spreading case histories. The database was divided into two data sets: one that consisted of all data, and one that consisted of the data corresponding to ground surface displacements less than 2 m. The second data set was considered to be more applicable to typical engineering design situations. The data sets were further subdivided into ground slope and free-face subsets.

Bardet et al. (1999), recognizing that reliable information on fines content and mean grain size was often sparse or missing from case history data, developed two different regression models for each data set: a six-parameter model of the same form used by Bartlett and Youd (1992) and a four-parameter model identical to the six-parameter model except for elimination of the fines content and mean grain size terms. The parameters for each model were determined by multiple linear regression.

The six-parameter models, which can be used when grain size information is available, provide a better match to the observed displacements than the four-parameter models. The relationship developed considering both free-face and ground slope data is

$$\begin{aligned} \log(D_H + 0.01) = & -13.522 + 1.050M - 0.778 \log R - 0.013R + 0.370 \log W_{ff} \\ & + 0.106 \log S_{gs} + 0.270 \log T_{15} + 3.481 \log(100 - F_{15}) \\ & - 0.715 D50_{15} \end{aligned}$$

For ground slope conditions, improved accuracy can be obtained from

$$\log (D_H + 0.01) = -14.212 + 0.800M - 1.198 \log R - 0.006R + 0.071 \log S \\ + 0.373 \log T_{15} + 5.090 \log (100 - F_{15}) - 0.704 D50_{15}$$

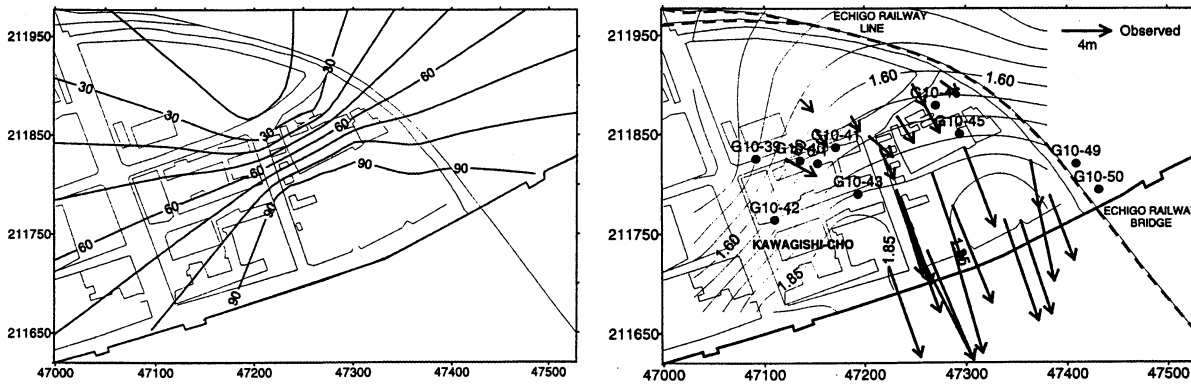
The four-parameter models are recommended for use when grain size information is not available. The relationship based on both free-face and ground slope data is

$$\log (D_H + 0.01) = -6.909 + 1.001M - 0.289 \log R - 0.021R + 0.090 \log W_{ff} \\ + 0.203 \log S_{gs} + 0.289 \log T_{15}$$

For ground slope conditions, improved accuracy can be obtained from

$$\log (D_H + 0.01) = -8.410 + 1.239M - 0.358 \log R - 0.024R + 0.266 \log S \\ + 0.373 \log T_{15}$$

Bardet et al. (1999) also developed a procedure for computing the probability of exceeding some level of permanent displacement. An example of its application, for an observed lateral spread from the 1964 Niigata earthquake, is shown below. The Bardet et al. (1999) procedure was used, along with subsurface data from that site, to compute contours of the probability of exceeding 2 m permanent displacement (below, left). The actual measured displacements (below, right) are consistent with the probability contours.



Lateral spreading displacements are currently predicted only at the ground surface. The variation of lateral spreading displacements with depth can also be important, particularly when deep foundations are involved. Development of procedures for prediction of lateral spreading displacement profiles are needed.

The extent to which lateral spreading deformation occurs in the field depends on the rate at which the elements of soil within a slope stiffen as the soil dilates at high stress ratios.

Currently, little data are available to indicate exactly how this stiffening takes place, and to indicate the factors that control the rate of stiffening. While some laboratory data have been generated in element tests, much more is needed. The questions of how stiffening proceeds, how it is influenced by effective confining pressure, grain size distribution, grain shape, fines content, fines plasticity, and stress/strain history are all potentially significant and should be investigated by programs of laboratory element and model testing (see inset). The goal of this work would be to fully characterize phase transformation behavior so that it could be better represented in constitutive models. These models would then be implemented into analytical platforms like OpenSees to allow improved prediction of the performance of structures in liquefiable soils.

#### **4.4.2 Pore-Pressure Redistribution**

Soil liquefaction involves the generation, redistribution, and eventual dissipation of excess porewater pressure. The role of porewater pressure generation in the softening and weakening of liquefiable soils has long been appreciated by geotechnical engineers. Similarly, the role of pore-pressure dissipation and coincident soil reconsolidation in producing post-liquefaction ground settlement has also been recognized. The role of porewater redistribution, however, has not received as much attention.

Early theoretical work on the mechanism of sand boils (Housner, 1958; Ambraseys and Sarma, 1969; Scott and Zuckerman, 1972; and NRC, 1985) attributed the formation of sand boils to inhomogeneity in permeability near the ground surface. Many natural and man-made liquefiable sand deposits contain finer, more impervious silty or clayey layers (a typical example is soil strata generated by hydraulic filling (Seed, 1987)). During and after earthquake shaking, upward porewater flow driven by the hydraulic gradients induced by excess porewater pressure generation will cause the effective stress to decrease in the upper portion of the sand deposit. Dilation of the sand due to reduced effective stresses and the mechanical behavior of the soil can reduce the residual strength of the sand to a value less than or equal to that required to maintain static equilibrium, thereby triggering flow liquefaction after earthquake shaking has ended (Boulanger and Truman, 1996). In the extreme case, liquefaction-induced void-ratio redistribution may result in a water-rich seam entrapped underneath a relatively impervious interface. Several researchers, (e.g., Scott and Zuckerman, 1972; Liu and Qiao, 1984; Elgamal et

al., 1989; Adalier, 1992) observed water interlayer formation along the boundary of lower coarser and upper finer layers in small-scale tests of stratified deposits. In these studies, the occurrence of sand boils was also reported. Recently, Kokusho (1999) (Figure 4.1) and Kokusho et al. (1999) conducted 1D and 2D liquefaction shaking table tests to demonstrate the evolution of a water film trapped below a silt seam, and its key role in dictating the time of occurrence and extent of lateral deformation in sloping ground. In a 2D embankment test, the portion of the embankment above the water interlayer started to slide several seconds after the shaking event, resulting in a (delayed) flow failure.

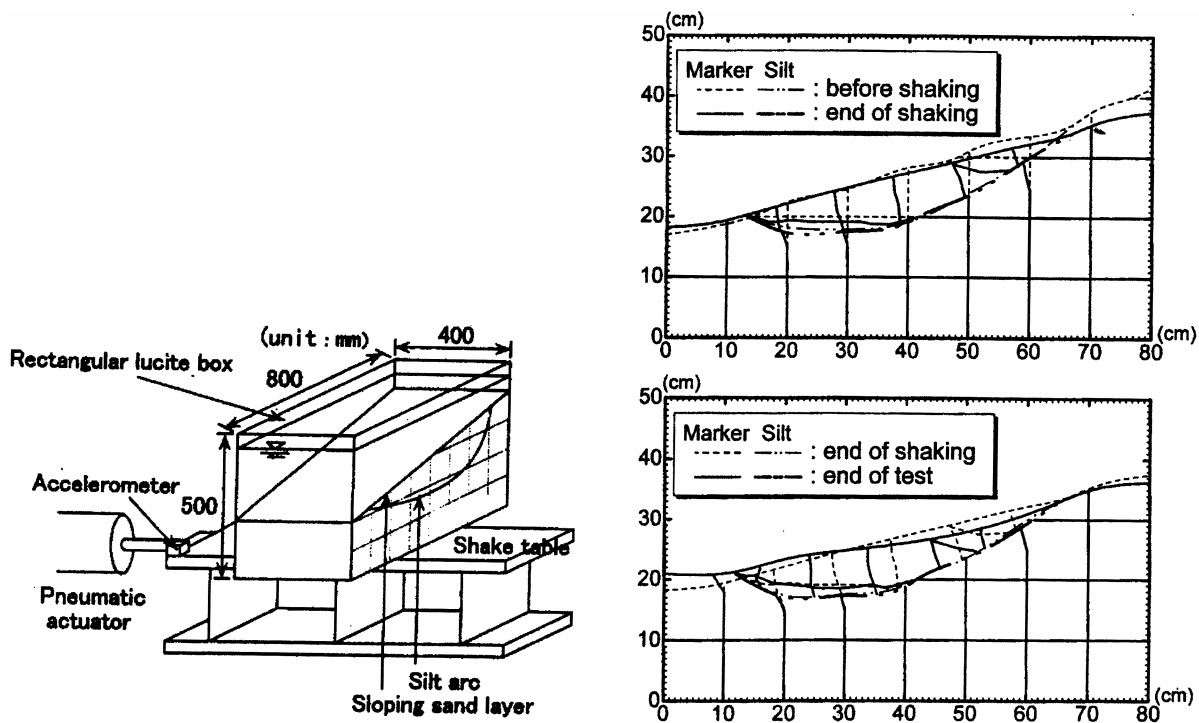


Fig. 4.1 Schematic illustration of apparatus and results of shaking table tests on saturated sand with silt layer (after Kokusho, 1999).

(a) *Effects on Site Response*

Because porewater redistribution requires some period of time, its effects on site response are likely to be minimal. However, the redistribution of porewater in a main shock could have some influence on the response in an aftershock that occurred shortly thereafter. Altogether, the effects of pore-pressure redistribution on the ground motions that are transmitted to a structure are likely to be small.

**(b) *Effects on Ground Failure***

Pore-pressure redistribution is being increasingly recognized as having a significant influence on ground failure. Field and laboratory evidence suggest that pore-pressure redistribution does occur following strong ground shaking and can lead to permanent deformations that occur after earthquake shaking has ended. This type of failure leads to some ambiguity in the classification of liquefaction-induced ground failures.

Evaluation of the effects of pore-pressure redistribution on the performance of structures is really in its infancy, and a number of factors require investigation before reliable procedures for consideration of pore-pressure redistribution can be developed. Consideration of pore-pressure redistribution requires simultaneous solution of nonlinear diffusion and wave equations. This can be accomplished by casting the governing equations in the form of Biot (1956a,b) in which the hydraulic and mechanical components of the response are fully coupled. Fully coupled solutions have been developed, but their use to date has largely been limited to the research arena.

In view of the potential for a water-interlayer formation underneath an impervious layer, Seed (1987) pointed out the difficulty in obtaining reliable estimates of residual shear strength based on laboratory sample tests. Thereafter, a number of centrifuge model tests were conducted to investigate the effect of permeability variation in liquefiable strata, including Arulanandan et al. (1988); Arulanandan and Scott (1993, 1994); Fiegel and Kutter (1994); Zeng and Arulanandan (1995); Balakrishnan et al. (1997); and Balakrishnan and Kutter (1999). Most of these experiments employed clean liquefiable sand profiles overlain by a clay/silt layer. The above experimental studies are generally motivated by relevant case histories such as the San Fernando Dam (Seed et al. 1975, 1989; Davis and Bardet 1996), and observed effects of liquefaction on slopes and bridge foundations (Berrill et al. 1997; Boukouvalas et al. 1999).

Development of analytical procedures for consideration of pore-pressure redistribution, however, may be the easier half of the problem. Because porewater tends to accumulate in the vicinity of permeability gradients, the three-dimensional permeability field must be known to accurately evaluate pore-pressure redistribution effects. Research into the effects of pore-pressure redistribution on performance should be undertaken to determine the level of permeability gradient that is required to produce significant effects on performance; once that is

known, identification of practical procedures for evaluation of the in situ permeability field can be undertaken.

#### **4.4.3 Residual Strength**

Estimation of residual strength is one of the most difficult tasks currently faced by geotechnical earthquake engineers.

Two basic approaches for the estimation of residual strength have developed over the years, one based on laboratory testing and one based on back-calculation from flow slide case histories. Currently, a very high level of uncertainty is associated with each of these residual-strength prediction approaches.

##### ***(a) Laboratory Testing Approach***

An approach to estimation of residual strength based on careful sampling and subsequent laboratory testing was proposed by Poulos et al. (1985). In this approach, undisturbed samples are obtained by careful piston sampling or, if possible, by freezing and coring. The in situ void ratio is determined and the specimens are then consolidated to higher effective confining pressures (to ensure contractive behavior) and sheared monotonically under undrained conditions. A series of triaxial tests on reconstituted specimens is then performed to determine the slope of the steady-state line. This slope is then used to correct the measured steady-state strength for the undisturbed specimen back to the in situ void ratio.

This procedure suffers from the practical difficulty of accurately measuring the in situ void ratio, and from the high sensitivity of steady-state strength to void ratio. The very tendency of liquefiable soils to change in volume when sheared also makes undisturbed sampling extremely difficult — the insertion of even a thin-walled sampler into such a soil will cause the soil to densify somewhat. Because steady-state lines are generally quite flat, even a small degree of densification can lead to a large increase in the perceived value of steady-state strength. These practical difficulties lead to significant uncertainty in the values of residual strength obtained by the laboratory testing approach.

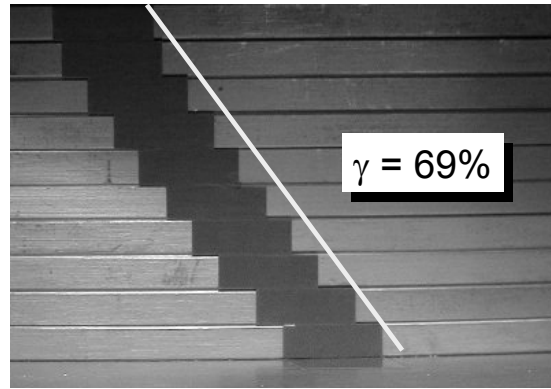
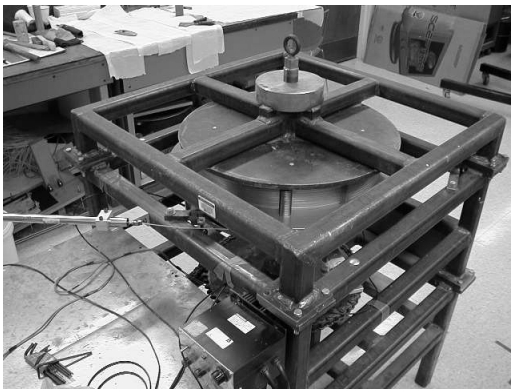
Nevertheless, laboratory testing offers the opportunity to better understand the mobilization of residual strength, and to identify the factors that control it. Though it may not allow the true steady state of deformation to be reached, triaxial testing has shown that grain size distribution tends to change the slope of the steady-state line and particle shape tends to change its position. New testing devices may be capable of reaching the steady state of deformation and providing new insights into the factors that influence residual strength (see inset).

.....

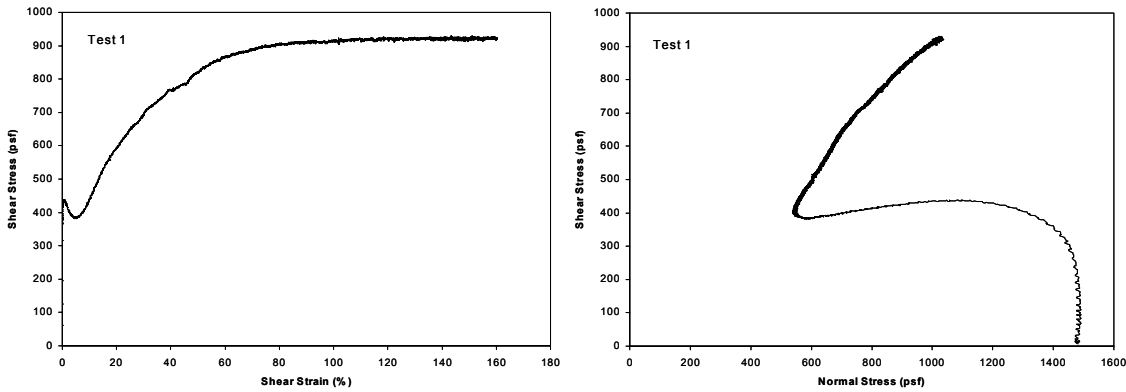
### **PEER Core Research Program — Residual-Strength Testing**

A laboratory investigation of the residual shear strength of liquefied soil is being undertaken using a new testing device at the University of Washington. PEER researchers Steven Kramer and research assistant, C. H. Wang are using the new Ring Simple Shear Device (RSSD) to test sands at high shear strains under uniform stress and strain conditions. The RSSD is capable of shear strains exceeding 100%.

The RSSD combines elements of the ring shear and simple shear testing systems. By placing a soil specimen in the annular space between two sets of stacked rings (below), applying a normal stress to the top of the soil specimen, and then applying torsion to the top of the specimen, the soil can be sheared to high strain levels. The rings



are ground, polished, and lubricated, so they provide negligible resistance to torsion. The relative movement of the rings indicates the level of strain in the soil within the test specimen. Stress-strain and stress path curves for an RSSD test are shown below. Note the existence of both the quasi-steady state (strength  $\sim 380$  kPa) and the steady state (strength  $\sim 920$  kPa), the difference between the two, and the strain levels at which each are mobilized.



The RSSD is being used in an extensive testing program to evaluate the influence of various factors such as grain size distribution, particle size, particle shape, etc., on the residual strength of liquefiable soils.

.....

**(b) Back-Calculation Approach**

Recognizing the practical difficulties associated with the laboratory testing approach, Seed (1986) proposed an alternative approach based on back-calculation of the apparent residual strength from actual flow slide case histories. This procedure involved the interpretation of published or unpublished flow slide case histories.

For a typical case history, the geometry of the failure surface must be determined, typically by examining the pre-failure and post-failure slope geometries. This step typically involves a considerable degree of subjective interpretation, as the deformations may be large, may reflect an unknown degree of progressive failure (i.e., the final geometry may not be the result of a single failure), and the mechanism of deformation may not be apparent. Furthermore, the final geometry may be significantly influenced by inertial forces that develop during the failure — a liquefied slope may have some non-zero velocity at the point at which its changed geometry has reduced the driving shear stresses to the actual residual strengths; those velocities will produce additional deformations that do not reflect the residual strength of the soil.

Once the geometry of the overall failure surface has been determined, the spatial extent of the portion of the failure surface that extends through the liquefied soil layer(s) must be

identified. This determination also involves subjective interpretation with information that is frequently quite sparse.

The properties of the non-liquefied soil along the failure surface must be determined from available information, which is rarely plentiful and often deficient. Then, a series of static, limit equilibrium slope stability analyses are performed with a different undrained strength being assigned to the liquefied zone for each analysis. The limit equilibrium analyses require specification of the slope geometry. Such analyses have been performed using the pre-failure geometry, which clearly provides an upper bound to the residual strength. They have also been performed using the post-failure geometry, which, due to inertial effects, will produce a lower bound residual strength. Other analyses (e.g., Stark et al., 2000) have attempted to correct for inertial effects. The results of the limit equilibrium analyses are used to determine the value of undrained strength that gives  $FS = 1.0$ . This value is taken as the residual strength of the soil involved in that case history.

In the back-calculation approach, a single value of  $(N_1)_{60}$  is assigned to each case history. Assignment of this value also requires considerable interpretation; the question of whether to use the average, lower bound, or some other value of the  $(N_1)_{60}$  values from the liquefied zone remains open.

The paucity of data and considerable degree of interpretation required to perform back-calculation analyses of case histories lead to significant uncertainties in residual strength. Quantification of these uncertainties would allow probabilistic estimation of residual strength.

## **4.5 SUMMARY**

A number of contemporary issues need to be addressed for improved performance evaluation of structures located in areas near or underlain by liquefiable soils. These issues are associated with the problems of liquefaction susceptibility, initiation, and effects.

While more field and laboratory data on the liquefaction susceptibility of silts and gravelly soils would be useful, the general problem of liquefaction susceptibility does not appear to be critical for the immediate development of performance-based earthquake engineering.

Practical procedures for evaluating the potential for initiation of liquefaction are available, are verified by field experience, and are widely used in practice. Nevertheless,

evaluation of liquefaction potential in the framework of performance-based earthquake engineering requires unbiased estimates of the probability of liquefaction. The most commonly used procedures for liquefaction potential evaluation are deterministic and contain an unknown degree of conservatism. Available probabilistic procedures indicate very high levels of uncertainty in liquefaction resistance.

Well-validated, physically reasonable, practical procedures for probabilistic evaluation of the major effects of liquefaction are not currently available. The development of procedures which are consistent with the known mechanics of liquefiable soil is needed. Such procedures should be capable of unbiased predictions of the probabilities of achieving different levels of geotechnical performance.

# 5 State-of-the-Art Approaches to Liquefaction Modeling

## 5.1 INTRODUCTION

The preceding chapters have shown that reliable prediction of structural performance requires the development of models capable of predicting the mechanical and hydraulic behavior of liquefiable soils. Within PEER, a number of soil constitutive models (UC Berkeley, UC Davis, UC San Diego, and U. Washington) are currently under development (and/or refinement) for liquefaction analysis. During this development process, emphasis has been placed on accurate modeling of liquefaction-induced shear deformation (lateral spreading) and settlement. In this chapter, the UC San Diego model is used as an example to present: (1) a number of fundamental issues and challenges associated with numerical modeling of liquefaction, (2) a strong and long-term collaborative effort among the PEER researchers in experimental and computational modeling of liquefaction, and (3) accomplishments in liquefaction modeling during the early years of the PEER research program.

In addition to the above, a section is included to describe a number of noteworthy recent developments by the UC Davis research team and co-workers. These important developments define a more general analytical framework for incorporating both flow liquefaction and cyclic mobility responses, as well as material and stress-induced anisotropy. Finally, a summary of some new trends in observation (shear banding) and modeling (micromechanics, fluid mechanics) of soil pre- and post- liquefaction behavior is also presented. Advances in these areas not only provide us with insights, but also help define further research needs (from the practical application point of view).

## 5.2 DESIRABLE FEATURES IN A LIQUEFACTION SOIL MODEL

Soils exhibit a wide range of complex response characteristics when subjected to arbitrary loading. Among the most salient features are nonlinear stress-strain response, shear-volume coupling, and dependence of material properties on effective confinement and loading direction. All these phenomena may have a significant influence on the triggering and subsequent evolution of soil liquefaction. Therefore, a realistic liquefaction soil model should account for these important response characteristics. In addition, the potentially large post-liquefaction shear and volume deformations should be simulated.

Specifically, desirable features in a liquefaction soil model include

1. *Nonlinearity in shear stress-strain response.* Typically, under drained monotonic loading, as the shear strain continuously increases, the material tangent shear modulus gradually decreases and eventually approaches zero. Such a shear stress-strain curve is known as the *back-bone* curve (Kramer, 1996). This curve is often described mathematically by a hyperbolic function such as the two-parameter Kondner model or the four-parameter Ramberg-Osgood model (Ishihara, 1996).
2. *Hysteresis response under cyclic loading.* Soil exhibits hysteresis in stress-strain response (shear and volume), when subjected to cyclic loading. For the shear components (drained loading), this response characteristic may be approximated by a Masing-type rule (Kramer, 1996).
3. *Dependence of low-strain shear modulus and shear strength (friction angle) on effective confinement.* Dependence of shear modulus on the effective confinement is usually described in terms of a power law (with the power coefficient taken as 0.5 in most cases; Ishihara, 1996). Friction angle is found to be larger at low confinement levels, and decreases with increased confinement (Lambe and Whitman, 1969; Sture, 1999).
4. *Dependence of shear strength on Lode angle.* It is well known that soil shear strength is a function of the Lode angle (e.g., Lade and Duncan, 1973). For instance, shear strength in triaxial extension may be significantly lower than that in triaxial compression. Accounting for the Lode angle effect is particularly important in multi-directional loading situations (Peric and Ayari, 2000).

5. *Densification/consolidation of soil skeleton and associated excess pore-pressure buildup due to shear loading.* Accurate quantification of this response is essential, as the rate of densification often dictates the susceptibility to, and the triggering of liquefaction.
6. *Dilation of soil skeleton and associated increase in effective confining pressure at large shear strain excursions.* This dilation is important in that it may provide substantial instantaneous shear strength and limit the extent of shear strain during liquefaction (cyclic-mobility). A dilative excursion may also increase the rate of densification (or pore-pressure buildup) in the subsequent loading cycle (Nemat-Nasser and Tobita, 1982).
7. *Attainment of critical void ratio state (or critical state) where shearing progresses with minimal change in volume (drained) or pore-pressure (undrained).* Flow liquefaction may ensue when the available shear strength at the critical state is insufficient to resist the acting static shear load.
8. *Accumulation of cyclic shear strain under “downslope” shearing conditions (e.g., near foundations or slopes, behind and below retaining structures).* Satisfactory modeling of this response is essential for realistic prediction of liquefaction-induced deformations.
9. *Development of potentially large post-liquefaction volume reduction due to sedimentation (densification and re-consolidation).* Such volume reduction may be reach 5% or more for very loose soils and extremely strong shaking events (Kramer, 1996).

The last four points are directly related to the liquefaction process, and are among the most challenging tasks. In addition, the overall computational analysis framework (e.g., finite element formulation) should allow for coupling between the soil solid and fluid phases (effective-stress analysis), with pore fluid redistribution capability.

### **5.2.1 Practical Calibration Procedure**

Given the complexity of liquefaction response phenomena, it is not surprising that most numerical simulation models involve a large number of parameters (typically 10 to 20). Therefore, relatively simple and effective model calibration procedures are essential in order for these models to be of any practical use. One approach of general applicability is to calibrate model parameters based only on information that is easily available to the practitioners. For instance, this information can be based on: (1) SPT blow counts and/or CPT values, (2) ranges of

relative density (or void ratio), (3) ranges of plasticity index, and (4) estimates of soil permeability (e.g., gravel, sand, silt, or clay permeability ranges).

### **5.3 LIQUEFACTION MODELS**

#### **5.3.1 Available Liquefaction Models**

A number of constitutive models have been developed to simulate soil response during liquefaction (e.g., Prevost, 1985; Pastor and Zienkiewicz, 1986; Matsuoka and Sakakibara, 1987; Wang et al., 1990; Nishi and Kanatani, 1990; Iai, 1991; Muraleetharan, 1993a, b; Muraleetharan et al., 1994; Anandarajah, 1993; Aubry et al., 1993; Bardet et al., 1993; Dafalias, 1994; Dafalias and Manzari 1999; Byrne and McIntyre, 1994; Proubet, 1991; Li, 1990, 1993, 1997; Li and Dafalias 2000; Kimura et al., 1993; Tobita and Yoshida, 1995; Manzari, 1996; Manzari and Dafalias, 1997; Lade and Yamamuro, 1999; Borja et al. 1999a, b; Kramer and Arduino, 1999; Arduino et al. 2001). Many essential features of cyclic mobility have been satisfactorily modeled by Iai (1991, 1998, Figure 5.1), Dafalias and Manzari (1999), Kramer and Arduino (1999), and Li et al. (2000).

Currently, few reported results show the performance of available constitutive models for the important situations of a superposed driving shear stress (e.g., below foundations, lateral spreading, retaining quay walls, embankment slopes, etc.). These situations necessitate a high degree of control over the accumulated cycle-by-cycle shear deformations (Figure 5.2), as depicted in Figure 5.3. Currently, similar reliable constitutive models are needed for use in predictive computational simulations.

Stress-strain

Stress path

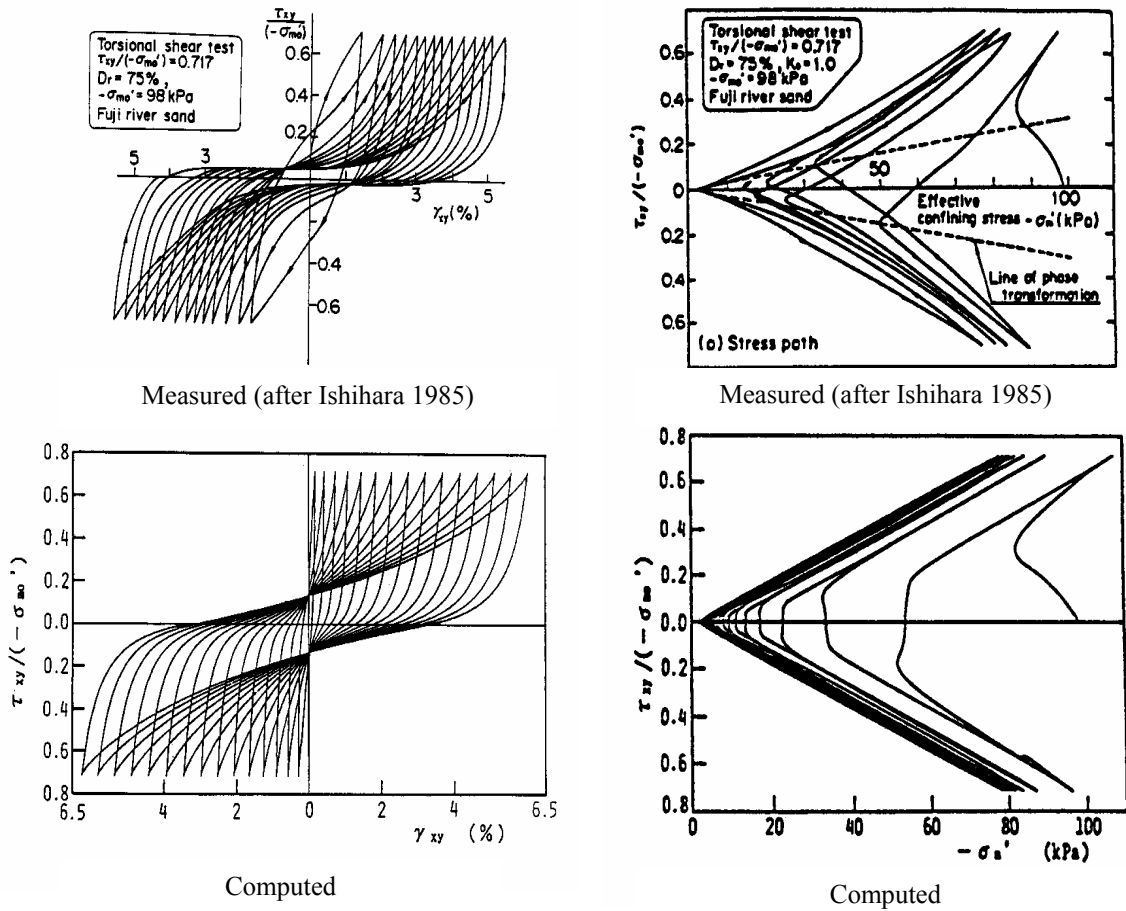


Fig. 5.1 Measured and numerically simulated shear behavior of Fuji River Sand (Ishihara, 1985; Iai, 1991).

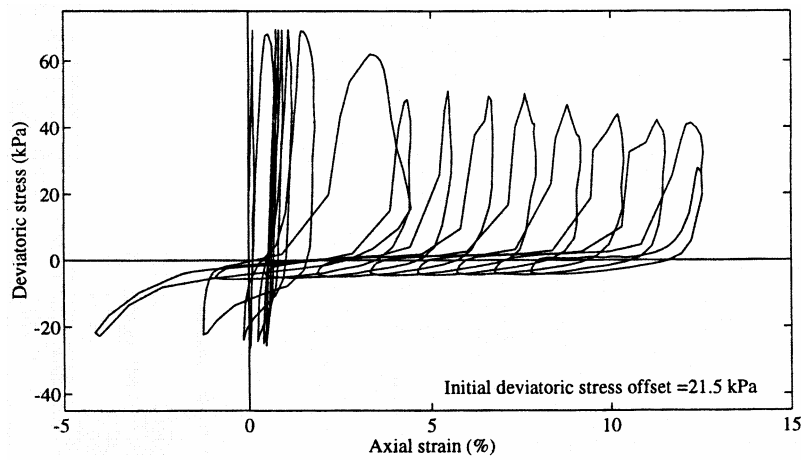


Fig. 5.2 Stress-strain and excess pore-pressure histories during an undrained, anisotropically consolidated cyclic triaxial test of Nevada Sand at  $D_r=40\%$  (Arulmoli et al., 1992).

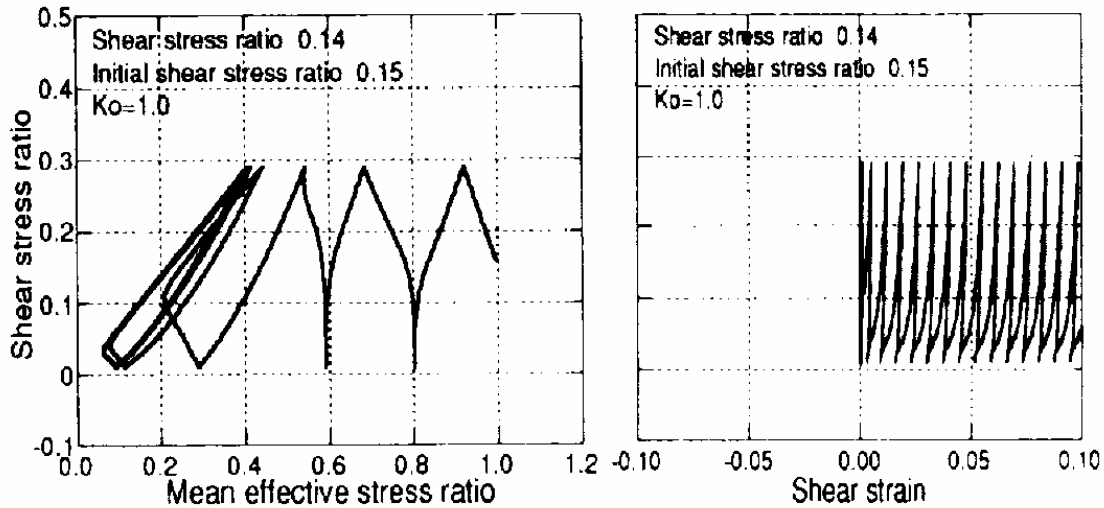


Fig. 5.3 Computed simulation of undrained torsional shear-test response (Tateishi et al., 1995).

### 5.3.2 UCSD Model Description

In the UCSD liquefaction model, emphasis is placed on controlling the magnitude of cycle-by-cycle permanent shear-strain accumulation in clean medium-dense cohesionless soils (Parra, 1996; Yang, 2000). Specifically, the experimentally observed accumulation of permanent shear strain (e.g., Arulmoli et al., 1992, Figure 5.2) was modeled by using strain-space parameters (Yang, 2000), within a multi-surface stress-space model (Prevost, 1985). Furthermore, appropriate loading-unloading flow rules were devised to reproduce the observed strong dilation tendency (Figure 5.2), which results in increased cyclic shear stiffness and strength (Parra, 1996). The main components of this model are summarized below.

#### (a) Yield Function

Following the classical plasticity convention (Hill, 1950), it is assumed that material elasticity is linear and isotropic, and that nonlinearity and anisotropy result from plasticity. The selected yield function (Prevost, 1985; 1989; Lacy, 1986) forms a conical surface in stress space with its apex at  $p_0$  along the hydrostatic axis (Figure 5.4). In the context of multi-surface plasticity (Iwan, 1967; Mroz, 1967; Prevost, 1985), a number of similar yield surfaces with the common

apex  $p_0$  and different sizes form the hardening zone (Figure 5.4). The outmost surface is the envelope of peak shear strength (failure surface). Each surface is associated with a constant stiffness (elastoplastic modulus), and the stiffness value typically decreases with the surface size. Note that the Lode angle effect can be partially accounted for by positioning the failure surface center on a line other than the hydrostatic axis (Figure 5.4).

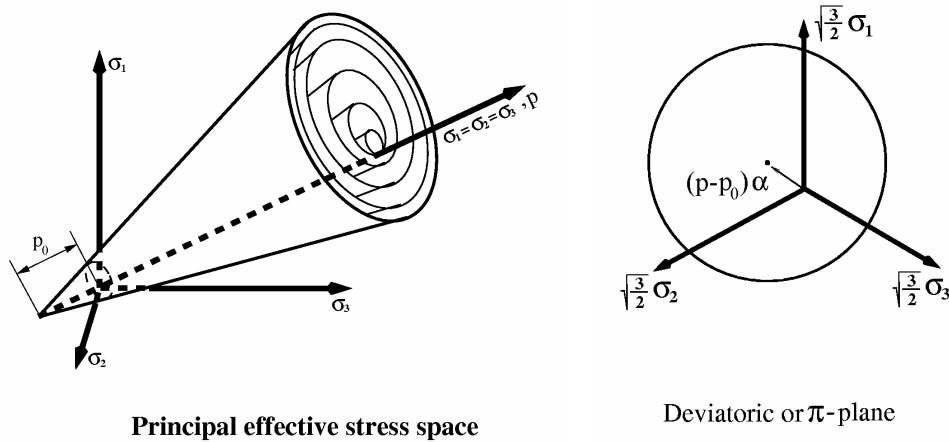


**Fig. 5.4 Conical yield surface in principal stress space and deviatoric plane (after Prevost, 1985; Lacy, 1986; Parra, 1996; and Yang, 2000).**

**(b) Hardening Rule**

A purely deviatoric kinematic hardening rule (Prevost, 1985) is employed in order to generate soil hysteretic response under cyclic loading. This kinematic rule dictates that all yield surfaces may translate in stress space within the failure envelope (Parra, 1996; Yang, 2000).

When subjected to drained monotonic shear loading, this hardening rule generates a piecewise-linear, gradually softening back-bone shear stress-strain curve (Figure 5.5). Therefore, the sizes and elastoplastic moduli associated with all yield surfaces can be calibrated by numerically matching experimental shear stress-strain data (see model calibration below).

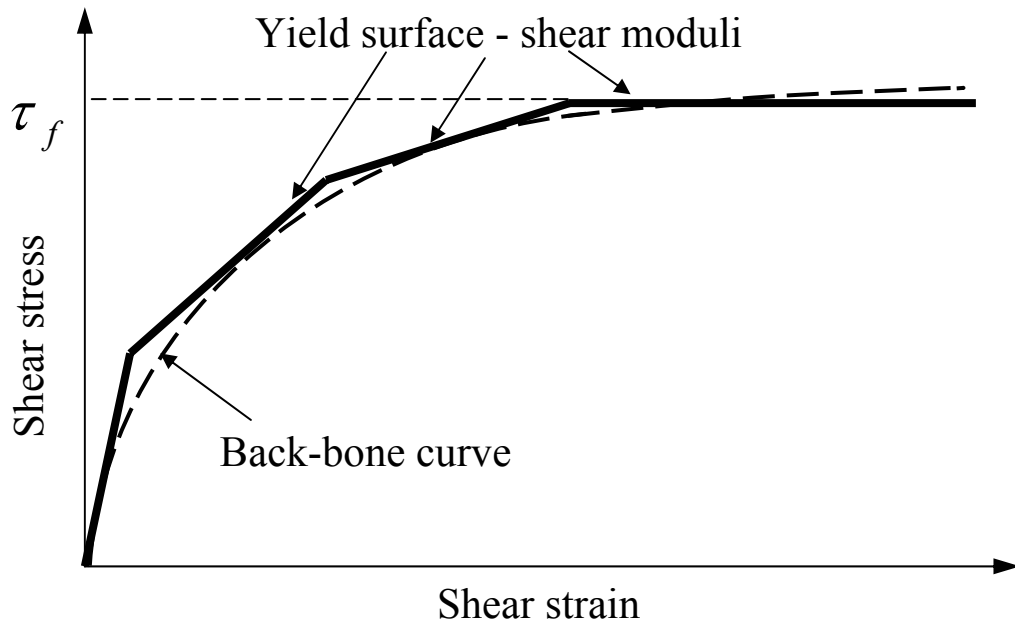


Fig. 5.5 Piecewise linear representation of soil nonlinear shear stress-strain response ( $\tau_f$  = model peak shear strength).

(c) **Flow Rule**

During shear loading, the soil contractive/dilative behavior is handled by a non-associative flow rule (Parra, 1996) to achieve appropriate interaction between shear and volumetric response. In particular, nonassociativity is restricted to the volumetric component ( $P''$ ), of the plastic flow tensor (outer normal to the plastic potential surface in stress-space). Therefore, depending on the relative location of the stress-state (Figure 5.6, also shown as Figure 2.21 earlier) with respect to the *phase transformation* (PT) surface (see Section 2.3.2(b)), different expressions for  $P''$  were specified for (Parra, 1996):

1. The contractive phase, with the stress-state inside the PT surface (Figure 5.6, Phase 0-1),
2. The dilative phase during loading, if the stress-state lies outside the PT surface (Figure 5.6, Phase 2-3), and
3. The contractive phase during unloading, with the stress-state outside the PT surface (Figure 5.6, Phase 3-4).

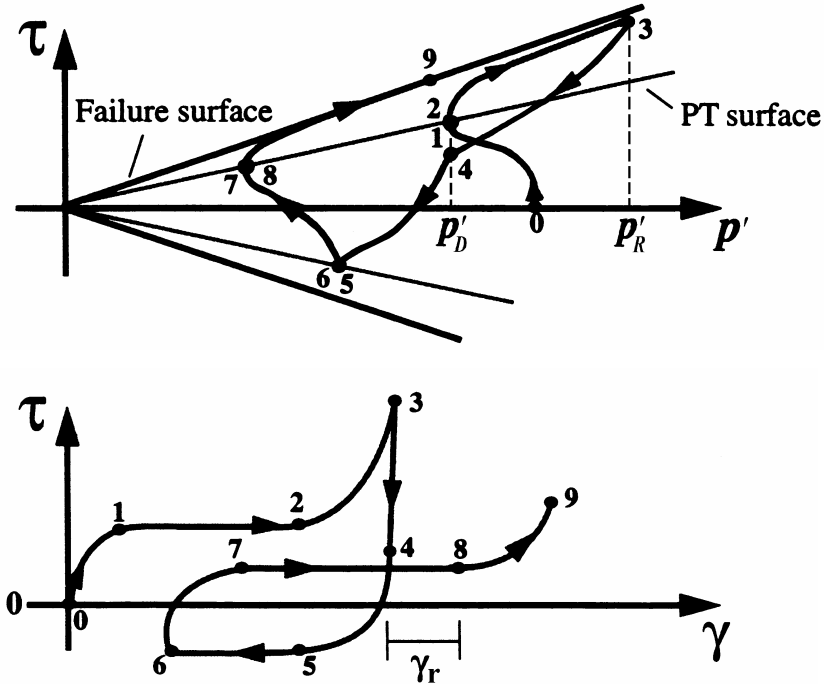


Fig. 5.6 Schematic of constitutive model response showing the octahedral stress  $\tau$ , the effective confining pressure  $p$ , and the octahedral strain  $\gamma$  relationships (Parra, 1996; Yang, 2000).

At low effective confining pressure (e.g., below 10 kPa), when the stress state reaches the PT surface while loading, permanent shear strain may accumulate rapidly with essentially no change in shear stress (Figure 5.6, Phase 1-2). This is achieved by activating a *perfectly plastic zone* (PPZ) before the initiation of dilation outside the PT surface (Figure 5.6, Phase 2-3). The PPZ is defined in deviatoric strain space as a circular, initially isotropic surface (Yang, 2000). Depending on the current strain state and plastic loading history, the PPZ may enlarge and/or translate in deviatoric strain space to model the accumulation of permanent shear deformations (Yang, 2000).

### 5.3.3 Model Calibration

The model may be calibrated entirely based on results from conventional laboratory sample tests. Specifically, these laboratory tests include

1. Monotonic drained triaxial/shear tests conducted at a constant mean confining pressure (Figure 5.7). Data from this type of experiment mainly serves as a basis for defining the

low-strain (linear) soil shear stiffness and maximum shear strength (or friction angle) at the corresponding effective confining pressure.

2. Monotonic undrained triaxial/shear tests (Figure 5.8). Results of this type of experiment serve to define constitutive model parameters that control contraction and dilation behavior.
3. Undrained cyclic triaxial/shear tests, possibly with a static shear stress bias (Figure 5.9). Results of this type of liquefaction experiment serve to define constitutive model parameters (e.g.,  $\gamma_r$  in Figure 5.6) that control the amount of cyclic accumulation of liquefaction-induced shear strain (Parra, 1996).

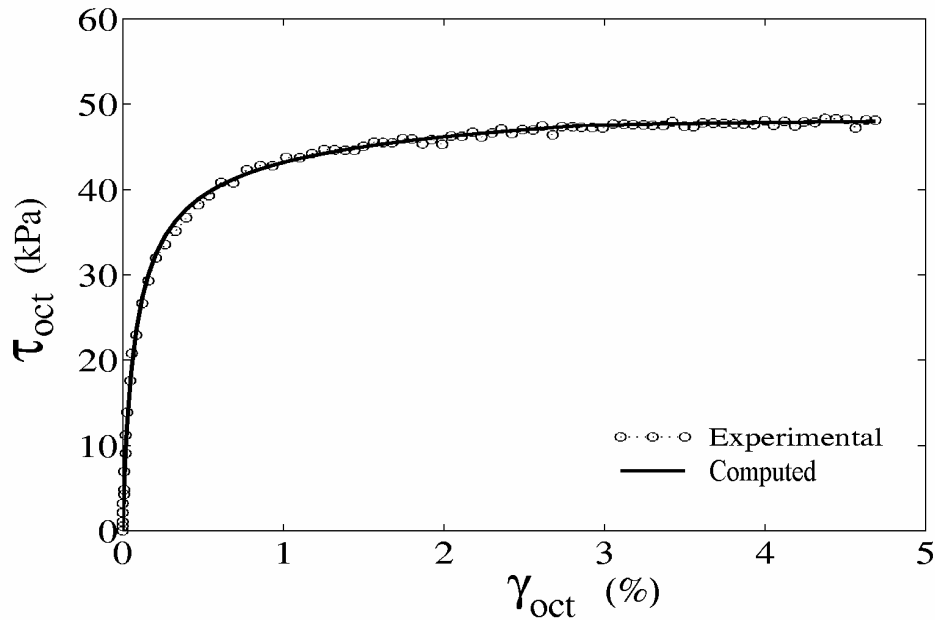


**Fig. 5.7** Experimental and computed (UCSD model) stress-strain curves for an isotropically consolidated, drained monotonic triaxial loading test (VELACS Test No. 40-100, Arulmoli et al., 1992;  $\tau_{oct}$  and  $\gamma_{oct}$  are octahedral quantities).

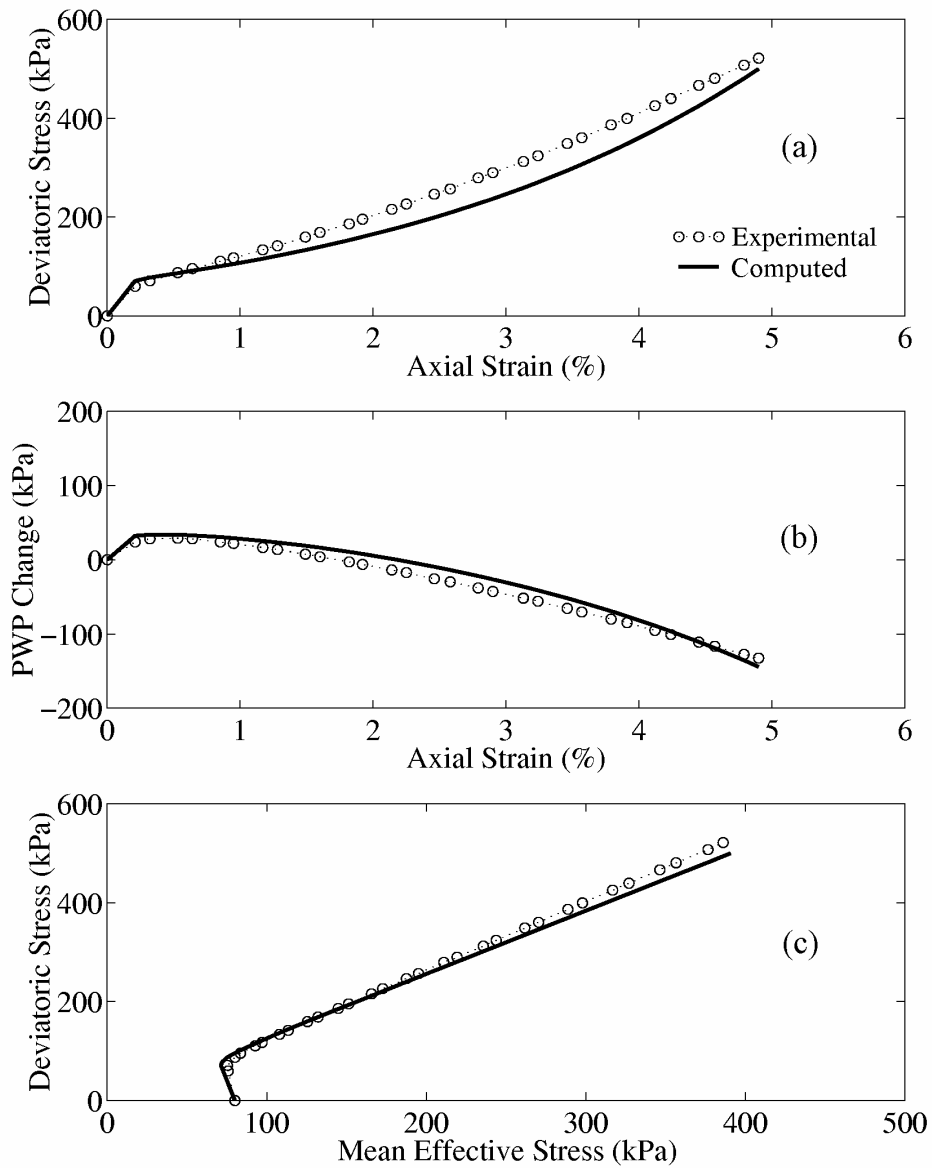


**Fig. 5.8** Experimental and computed (UCSD model) results of an isotropically consolidated, undrained monotonic triaxial loading test (VELACS Test No. 40-04, Arulmoli et al., 1992; PWP is porewater pressure).

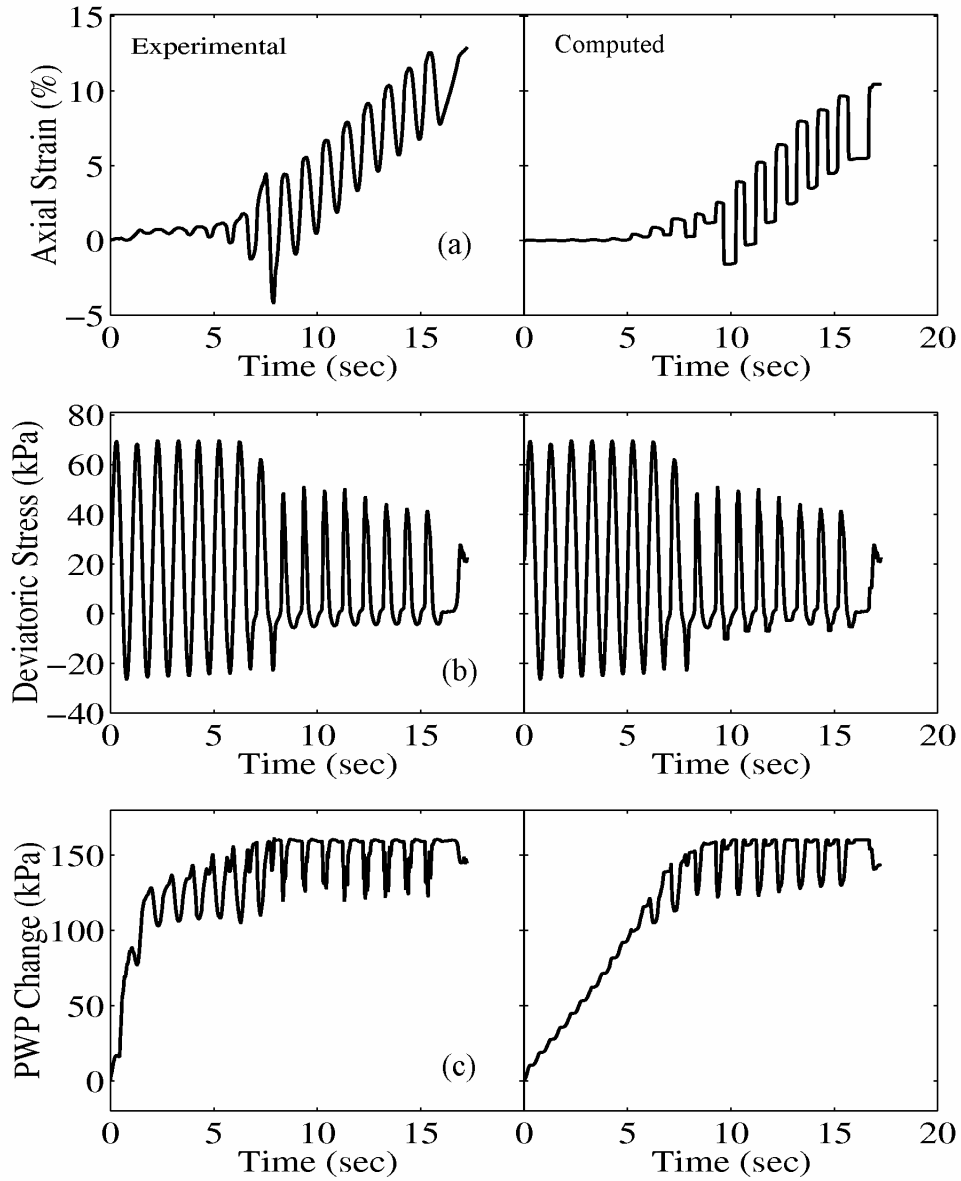


**Fig. 5.9** Experimental and computed (UCSD model) results of an anisotropically consolidated, undrained cyclic triaxial loading test (VELACS Test No. 40-58, Arulmoli et al., 1992), (continued on next page).

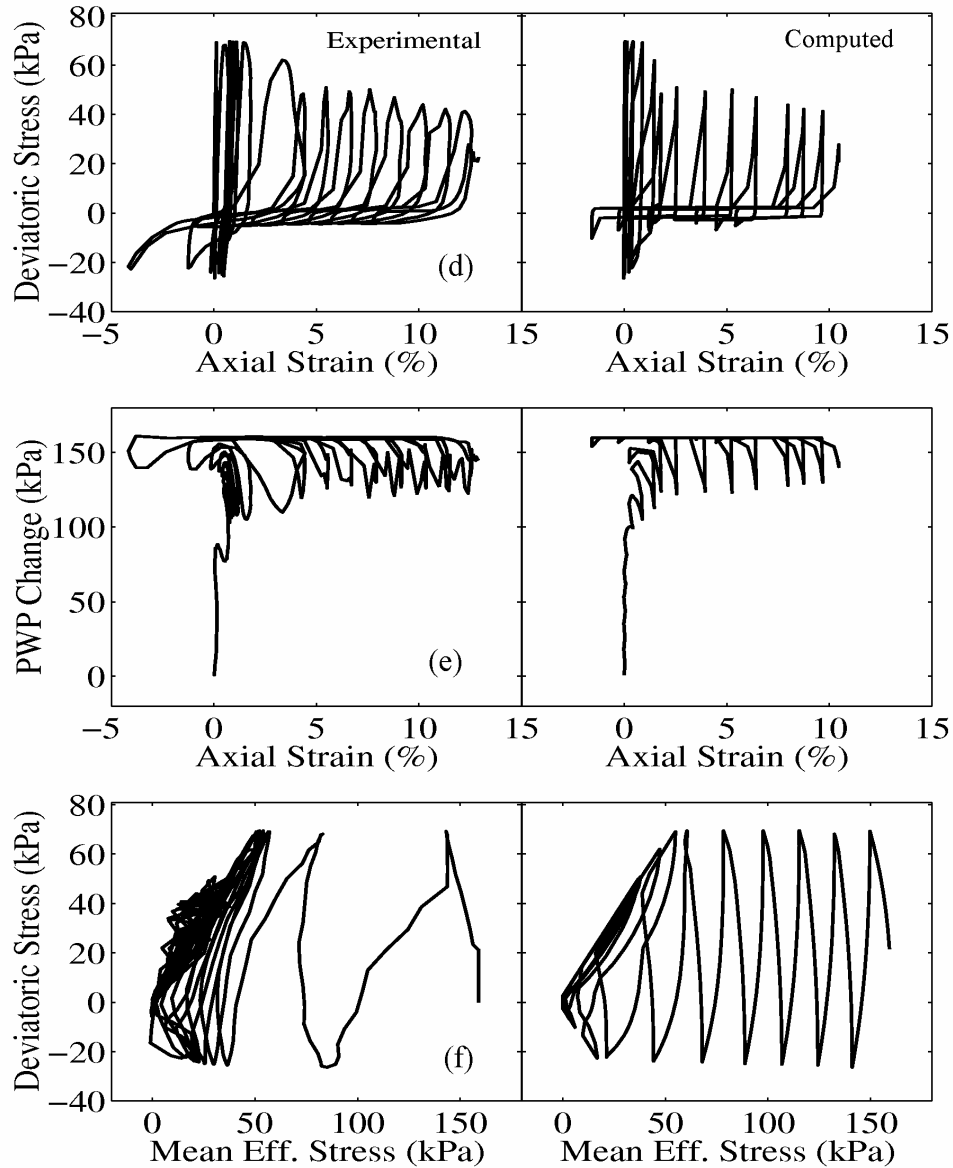


**Fig. 5.9 (cont'd):** Experimental and computed (UCSD model) results of an anisotropically consolidated, undrained cyclic triaxial loading test (VELACS Test No. 40-58, Arulmoli et al., 1992).

#### 5.4 MODEL PERFORMANCE

The UCSD constitutive model was incorporated into a general-purpose two-dimensional (2D plane-strain and axisymmetric) finite element program CYCLIC (Parra, 1996; Yang, 2000). CYCLIC implements the two-phase (solid-fluid), fully coupled numerical formulation of Chan

(1988) and Zienkiewicz et al. (1990). Most of the numerical model simulations discussed in this section were conducted using CYCLIC.

#### **5.4.1 Simulation of UC Berkeley Laboratory Sample Tests**

Numerical simulations were conducted directly using the UCSD liquefaction model to reproduce the essential response characteristics of dense Nevada sand (at  $D_r$  of about 90%). In this experimental program, effort was directed toward complementing existing information by a set of data at high relative densities (where liquefaction-induced deformations are still objectionable, despite the high  $D_r$ ). The numerical simulations were based on results from three stress-controlled undrained cyclic shear tests conducted using the UC Berkeley bidirectional simple shear device (see Section 4.4.1, and Kammerer et al. 2000 for a detailed description of the experimental program). These three tests (NS8, NS11, and NS12) varied in the initial vertical effective confining pressure (96 kPa, 44 kPa, and 36 kPa), the cyclic stress ratio (CSR = 0.26, 0.22, and 0.53), and the amplitude of static stress bias ( $K_\alpha = 0.0, 0.08, \text{ and } 0.09$ ). A single set of model parameters was calibrated to simulate all three tests (Figure 5.10 shows NS11 and NS8 results).

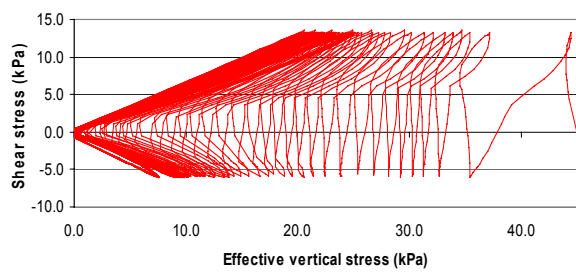
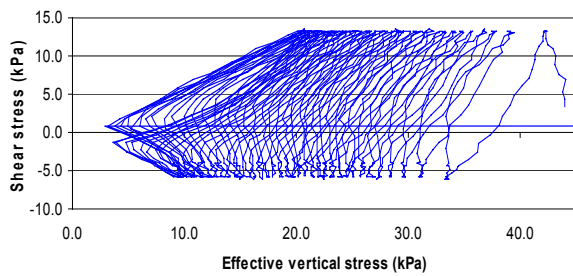
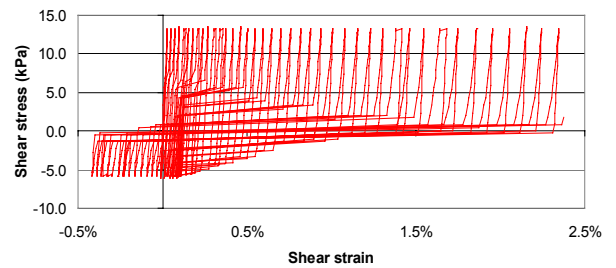
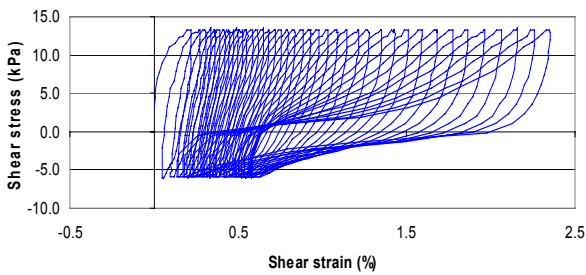
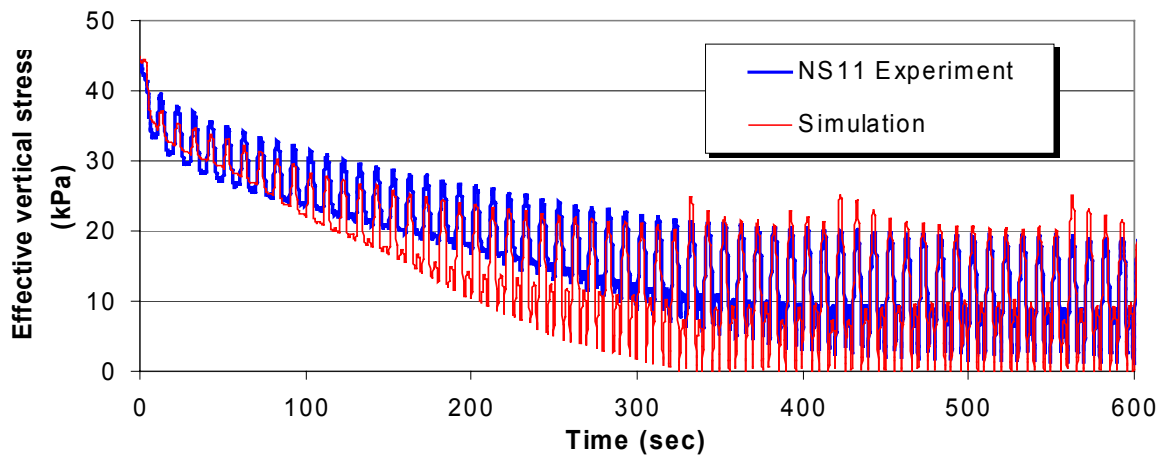
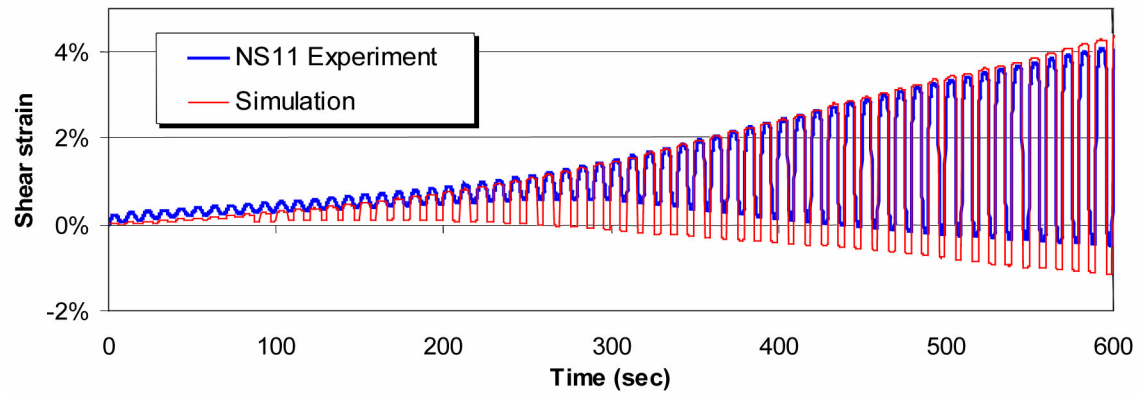
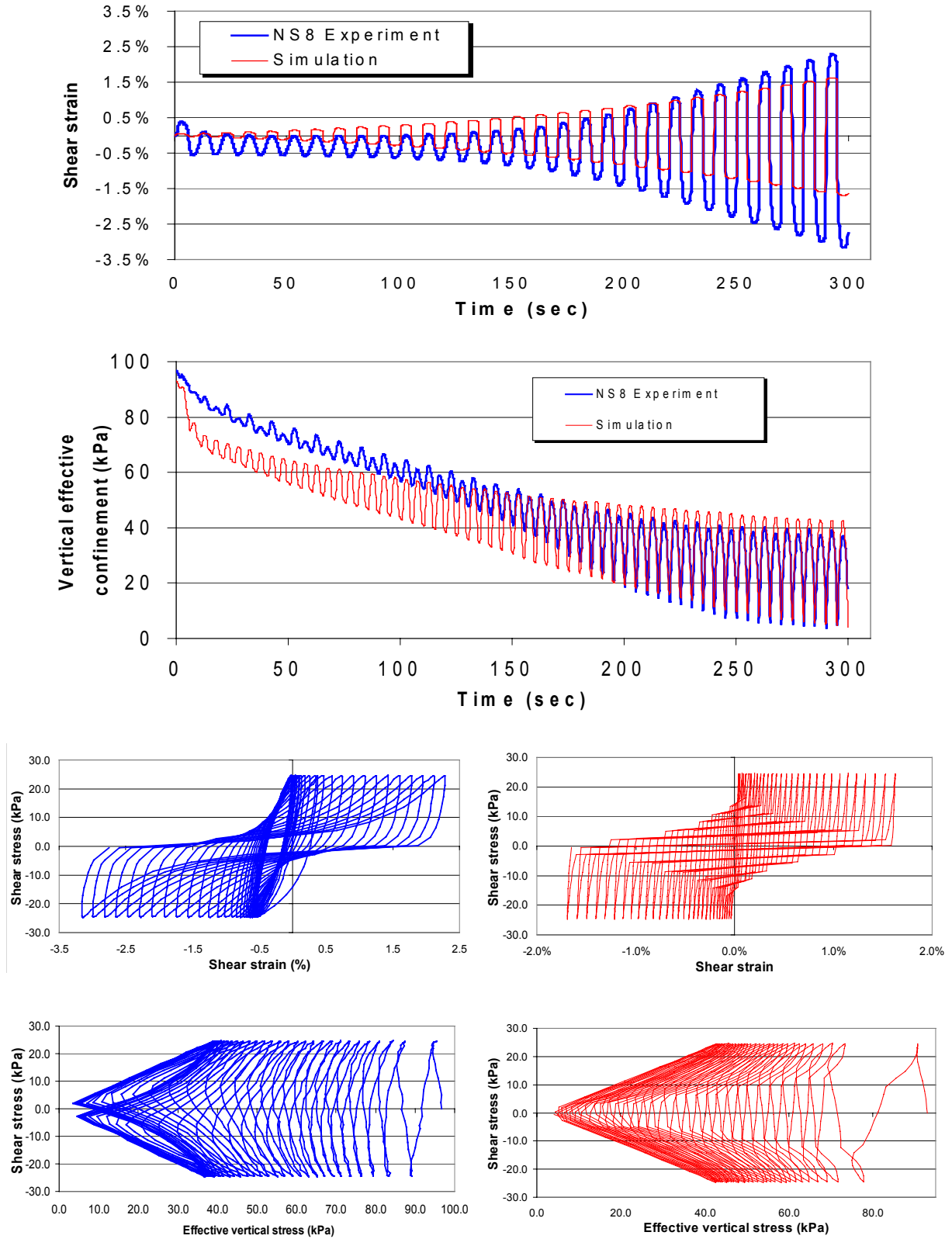


Fig. 5.10a NS 11 experimental (left) and computed (right, UCSD model) response of dense Nevada sand (Kammerer et al., 2000).



**Fig. 5.10b** NS 8 experimental (left) and computed (right, UCSD model) response of dense Nevada sand (Kammerer et al., 2000).

### 5.4.2 Simulation of UC Davis Centrifuge Test

The UC Davis geotechnical centrifuge has been used to evaluate liquefaction remediation effects at bridge sites (Balakrishnan and Kutter, 1999). In one test, a river and its flood banks were modeled (Figure 5.11). The soil profile was prepared with a dense-sand ( $D_r = 80\%$ ) bottom layer overlain by medium density sand ( $D_r = 50\%$ ), with a sloping surface deposit of over-consolidated clay on top. The rigid model container was inclined at an angle of  $1.7^\circ$  ( $3.0\%$ ) to the centrifugal acceleration field.

A numerical simulation was conducted using CYCLIC (Yang, 2000). The model response was assumed to be approximately 1D in the south central (A-A) section (Figure 5.11). Therefore, a 1D profile of this location (Figure 5.11) was adopted in the numerical analysis (base excitation was a scaled version of the 1995 Kobe ground motion recorded at 80 m depth with a  $0.73\text{ g}$  peak, Balakrishnan et al., 1997). In general, the computed excess pore pressure (Figure 5.12) and lateral displacement histories (Figure 5.13) show overall general agreement with the experimental measurements (Yang, 2000).

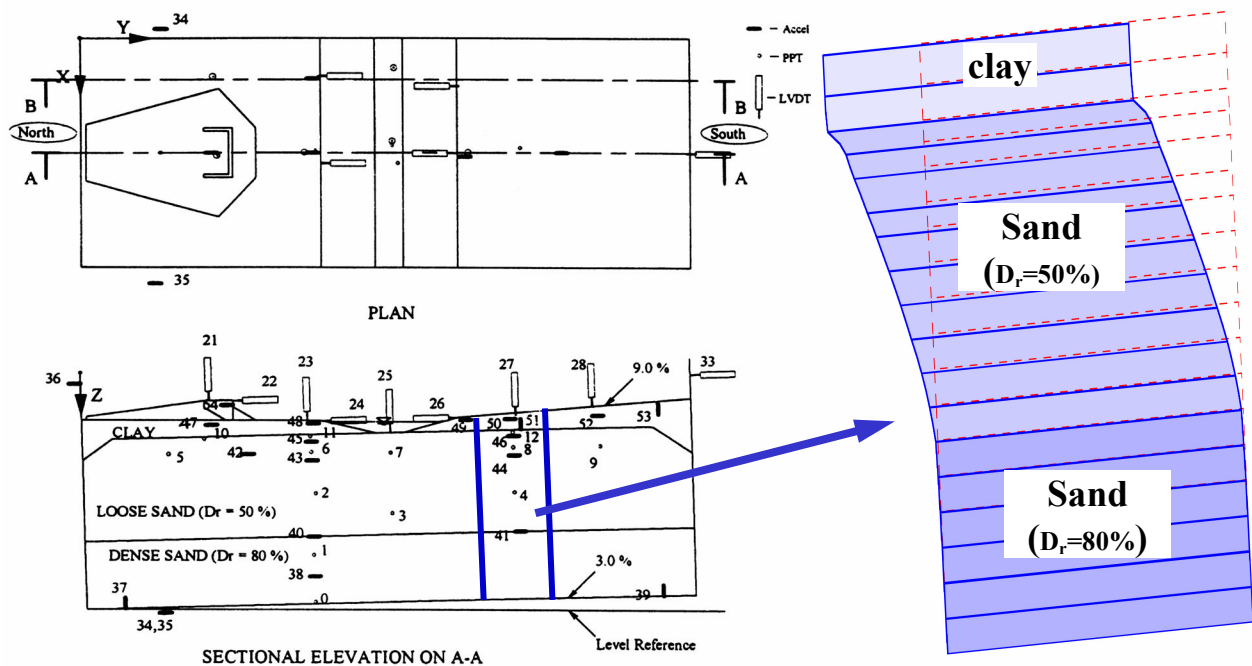
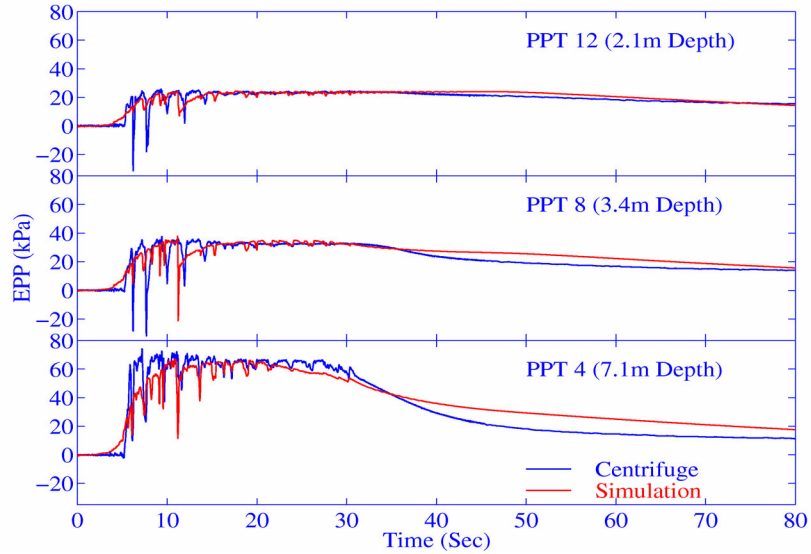
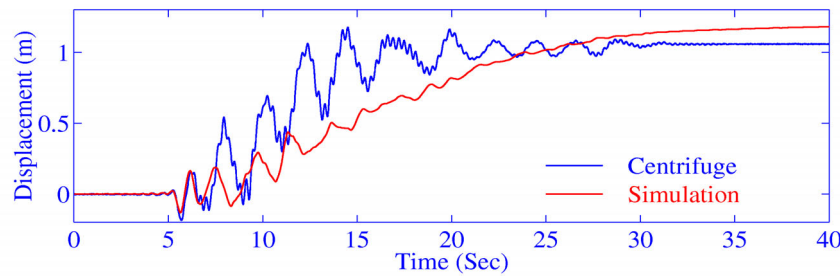


Figure 5.11 UC Davis centrifuge model configuration and numerical model simulation (Balakrishnan et al., 1997; Yang, 2000).



**Fig. 5.12 Recorded and computed excess pore-pressure time histories along the soil profile (Yang, 2000).**



**Fig. 5.13 Recorded and computed surface lateral displacement time histories (Yang, 2000).**

### 5.4.3 Simulation of RPI (VELACS) Centrifuge Test, and Permeability Effects

A numerical study was conducted recently (Yang and Elgamal, 2001) to highlight the influence of permeability variation on the overall site response in both uniform and non-uniform soil strata. In this study, a 1D numerical model was employed to represent a 10-m-thick uniform soil profile, inclined by  $4^\circ$  to simulate an infinite-slope response. This configuration is identical to that of the VELACS Model-2 centrifuge experiment (used earlier for calibration) conducted at RPI (Dobry et al., 1995; Taboada, 1995). Three numerical simulations were conducted, with permeability coefficients  $k = 1.3 \times 10^{-2}$  m/sec (gravel permeability),  $k = 3.3 \times 10^{-3}$  m/sec (VELACS Model-2 sandy gravel calibration simulation), and  $k = 6.6 \times 10^{-5}$  m/sec (clean sand permeability) respectively. The same Nevada sand constitutive model parameters (at  $D_r$  of about

40%) were employed in all three cases in order to maintain focus on permeability effects. In this regard, the adopted sand model parameters represents the behavior of a medium-density frictionless granular material.

The VELACS centrifuge Model-2 input excitation (harmonic, mainly 2 Hz motion, Taboada, 1995) was employed as the base excitation. Computed lateral displacements for the three simulations are displayed in Figure 5.14, along with the experimental response of VELACS Model 2 test (Dobry et al., 1995; Taboada, 1995). It is clearly seen that: (i) computed lateral deformations with the sandy gravel- $k$  value are close to the experimental responses (part of the calibration process) and (ii) the extent of lateral deformation in this uniform profile is inversely proportional to soil permeability, i.e., a higher  $k$  results in smaller lateral deformation (near the surface, the lateral deformation of the sand- $k$  simulation was about 2.5 times that of the gravel- $k$  simulation). The relationship between  $k$  and lateral deformation is a consequence of the effect of permeability on excess porewater pressure (Figure 5.15) throughout the soil profile. Figure 5.16 shows that rapid excess porewater pressure dissipation took place in the gravel- $k$  model (even during the strong shaking phase), resulting in a low excess porewater pressure profile. Consequently, high effective confining pressure was maintained with less reduction in shear stiffness and strength. In the sand (low  $k$ ) profile, soil response was essentially undrained, resulting in the liquefied region reaching a depth in excess of 5 m.

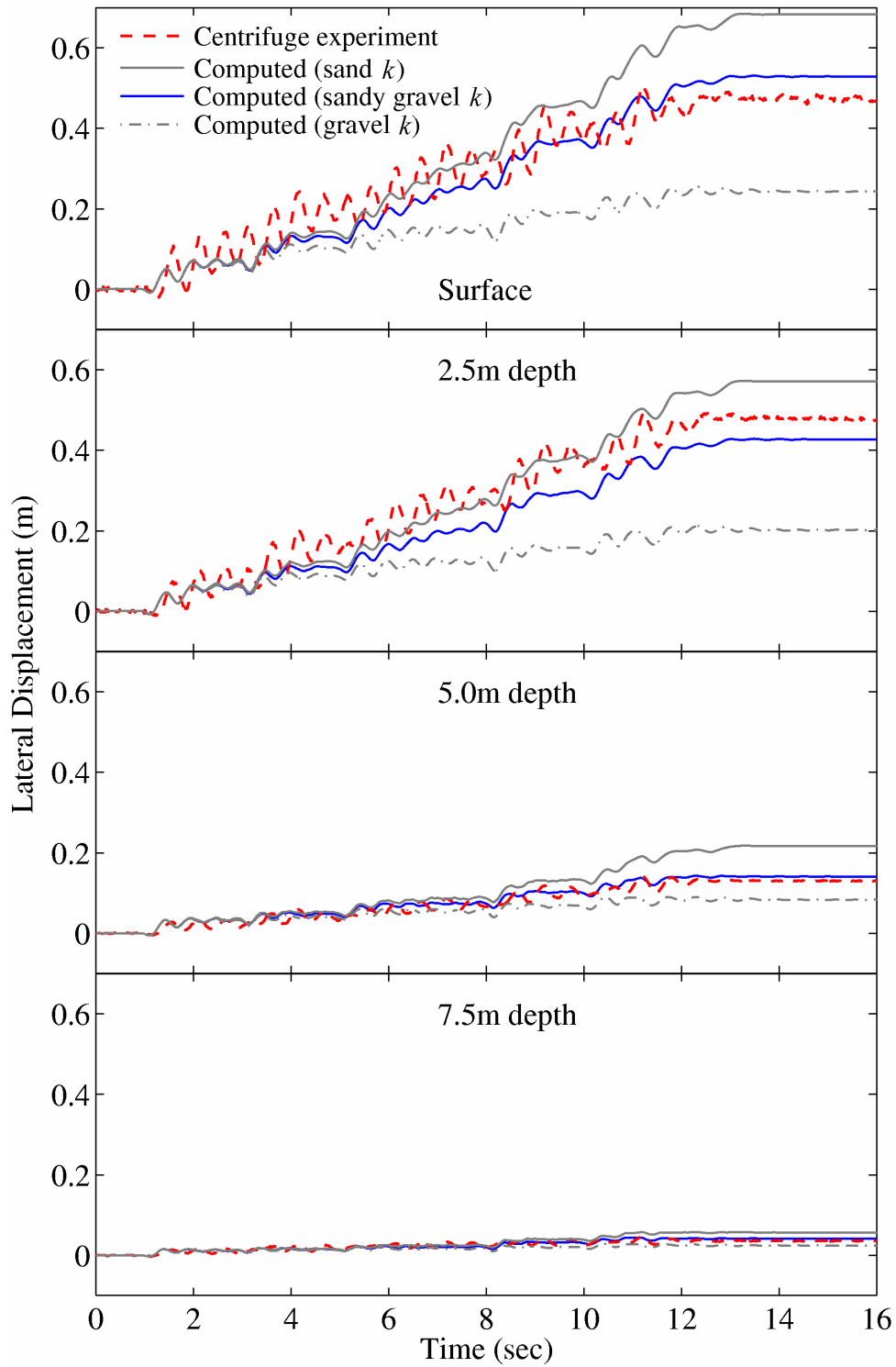


**Fig. 5.14 Lateral displacement histories in uniform soil profile with different permeability coefficients (Yang and Elgamal, 2001).**

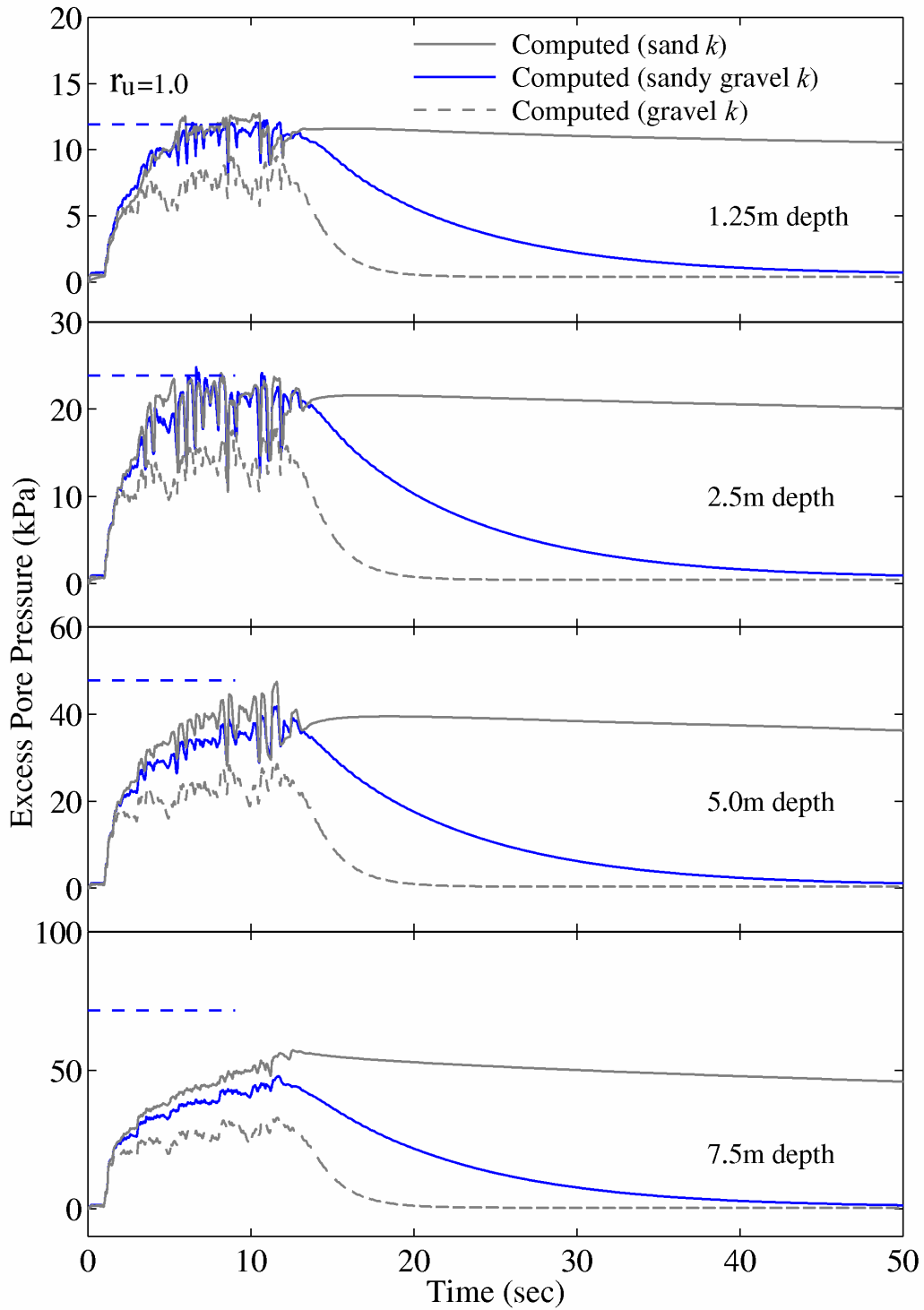


Fig. 5.15 Excess pore-pressure histories in uniform soil profile with different permeability coefficients (Yang and Elgamal, 2001).

#### 5.4.4 Permeability Variation Effects

In an additional simulation (Yang and Elgamal, 2001), an inclined sand profile ( $4^\circ$  inclination, 13m in depth) with an embedded low-permeability (silt) layer was subjected to 15 sec of sinusoidal motion (0.08 g peak amplitude, at 1 Hz).

At the end of shaking, the element underneath the silt- $k$  layer had not increased in void ratio sufficiently to reach the prescribed no-dilation critical-void-ratio state (Figure 5.16). The remaining tendency for dilation produced sufficient shear strength to halt further lateral deformation of the  $4^\circ$  slope. However, continued post-liquefaction sedimentation (settlement below the silt- $k$  interlayer) eventually allowed the element underneath the silt layer to reach the critical-void-ratio state. Thereupon, the lack of dilation and the liquefaction condition ( $r_u=1.0$ ) resulted in a delayed flow failure (Figure 5.16). Such delayed flow failure after the end of dynamic/seismic excitation has been reported in the literature by a number of investigators (e.g., Ishihara 1984, Seed, 1987; Harder and Stewart 1996, Berrill et al., 1997; Boukouvelas et al., 1999; Kokusho, 1999; Kokusho et al. 1999).

The influence of a low-permeability interlayer on the overall profile response may be visualized in Figure 5.16, in terms of excess porewater pressure and deformation profiles along the soil column at 16.5 sec (end of shaking) and 80.0 sec:

- (1) A very high pore-pressure gradient developed in the silt- $k$  layer. Below this layer, the post-shaking re-consolidation process eventually results in a constant excess porewater pressure distribution. This constant value is equal to the initial effective confining pressure (overburden pressure) imposed by the silt and layers above. Dissipation of this excess porewater pressure through the low-permeability silt may take a very long time in practical situations (if no sand boils develop).
- (2) After the shaking phase, large shear-strain concentration and void-ratio increase occurred immediately beneath the silt- $k$  layer. Meanwhile, negligible additional shear strain was observed in the rest of the profile. The concentration of void-ratio increase below the silt- $k$  interlayer was mainly due to (i) post-liquefaction settlement of the underlying sand and (ii) virtual lack of settlement of overlying soil due to the relatively impervious silt- $k$  interlayer.

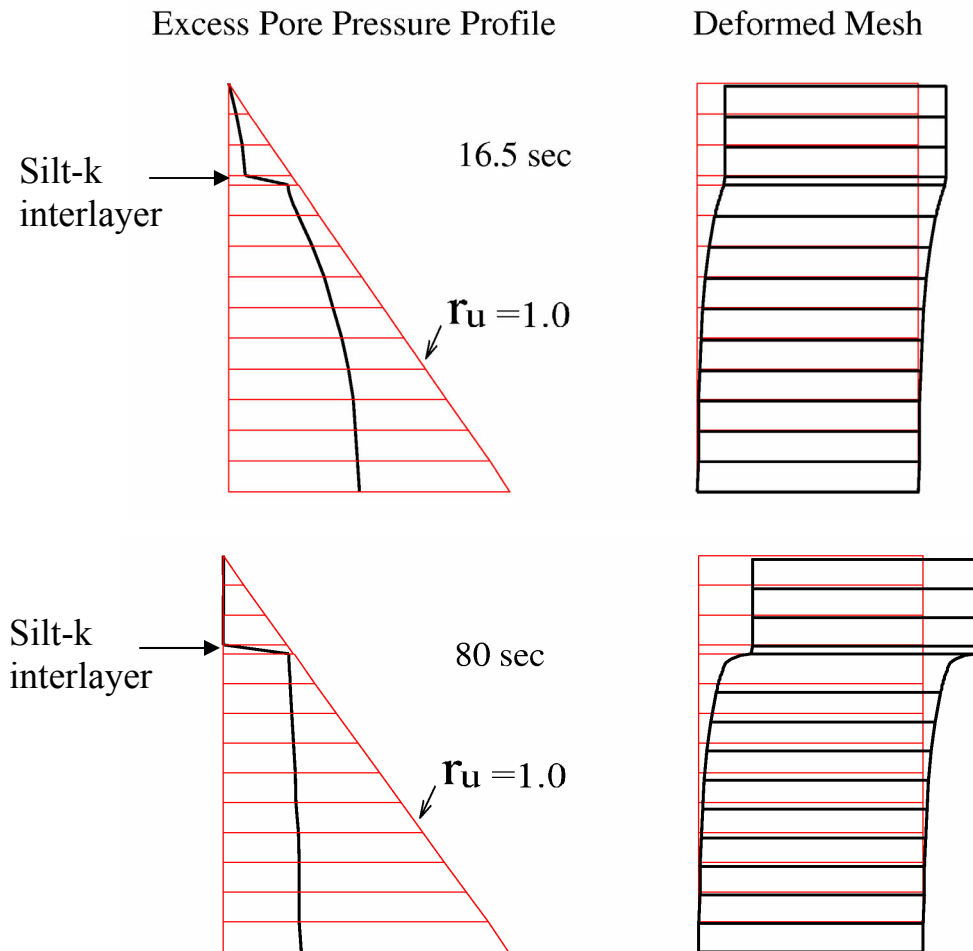


Fig. 5.16 Excess pore-pressure profile and deformed mesh for clean sand profile with a silt-*k* interlayer (deformations are not to scale and are exaggerated for clarity; Yang and Elgamal, 2001).

#### 5.4.5 Simulation of RPI Centrifuge Embankment Tests

A liquefaction countermeasure centrifuge experimental study was conducted (Adalier 1996; Adalier et al., 1998) using the centrifuge at Rensselaer Polytechnic Institute. The dynamic stability of a 4.5 m (prototype scale) clayey sand embankment (Figure 5.17) supported on 6 m of medium saturated sand (Nevada sand at  $D_r$  of about 40%), was systematically studied with and without liquefaction countermeasures. The sand modeling parameters were calibrated based on earlier laboratory (see Sections 5.3.3 and 5.4.3; Arulmoli et al., 1992) and centrifuge tests (Dobry et al., 1995). In this report, numerical simulation results of one of the employed liquefaction countermeasures (sheet-pile enclosure, Figure 5.17) are discussed, along with the

benchmark model (without remediation). The reader is referred to Adalier et al. (1998) for other retrofit techniques employed.

The centrifuge models were numerically simulated. Each model was shaken at 0.18 g peak excitation in prototype scale, with a uniform harmonic base input motion of 10 cycles at 1.6 Hz prototype frequency. The deformed meshes in Figure 5.18 show major lateral displacement and shear below the embankment toe in the foundation soil (which liquefied due to the imparted dynamic excitation) with no remediation implemented. On the other hand, the sheet-pile enclosure countermeasure resulted in nearly perfect containment of the foundation soils below the embankment (Figure 5.18). The computed shear stress-strain responses in Figure 5.19 also indicate the large cycle-by-cycle shear strain accumulation under the embankment toe in the benchmark model (in contrast to minimal permanent shear deformation for the sheet-pile case).

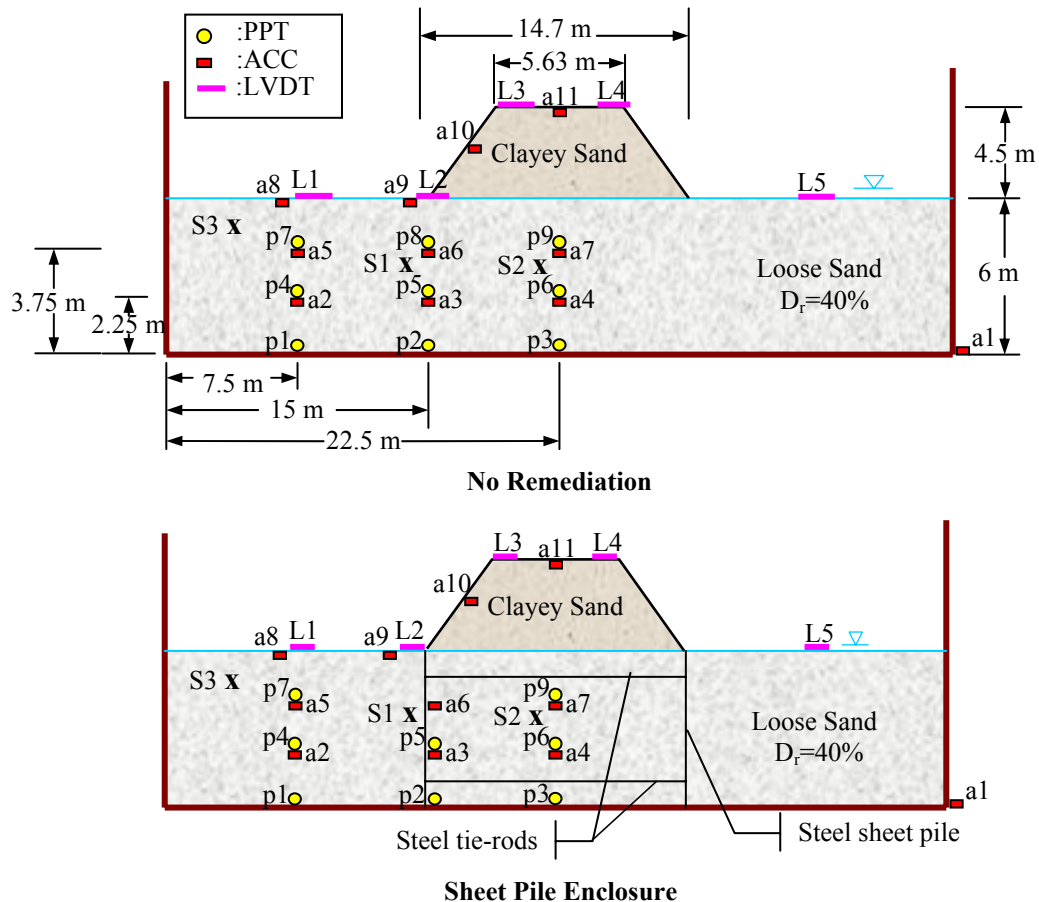


**Fig. 5.17 Centrifuge model setup (Adalier et al., 1998, PPT is Pore-Pressure Transducer, ACC is Accelerometer, LVDT is Linear Variable Differential Transducer).**

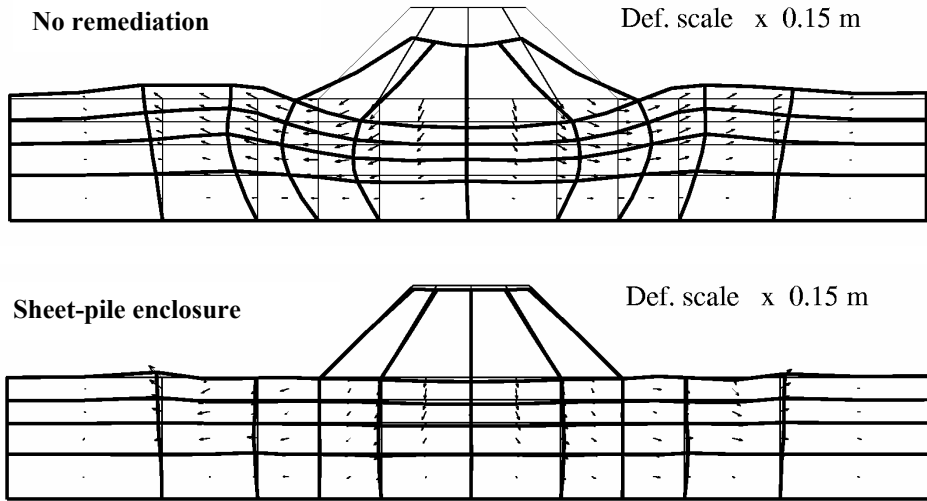


**Fig. 5.18** Computed deformed configuration (benchmark with no remediation and sheet-pile enclosure, Parra, 1996).

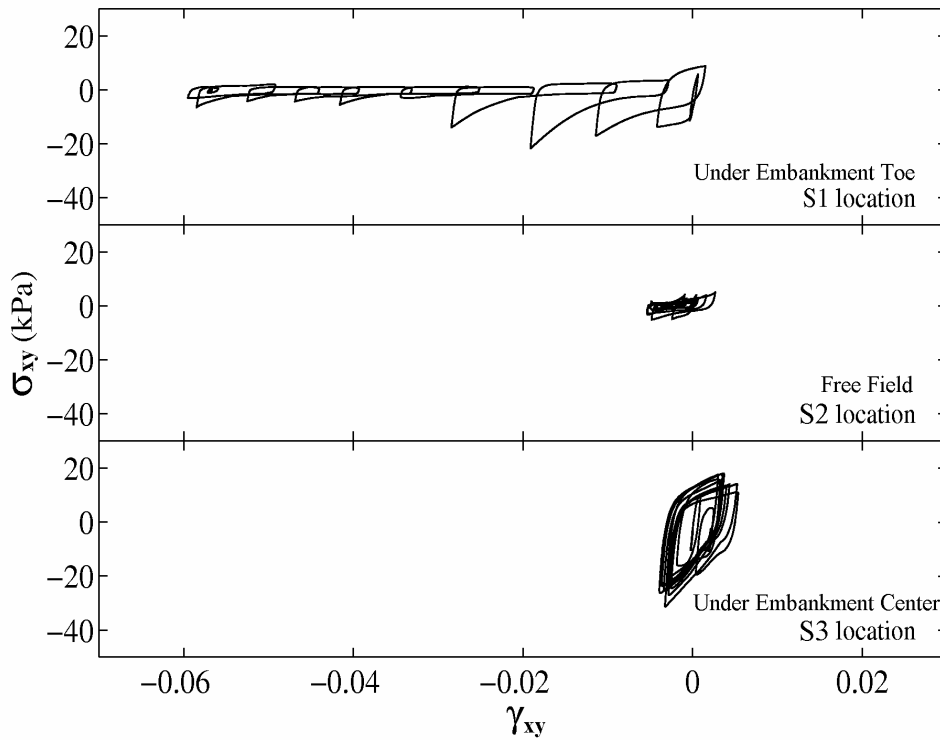


**Fig. 5.19a** Computed shear stress-strain histories (no remediation, Parra, 1996).

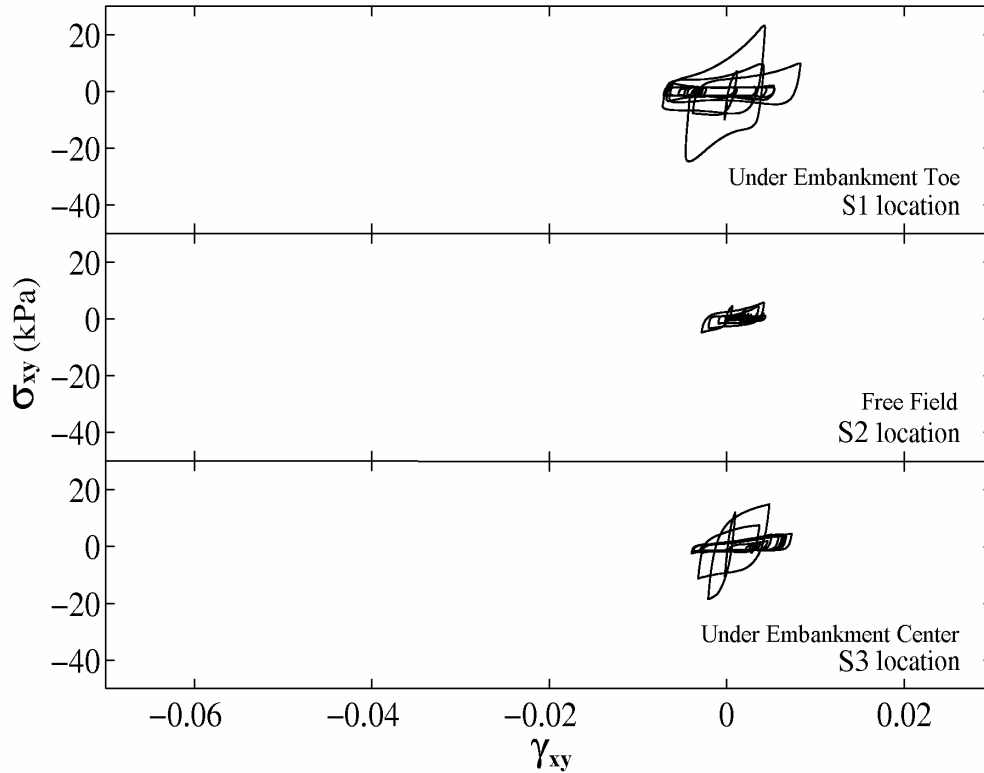
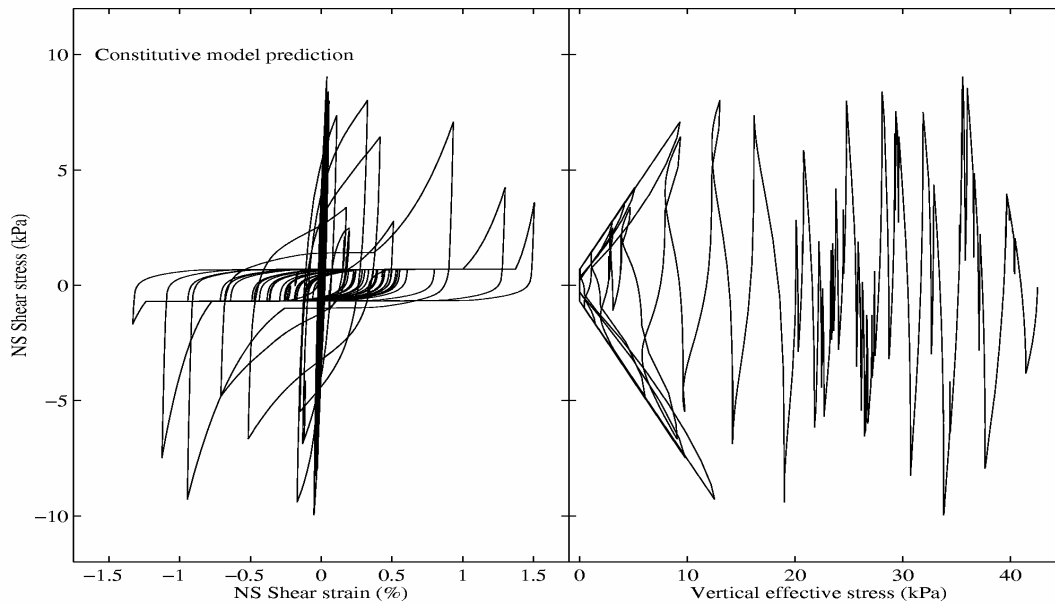


Fig. 5.19b Computed shear stress-strain histories (sheet-pile enclosure, Parra, 1996).

#### 5.4.6 Simulation of Field Data

##### (a) *Wildlife Refuge Site*

A preliminary computational simulation (Zeghal et al., 1996) of the identified liquefaction response in Figure 2.7 using the UCSD constitutive model is shown in Figure 5.20. In addition to the loss of stiffness and strength associated with pore-pressure buildup, the model also captures the regain in stiffness and strength at large strain excursions. The associated dilative response during these instants occurs near the condition of liquefaction along the phase transformation line.



**Fig. 5.20 Wildlife-Refuge computed NS shear stress-strain and effective stress path during the Superstition Hills 1987 earthquake (Zeghal et al., 1996).**

**(b) Port Island**

To achieve the best possible match between the identified stress-strain responses and the computed counterparts, the employed soil model parameters were derived (Elgamal et al., 1996; Zeghal et al., 1996) using a nonlinear optimization technique (Bard, 1974; Gill, 1981). Optimization was performed in a weighted manner where (1) the initial phase of response before pore-pressure buildup was used primarily to identify the low-amplitude soil properties, (2) the next phase of pore-pressure buildup was employed for calibrating the related modeling parameters, and (3) the remaining response was used to calibrate the corresponding post-liquefaction model response. Based on the above, the optimized model stress response is shown in Figure 5.21, along with the counterpart evaluated earlier from seismic response (Elgamal et al., 1996). These parameters represent average dynamic properties of the soil layers between the accelerometers located at elevations 0 m, 16 m, 32 m, and 83 m. Using the CYCLIC program, 1D site response was conducted. The N44W earthquake record at 83 m depth was employed as input excitation. As may be expected, close agreement was found between the computed and recorded accelerations (Figure 5.22). The computed excess pore-pressure time history at 8 m

depth showed that an abrupt rise occurred mainly during the phase of strongest excitation (Stage 2, 4-7 sec), causing the upper soil layers to lose stiffness and strength.

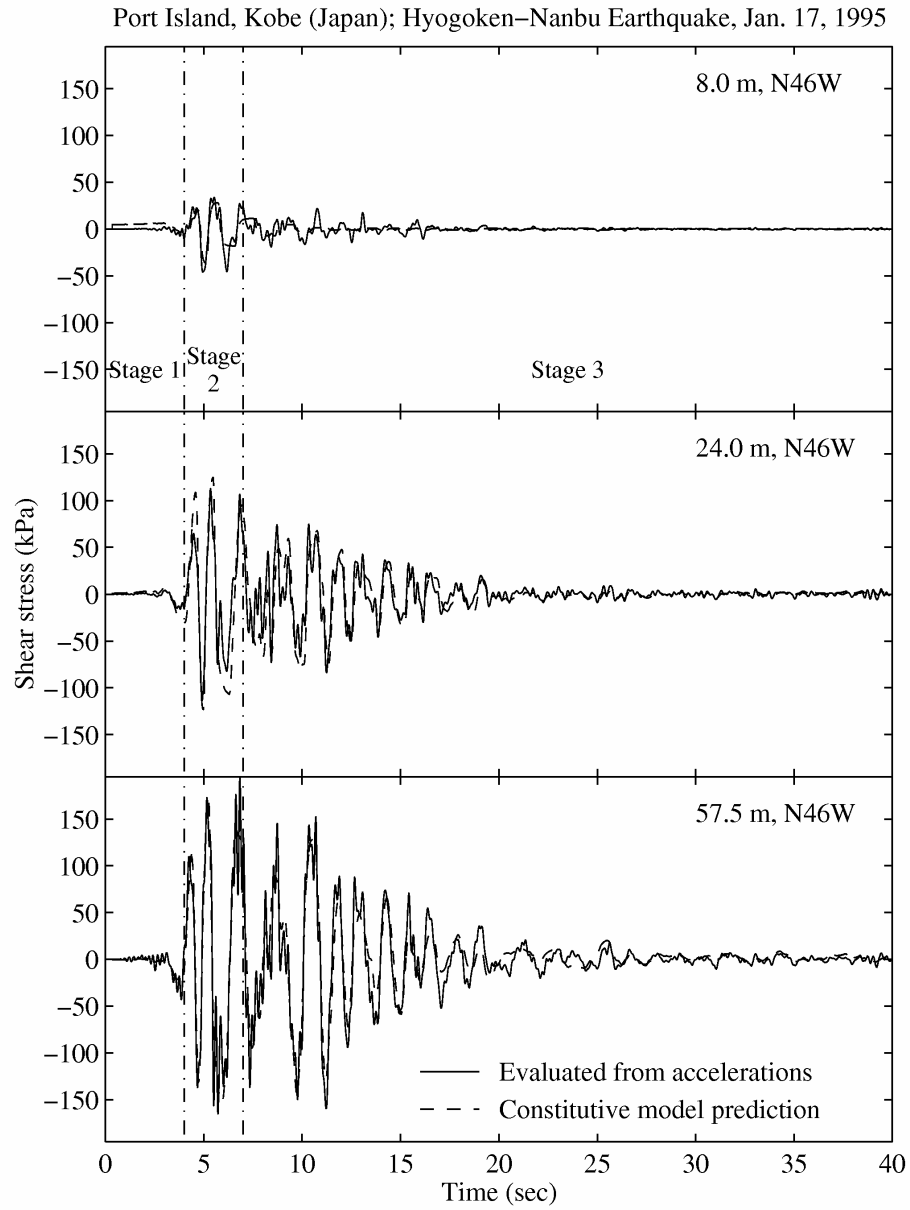


**Fig. 5.21** Port Island shear stress histories estimated from acceleration histories and corresponding constitutive model prediction (Elgamal et al., 1996; Zeghal et al., 1996).

Port Island, Kobe (Japan). Hyogoken-Nanbu Earthquake, Jan. 17, 1995

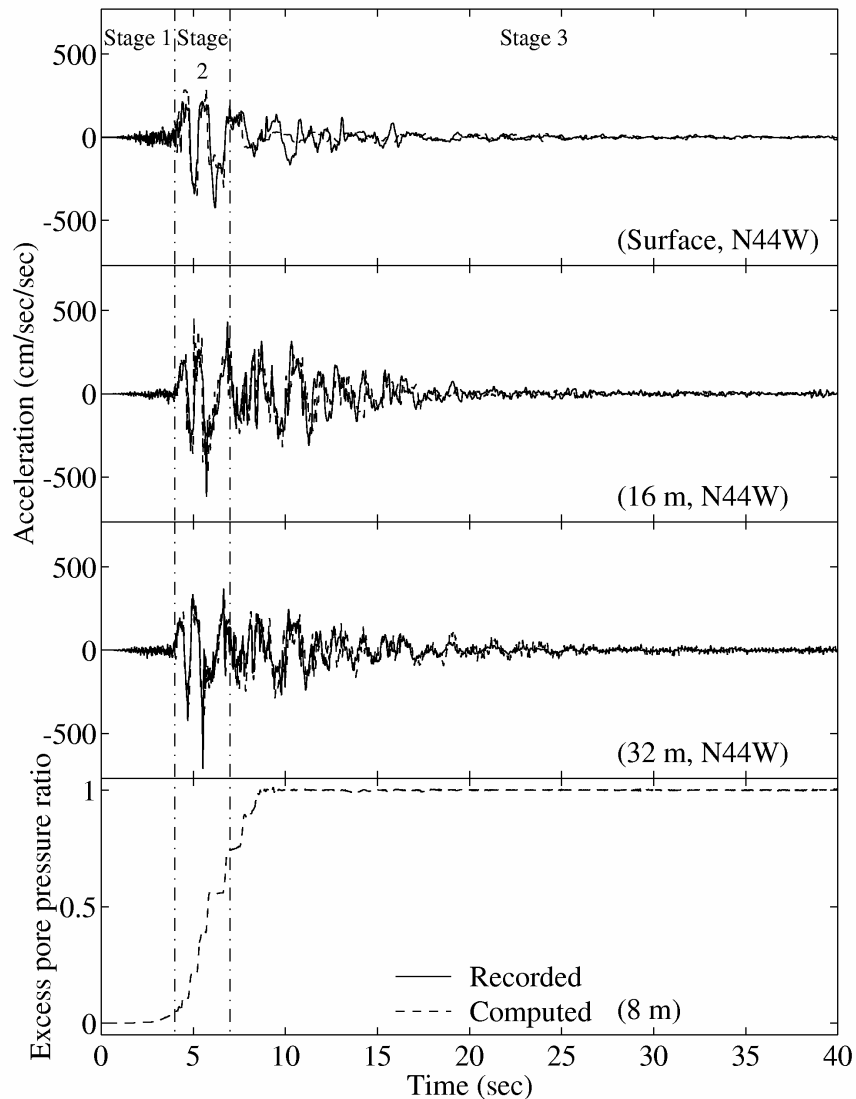


Fig. 5.22 Port Island recorded and computed accelerations at surface, 16 m and 32 m depth, and computed excess pore-pressure ratio at 8m depth (Elgamal et al., 1996; Zeghal et al., 1996).

## 5.5 RECENT UC DAVIS CONTRIBUTIONS

A long-term effort has been under way at UC Davis to advance the state of the-art in soil constitutive modeling. Particular emphasis has been placed on the modeling of liquefaction response within a unified framework (flow liquefaction and cyclic mobility). The prominent research team led by Professor Yannis F. Dafalias, includes Professor A. Rajah Anandarajah

(Johns Hopkins University), Professor Boris Jeremić (UC Davis), and Professor Xiang-Song Li (Hong Kong University of Science and Technology), and Professor Majid T. Manzari (George Washington University). This section summarizes a number of their recent contributions.

### 5.5.1 State-Dependent Dilatancy

Among the most significant recent advances in computational modeling of sand liquefaction behavior is the introduction and successful implementation of the state-dependent-dilatancy concept (Dafalias and Manzari, 1999; Li and Dafalias, 2000). Traditionally, constitutive models for cohesionless granular materials assume a constant void ratio  $e$ . Therefore, the same sand at different initial void ratios is modeled as different materials (Fig. 5.23a). This approach is not applicable in situations where significant changes in void ratio are expected. Further, experiments have shown that (Fig. 5.23b) even for the same initial void ratio, a sand may exhibit contractive or dilative behavior during shear loading, depending on its initial state relative to the critical state line (CSL) in  $e-p'$  space ( $p'$  is the effective confinement). Such a state-dependence cannot be reflected in a model that assumes constant  $e$ .

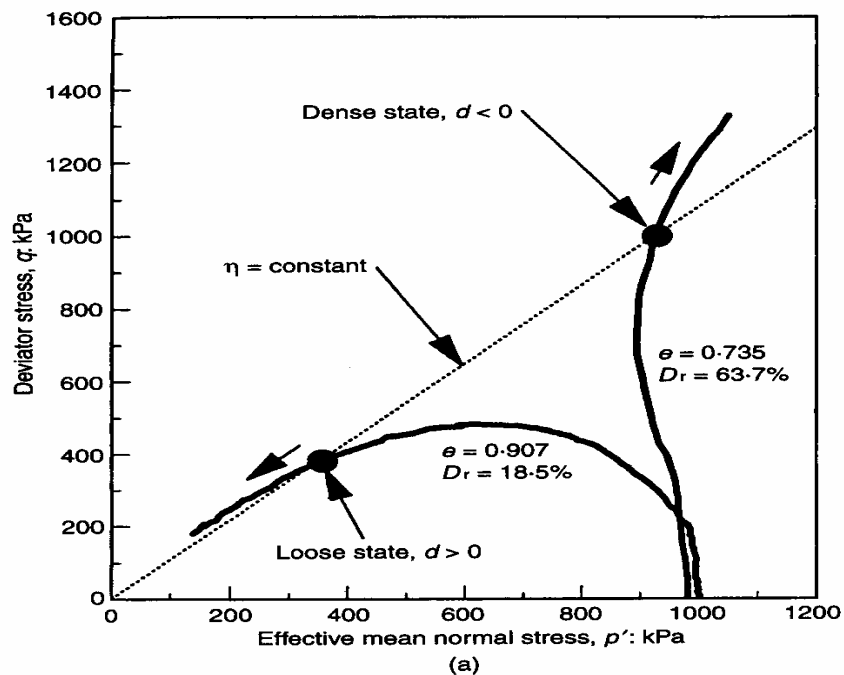
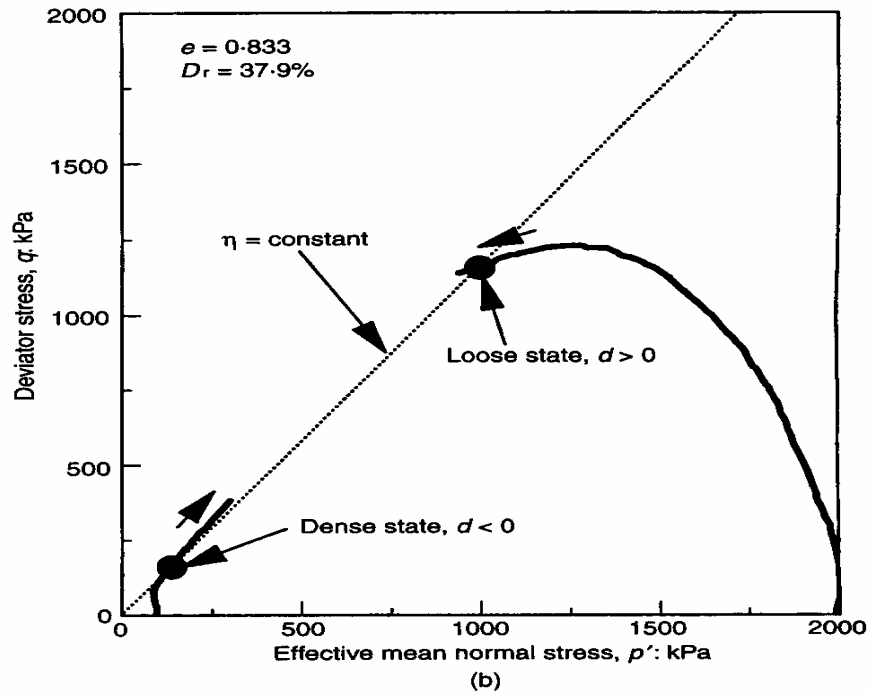


Fig. 5.23a Variation in dilatancy with material state (data from Verdugo and Ishihara, 1996): Undrained response with different densities (after Li and Dafalias, 2000).



**Fig. 5.23b** Variation in dilatancy with material state (data from Verdugo and Ishihara, 1996): Undrained response with the same density under different confinements (after Li and Dafalias, 2000).

In view of the importance of  $e$  in dictating soil shear response, Manzari and Dafalias (1997), and Li and Dafalias (2000) explicitly introduced  $e$  as a state variable in their models. Thus, a state-dependent dilatancy function  $d$  (ratio of plastic volumetric strain increment to effective plastic deviatoric strain increment) can be written in the following general form (Li and Dafalias, 2000):

$$d = d(\eta, e, Q, C)$$

where  $\eta$  is the effective stress ratio (ratio of octahedral stress to mean effective confinement),  $e$  the void ratio, and  $Q$  and  $C$  as collective terms, denote internal state variables other than  $e$  (e.g., the evolving tensor of anisotropy), and intrinsic material constants, respectively. The dilatancy function  $d$  must be zero upon reaching (Fig. 5.24): (1) the phase-transformation line and (2) the critical state (Li and Dafalias, 2000).

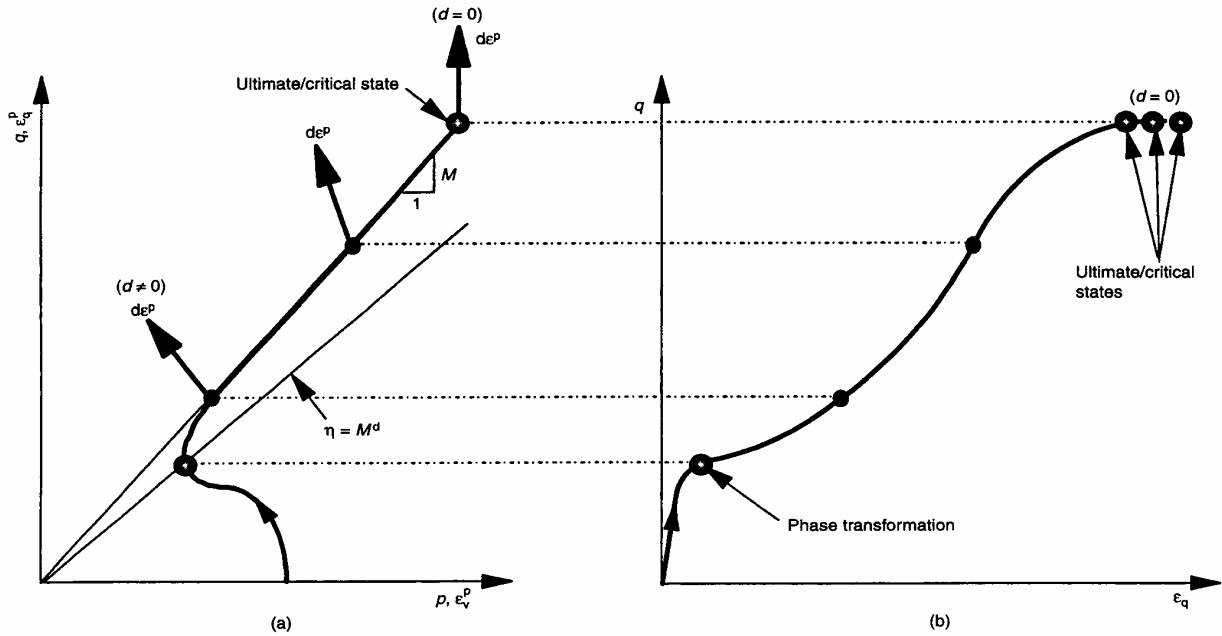


Fig. 5.24 Illustration of the dilative shear response: (a) stress path; (b) stress-strain response (after Li and Dafalias, 2000).

The explicit incorporation of  $e$  in a constitutive model elegantly groups the various soil response characteristics within a unified plasticity framework. Thus, a soil may be initially contractive or dilative, depending on whether its initial state is on the looser or denser side of the CSL (Fig. 5.23b); In addition, the soil may develop flow liquefaction or undergo cyclic mobility, depending on the associated changes in  $e$  and  $p'$ . One additional benefit of the state-dependence modeling approach is its simplicity in model calibration. Instead of using a different set of parameters for the same soil at different void ratios, only a single set of parameters is needed for a given material (regardless of its initial void ratio).

### 5.5.2 Stress-Induced Anisotropy during Loading/Unloading

Experimental studies (e.g., Nemat-Nasser and Tobita, 1982) have shown that during cyclic shear loading, the rate of volume contraction (or pore-pressure buildup) within a particular loading cycle is proportional to the level of dilation (or pore-pressure reduction) experienced in the last cycle. This important aspect has been incorporated in the Manzari-Dafalias model (Dafalias and

Manzari, 199), by defining the rate of volume reduction during a contractive phase to be a function of the volume increase in the preceding dilative phase.

### **5.5.3 Inherent (Material) Anisotropy**

Different from stress-induced anisotropy, inherent anisotropy is often believed to develop during soil deposition (or sample preparation), and is not significantly modified by the subsequent loading process. Li (2001) introduced inherent anisotropy in his model through a modified stress tensor  $\sigma \cdot \mathbf{K}$  (where  $\mathbf{K}$  is a symmetric second order tensor representing the inherent material fabric, and is assumed constant throughout the loading process). This formulation has been shown (Li, 2001) to successfully reproduce the experimentally observed soil plastic response during the rotation of principal stress directions (while the magnitudes of the principal stresses remained constant). The reader is referred to the original publication (Li, 2001) for more details.

## **5.6 NEW TRENDS IN MODELING OF SOIL MECHANICS BEHAVIOR AND LIQUEFACTION**

So far, discussions were focused on modeling soil behavior based on continuum solid mechanics. In this approach, soil is treated as a continuous medium, and soil response is described in terms of various macroscopic stress and strain measures. In most continuum mechanics formulations, deformed soil possesses continuous displacement and stress fields. Combined with finite element (or finite difference) techniques, continuum soil mechanics has resulted in numerical practical application codes that are being used by the geotechnical engineering society.

In recent years, a number of alternative approaches in observation and modeling of soil mechanical behavior (liquefaction response) have advanced significantly. These advances not only provide us with more insights, but also help define the direction of further research for practical applications. In the following, some of these noteworthy advances are briefly discussed.

### ***Observation and Modeling of Shear Banding***

In order to look at soil behavior more closely, experimentalists are employing advanced visualization techniques such as X-ray Computed Tomography (CT). Results accumulated from these experiments revealed that the continuous stress and displacement fields may not hold under conditions of large shear deformations. In summary, the following observations have been reported (Finno et al., 1997; Han and Vardoulakis 1991; Han and Drescher, 1993; Alshibli et al., 2000, Nemat-Nasser and Okada, 2001):

- (1) Under large shear deformations, non-uniformity in terms of concentration of shear deformations (the extreme of which is the development of shear bands) and redistribution of pore fluid seem to be an *intrinsic* characteristic of soil response. Observed material instability such as strain softening may be a direct consequence of strain localization mechanisms.
- (2) Strain localization typically initiates near a boundary or material imperfection, eventually leading to full development of shear bands. Shear bands may develop in soils under various conditions, whether dry or saturated, at a dense state or a loose state, under plane-strain shear, torsional shear, triaxial compression/extension, and other general loading situations. Once the shear band is formed, intense shear straining concentrates within the band, and the material response outside the band is nearly elastic.
- (3) The critical-state or steady-state soil response may occur only inside the shear bands, and not necessarily everywhere in a test sample.

The presence of such significant non-uniformity at large shear deformations can lead to much complexity in modeling efforts. To uniquely capture strain localization, it may be necessary to introduce a very small time scale (e.g., viscoplasticity approach, Loret and Prevost, 1990) or length scale (e.g., Cosserat continuum approach, Vardoulakis and Sulem, 1995) into the constitutive model. Either choice in turn requires very dense spatial and/or temporal discretization (i.e., small element sizes and/or time steps) when solving the field equations numerically (e.g., using finite element method).

An additional difficulty lies in the uncertainties in determining soil non-uniformity patterns in situ. Since triggering of strain localization is sensitive to boundary/material imperfections, reliable modeling of this problem depends on accurate description of the initial non-uniform material state. In view of such challenges, satisfactory numerical simulation tools must be ultimately calibrated on the basis of field observations.

### ***Particulate Mechanics***

Parallel to the developments in continuum soil mechanics, the field of particulate mechanics (or granular mechanics) has advanced substantially in the last twenty years. These advances have resulted in the discrete element method (DEM), in which particles (or particle groups) interact with one another. The DEM has been employed with success in modeling the response of laboratory soil samples including strain localization and shear banding phenomena (e.g., Bardet and Proubet, 1991; Thomas and Bray, 1999). However, given the huge number of particles and large variations in particle size, shape, and voids distribution typically involved in actual geotechnical problems, practical usage of DEM remains a major challenge today.

Granular mechanics also provides a physical basis for constitutive modeling using continuum soil mechanics. By investigating the response characteristics of individual soil particles and using statistical methods to sum-up the contribution of each particle to the overall response, researchers have been able to simulate many macroscopic phenomena such as shear-induced contraction, dilation, strain softening, and anisotropy. With the aid of these micromechanical insights, continuum soil mechanics has seen significant recent advances.

### ***Fluid Mechanics for Modeling Liquefaction***

Recently, a number of researchers (mainly in Japan) explored the possibility of formulating soil post-liquefaction response within a fluid mechanics context. This approach has been successful to a certain extent in simulating 1D soil lateral spreading response (e.g., Hamada, 1999).

## 5.7 IMPLEMENTATION ISSUES

The preceding sections of this chapter have described state-of-the-art approaches to constitutive modeling of liquefiable soil behavior. In order for PBEE to fully benefit from these new and advanced models, the models must be implemented into the PBEE framework described in Chapter 3. The implementation process raises important issues such as how the models are to be calibrated and how uncertainty is to be characterized.

### 5.7.1 Model Calibration

As described in Section 5.3.3, an advanced model such as the UCSD liquefaction model can be calibrated from the results of conventional (e.g. monotonic and cyclic, drained and undrained triaxial) tests. By performing a series of tests intended to illustrate various aspects of the response of the soil, the parameters that control the model's ability to represent those aspects of response can be verified.

While the testing and parameter identification portions of the laboratory-based calibration procedure are relatively straightforward, the acquisition/preparation of representative test specimens is not. Because the rate of excess pore-pressure generation has been shown to be sensitive to soil characteristics that are very difficult to replicate in reconstituted specimens (Section 2.3.2), testing of undisturbed specimens is required for accurate laboratory test-based model calibration. The use of unrepresentative laboratory test specimens can result in statistical bias (i.e. systematic underprediction or overprediction) of model-predicted rates of excess pore-pressure generation and/or other aspects of liquefiable soil behavior. The acquisition of undisturbed samples of liquefiable soil, however, generally involves ground freezing and coring, a process that is so expensive as to be practical only on rare occasions.

An alternative approach is to define the constitutive model parameters as functions of a smaller number of parameters that reflect in situ soil characteristics and are commonly available to practicing geotechnical engineers. Calibration on the basis of such characteristics as relative density or penetration resistance offers convenience and practicality, but is likely to produce less accurate predictions of response than would be obtained through soil-specific model calibration.

### **5.7.2 Uncertainty**

The PEER framework for PBEE, which applies to performance assessment and to performance-based design, is probabilistic in nature. As such, uncertainties in the parameters and models used to predict performance are important and must be quantified. This uncertainty can be considered to consist of two primary components: (1) intrinsic or inherent randomness in soil characteristics (e.g., density, penetration resistance, grain size characteristics, etc.) and (2) uncertainty in the predictive capabilities of the models used to assess performance, i.e., “model uncertainty.”

Sufficient laboratory data to characterize uncertainty in all of the parameters of a particular constitutive model, particularly those that control response under cyclic loading conditions, have not been compiled and documented in the engineering literature. Uncertainties in a number of relevant soil properties have been compiled for typical soils; a summary of those available in the literature is presented in the PEER report by Jones et al. (2001).

Model uncertainty is typically evaluated by statistical comparison of measured and model-predicted response for problems in which the input conditions are known. Ideally, a liquefaction model would be evaluated on the basis of its ability to predict the observed response of a series of full-scale liquefaction case histories in which all inputs (i.e., ground motions, site conditions, and soil properties) were known. Unfortunately, available full-scale case histories generally lack detailed information on one or more of these inputs; consequently, the difference between observed and model-predicted response may include effects of randomness in addition to those of model uncertainty. Isolation of model uncertainty requires response data for problems in which the inputs are well known or controlled. Physical model tests, such as geotechnical centrifuge tests, probably offer the best means for evaluation of model uncertainty.

### **5.7.3 Discussion**

In order to evaluate and/or predict the influence of liquefiable soil on the performance of structures, advanced constitutive models of the type described in this report will need to be implemented into the OpenSees analytical platform and into the probabilistic PBEE framework. Realization of the full benefits of these models will require evaluation of calibration procedures, possibly including multiple “levels” of calibration based on different levels of soil data, and of the uncertainty associated with each. Characterization of model uncertainty, likely through

comparisons of model predictions with response observed in geotechnical centrifuge tests, will be an important part of the verification/validation of OpenSees.

## **5.8 SUMMARY**

A number of key issues related to the state of the art in numerical modeling of liquefaction were discussed. Emphasis was placed on the consequences of liquefaction from the viewpoint of accumulated shear deformations, and ground settlement mechanisms. Foremost among these issues are the mechanisms of: (1) cyclic mobility and the complex shear-volume interaction and (2) estimation of site permeability variation and influence on resulting deformations. The above mechanisms directly influence the magnitude of liquefaction-induced deformations, and must receive much attention in future research efforts.

In this chapter, computational results were presented as pilot efforts to simulate the effects mentioned above. These results demonstrated the significance of these mechanisms from the performance-based engineering point of view. This in turn helps to dictate the path toward needed experimental data, and appropriate experimentation techniques. In this regard, PEER is integrating all liquefaction-related experimental results with parallel numerical efforts, within a unified framework. In addition, data from full-scale seismic observations remain a main source of calibration and validation.

## **6 Research Needs and Future Directions**

### **6.1 INTRODUCTION**

One of PEER's primary goals is the development of tools that support the advancement of performance-based earthquake engineering. After development and appropriate validation, PEER intends to make these tools available to the engineering community. An important tool, in the form of a computational platform (OpenSees) has been developed to facilitate incorporation of latest research findings into useful analytical tools. This computational platform will be employed by many PEER researchers as a common basis for prediction of the performance of soil-structure systems. PEER will ultimately develop analytical tools available through Internet-based distributed/parallel computational environments. A related ongoing effort involves development of an interactive website for on-line execution of a site amplification/liquefaction computational program (CYCLIC1D at <http://cyclic.ucsd.edu>).

This chapter describes research needs and anticipated future PEER research directed toward evaluation of the performance of structures founded on or near liquefiable soils. Preliminary steps taken in some of these research directions are also described.

### **6.2 RESEARCH NEEDS**

The preceding chapters have described current procedures that contribute to estimating the performance of structures founded on or near liquefiable soils. Also identified were a number of issues that need to be addressed in order to improve the earthquake engineering profession's ability to predict such performance accurately.

With respect to liquefaction, current research needs can be broken into three main categories: investigation of liquefaction behavior, development of predictive tools, and

collection of field data. These three categories are closely related, and an integrated program of research in all three should move forward.

### **6.2.1 Investigation of Liquefaction Behavior**

As emphasized throughout this report, advances in prediction of the effects of liquefaction on performance will require improved understanding of the behavior of liquefiable soil, i.e., the response to loading after initial liquefaction has been reached.

Among the most important of these fundamental research needs is characterization of post-liquefaction stress-strain behavior. Improved understanding of the manner in which strain accumulates during the contractive phase and stiffness increases during the dilative phase of post-liquefaction behavior is needed. This need should be addressed by laboratory (element) testing and model (centrifuge) testing on a variety of potentially liquefiable soils so that the soil characteristics that influence post-liquefaction stress-strain behavior can be identified.

Improved procedures for estimation of residual strength are needed, and the relationship between residual strength, steady-state strength, and quasi-steady-state strength must be clarified and defined with respect to performance-based earthquake engineering. Ongoing research is addressing the problem of steady-state strength and residual strength, but integration with other ongoing experimental research involving quasi-steady-state behavior is needed.

Improved understanding of the hydraulic aspects of liquefaction, i.e., porewater pressure redistribution and dissipation, is needed. Experimental testing of non-homogeneous specimens (i.e., specimens with spatially variable permeability) and model testing would provide useful data for evaluation of the relationship between permeability gradients and increased permanent displacements. This work would also lead to advances in the prediction of delayed flow slides, which have been observed in numerous earthquakes and are not addressed by current liquefaction hazard evaluation procedures.

### **6.2.2 Development of Predictive Tools**

Because the behavior of liquefiable soils is so complex, prediction of the performance of structures founded on or near liquefiable soils requires the use of advanced numerical analyses.

The accuracy of these analyses will depend on the accuracy of the constitutive model(s) used to represent the behavior of the soil, and on the capabilities of the analysis to represent the interaction of soils with elements such as foundations, retaining structures, etc.

As described in the following section (Section 6.3), PEER researchers have been adding geotechnical capabilities, including capabilities for modeling liquefiable soils, to a numerical analysis platform. This work, which is currently focusing on development of solid elements, implementation of constitutive models, development of interface elements and transmitting boundaries, and implementation of pile-soil interaction ( $p$ - $y$  and  $t$ - $z$ ) elements, should continue and be followed by thorough validation of the performance of each of those components by comparison with experimental (element and model test) results.

### **6.2.3 Collection of Field Data**

The ultimate test of performance prediction will come from the careful evaluation of case histories in which liquefaction occurred and influenced the performance of structures. Recent earthquakes in Turkey and Taiwan have produced numerous case histories of soil liquefaction. In some cases, particularly in Taiwan, the case histories are accompanied by ground motion recordings in closer proximity than have been available in most historical earthquakes. PEER's ongoing efforts at documenting case histories of liquefaction and lateral spreading in Turkey should be continued and expanded to other areas where such behavior has been observed.

### **6.3 OpenSees**

The Open System for Earthquake Engineering Simulation (OpenSees, <http://opensees.berkeley.edu/>) is a PEER sponsored project to develop a software framework for simulating the seismic response of structural and geotechnical systems (under the Direction of Professor Gregory Fenves, UC Berkeley). OpenSees is intended to serve as the computational platform for research in performance-based earthquake engineering at PEER. The core development team for the initial development of the project are all members of PEER; however as the framework grows it is hoped the development team will grow to include others in the larger engineering community. To encourage this growth, OpenSees is open source, i.e., the source code is available for free to anyone who wishes to use it.

### 6.3.1 Available Geotechnical Capabilities

Through its recent course of rapid development, OpenSees has built up very strong capabilities for dynamic analyses of elastic/inelastic structures by solving large systems of equations. Recently, a number of PEER researchers from UC Berkeley, UC Davis, UC San Diego, and U. Washington have been working very closely to develop and incorporate geotechnical components into OpenSees. This collaborative effort resulted in a significant contribution to the geotechnical capabilities of OpenSees. Specifically, the currently available elements and materials in OpenSees of geotechnical interests include

Element Type	Usage	Developed at
4-node quadrilateral element	2D drained soil domain	UC Berkeley
4-node mixed quadrilateral element	2D undrained (nearly incompressible) soil domain	UC Berkeley
8-node brick element	3D concrete or soil domain	UC Davis
Interface element	3D pile-soil interaction ( $p$ - $y$ and $t$ - $z$ ) effects and transmitting boundary effects	UC Berkeley

Material Type	Usage	Developed at
Pressure independent soil material	Undrained clay under fast loading	UC San Diego
Pressure dependent soil material	Sand, silt, and gravel materials (please see Chapter 5 for more details)	UC San Diego
Undrained fluid material (see note below)	An elastic material with very large bulk modulus and zero shear modulus to represent undrained fluid.	UC San Diego
Viscoelastic material	Lysmer-type transmitting boundary	U. Washington
Gap material	Gap in soil-pile contact problems	UC Berkeley

*Note:* Undrained fluid material can be coupled with pressure dependent/independent materials to analyze soil response under undrained loading conditions (numerical technique in OpenSees).

In addition, a generic template (developed at UC Davis) for easy implementation of a wide range of soil plasticity models has also been included (Figure 6.1). This template allows a user to create a new soil model in OpenSees by (1) supplying a yield function, a plastic potential

function, and a hardening rule and (2) selecting a built-in stress integration rule (e.g., forward or backward Euler). During computation, OpenSees will automatically update elasto-plastic stress/strain states, and calculate the corresponding tangent stiffness.

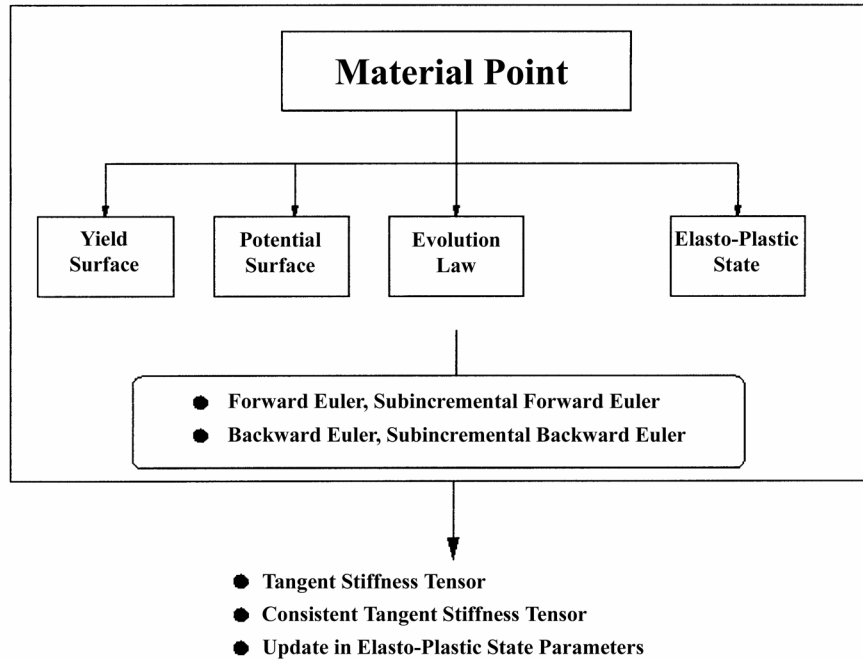


**Fig. 6.1 Schematic of a generic template for soil plasticity model generation (Professor Boris Jeremic, UC Davis).**

### 6.3.2 Validation

Validation of the geotechnical components has always been an integral part of the OpenSees development process. The “open” nature of the OpenSees platform allows for easy interaction and collaboration between members of the development team during both development and validation activities. This validation effort includes

- 2D modeling of an actual bridge site (UC San Diego, Figure 6.2). An actual bridge site (the Middle Channel bridge at Humboldt Bay, Eureka, California) is modeled using OpenSees, for probabilistic fragility analysis of bridge systems (a project in PEER Thrust Area 5). Initially, the bridge is modeled as an elastic beam-column system, and the surrounding soil as plastic materials. Viscoelastic materials are also deployed along the

two lateral sides of the mesh to better reflect energy radiation effects. Dynamic analyses are currently being conducted with this model to simulate bridge response under various strong shaking scenarios.

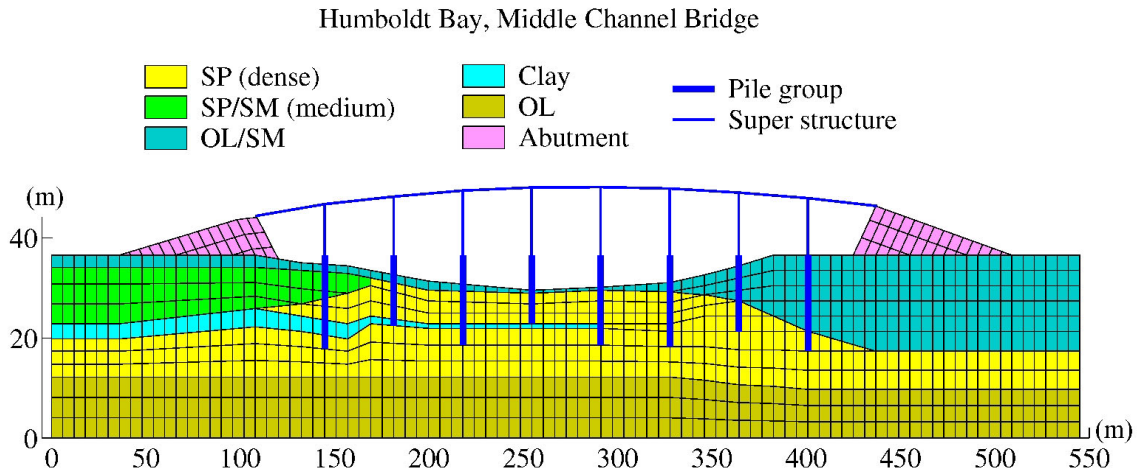


**Fig. 6.2 Two-dimensional modeling of Humboldt Bay, Middle Channel Bridge using OpenSees (UC San Diego).**

- 3D modeling of soil-pile interaction (UC Davis, Figure 6.3). A representative pier-foundation system of the above bridge (Figure 6.2) is modeled along with the surrounding soil using 3D brick elements. The 3D modeling enables more detailed study of soil-pile interaction effects that might not be fully accounted for by 2D modeling alone. Currently, the soil is modeled as a plastic material, and the pier-piles as an elastic material.

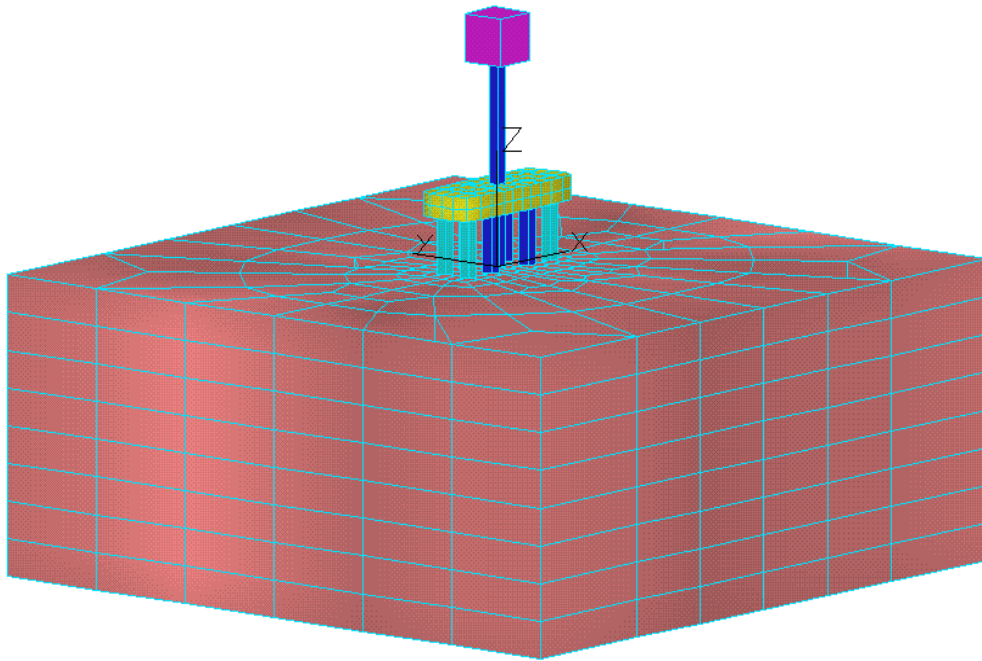


**Fig. 6.3 Three-dimensional modeling of soil-pile interaction using OpenSees (UC Davis).**

- 2D simulation of transmitting boundary effects (U. Washington, Figure 6.4). When a 2D rectangular mesh is subjected to a surface shear pulse, Figure 6.4. shows that (a) with a completely fixed boundary, energy input due to the shear pulse is trapped inside the mesh (observe nodal oscillation on the left part of Fig. 6.4) and (b) with a properly deployed transmitting boundary, the input energy can be completely absorbed at the boundary (the right part of Figure 6.4).

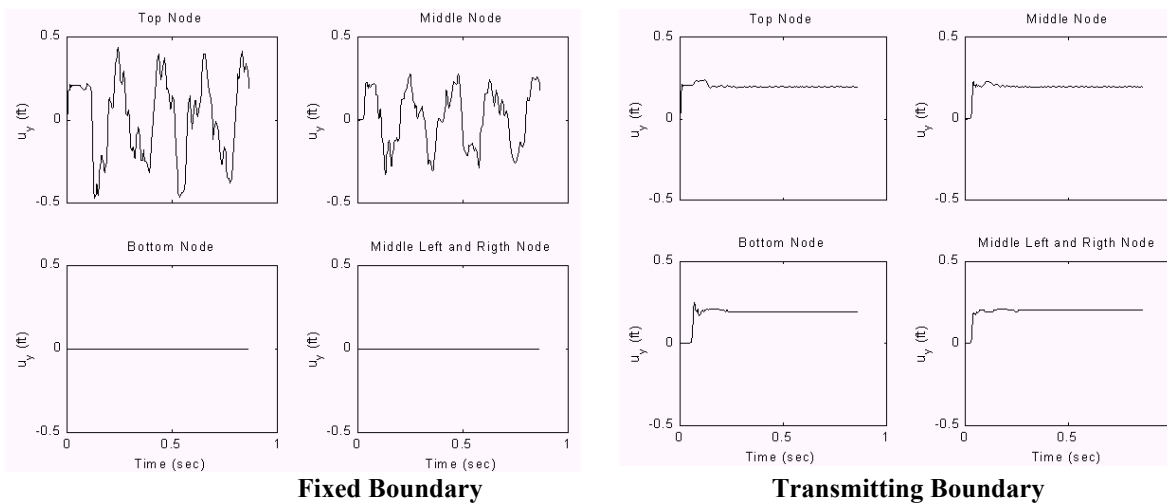
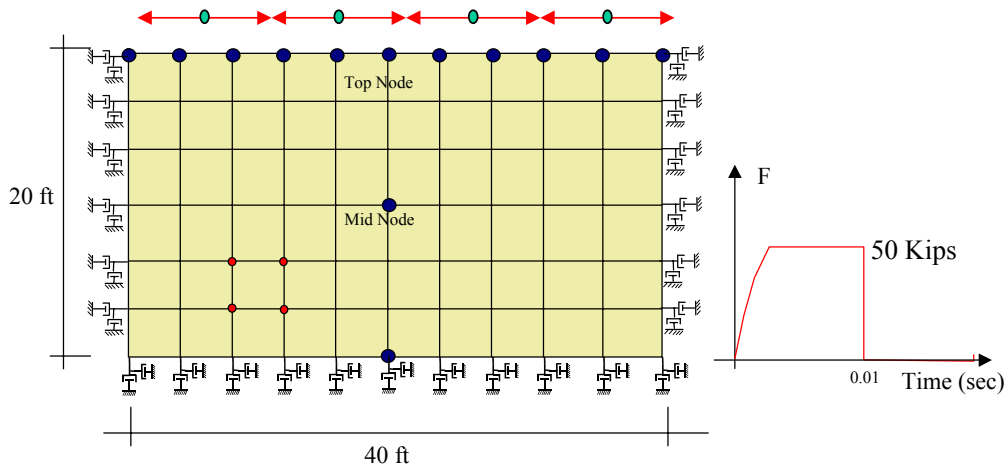


**Fig. 6.4 2D simulation of transmitting boundary effects using OpenSees (U. Washington).**

As more geotechnical/structural capabilities become available in OpenSees, the above models (Figures 6.2–6.4) will be further refined in order to achieve more accurate results.

### 6.3.3 Further Development

OpenSees is currently in a period of rapid growth. Current plans for further development of geotechnical components include a solid-fluid fully coupled formulation to more accurately represent porewater pressure generation, redistribution, and dissipation effects. Additional features that will be needed for more complete and reliable performance predictions include large-deformation capabilities and other well-established transmitting boundary techniques.

Incorporation of parameter sensitivity and optimization capabilities to facilitate performance-based earthquake engineering requirements is also under discussion. As more researchers and engineers are involved in this geotechnical development effort, it can be expected that a large library of user provided elements and materials will be generated and accessible to the general public.

## **6.4 INTERACTIVE WEBSITE**

PEER will ultimately make analytical tools (including OpenSees) available through Internet-based distributed/parallel computation environments. One ongoing effort along this line has been the development of an interactive website CYCLIC1D (<http://cyclic.ucsd.edu>). This website allows remote users to operate a two-phase (solid and fluid) fully coupled nonlinear finite element program (CYCLIC) developed for numerical simulation of earthquake ground response and liquefaction effects (see Chapter 5 for more details). Remote users can select the desired model parameters and excitation signal, run the computational code CYCLIC1D, and view/retrieve the computation results — all via a web browser. The experience gained from this website development exercise will help make other PEER analytical tools available over the Internet in the near future.

### **6.4.1 Website Available Functionality**

#### ***Predefined Material Library***

The library includes sand (loose to dense), silt, and clay materials. Each material has a set of predefined parameters. Calibration of model parameters for medium Nevada sand has been carried out. In the near future, the calibration process and effects of each parameter will be available in detail on the webpage.

#### ***Online 1D Soil Profile Generation***

The user can generate a 1D soil profile by specifying:

- (1) Soil profile height (any value from 5 m to 100 m),

- (2) Number of elements (10 – 100 elements),
- (3) Depth of water table,
- (4) Inclination angle of the soil profile (any value from 0.0 to 10.0 degrees can be chosen, with 0.0 degree representing level ground), and
- (5) Material type (each layer may be assigned a different material type, chosen from the above-described material library).

In the future, a library of 2D predefined meshes (e.g., for site-amplification, embankments, retaining wall/Quay wall, soil-foundation interaction) will be available, and the user will be able to modify the spatial properties of these meshes. Interested users may also submit their own finite-element mesh.

### ***Input Motion Library***

The input motion library includes a number of earthquake records (and harmonic excitations). A remote user can scale the amplitude and/or duration (frequency content) of a selected input motion. Shortly, the library will be extended to include a wide range of earthquake records covering a wide range of peak accelerations, strong motion duration, and frequency content (e.g., PEER strong motion records, <http://peer.berkeley.edu/research/motions>). A user-defined input motion submitted over the Internet will be an available option.

### ***Transmitting Boundary Option***

This option allows an input dynamic excitation to be specified as either a total motion (rigid base) or an incident motion (elastic halfspace).

## **6.4.2 Presentation of Results**

The computed results are graphically displayed over the Internet in terms of response histories including acceleration (and the corresponding response/Fourier spectra), velocity, displacement, excess pore pressure, shear stress, and shear strain (Figures 6.5–6.7). Animation of the excess pore pressure, acceleration, and displacement profiles during the shaking phase is also available. All output graphs and data files are available for downloading.

### Example Website Results

Figures 6.5 – 6.7 show the numerical simulation results of a 10-m-thick, medium dense ( $D_r$  of about 40%) clean Nevada sand stratum in a mild-slope situation (0.2g, 1 Hz sinusoidal motion, at a slope of  $6^\circ$ ). In Figure 6.6, the acceleration near the ground surface is seen to display asymmetric response with spikes that are directly related to the instances of excess pore-pressure drop during liquefaction. Associated shear deformation (lateral spreading) can also be seen to accumulate on a cycle-by-cycle basis (Figure 6.6). In Figure 6.7, the cyclic mobility characteristics are displayed in terms of: (1) high stiffness and strength in the shear stress-strain response during liquefaction, (2) phases of increase in shear strength (and increase in effective stress) as the stress path travels above the phase transformation line during cyclic loading, and (3) accumulation of permanent downslope shear strain.

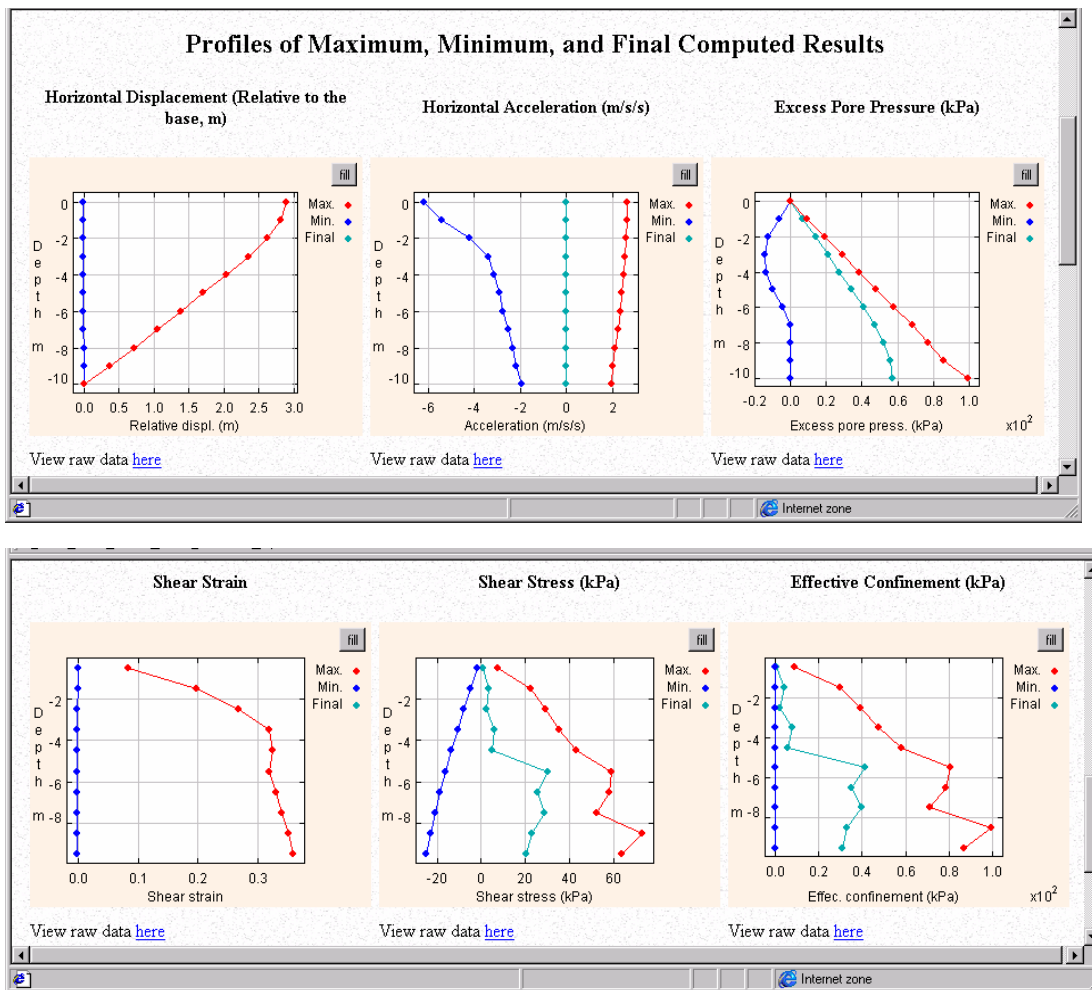
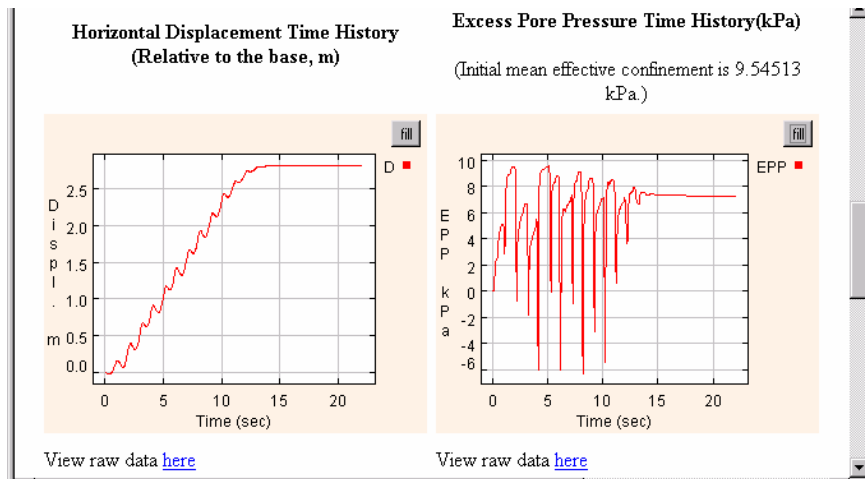
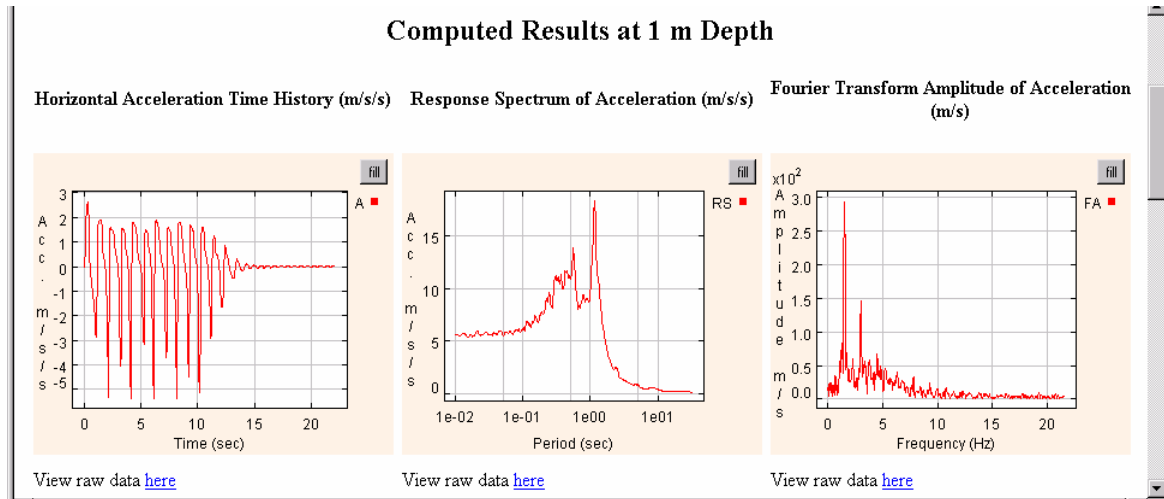
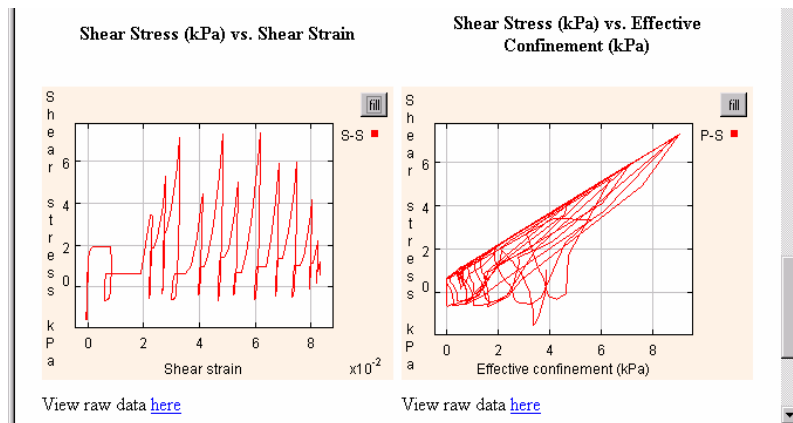


Fig. 6.5 Sample profiles of maximum, minimum, and final computed results (<http://cyclic.ucsd.edu>).



**Fig. 6.6** Sample computed acceleration, lateral displacement and excess pore-pressure histories at 1m depth (<http://cyclic.ucsd.edu>).



**Fig. 6.7** Sample computed shear stress-strain and stress path at 1.5m depth (<http://cyclic.ucsd.edu>).

## 6.5 SUMMARY

With respect to liquefaction, current research needs can be broken into three main categories: investigation of liquefaction behavior, development of predictive tools, and collection of field data. These three categories are closely related, and an integrated program of research in all three should move forward. Among the most important of these fundamental research needs is characterization of post-liquefaction stress-strain behavior (shear-volume interaction, role of permeability, and permeability variation). This work will lead to advances in the prediction of delayed flow slides, which have been observed in numerous earthquakes and are not addressed by current liquefaction hazard evaluation procedures. The above needs should be addressed by laboratory (element) testing and model (centrifuge) testing on a variety of potentially liquefiable soils so that the soil characteristics that influence post-liquefaction stress-strain behavior can be identified.

Improved procedures for estimation of residual strength are needed, and the relationship between residual strength, steady-state strength, and quasi-steady-state strength must be clarified and defined with respect to performance-based earthquake engineering. Ongoing research is addressing the problem of steady-state strength and residual strength, but integration with other ongoing experimental research involving quasi-steady-state behavior is needed.

The PEER OpenSees computational platform is progressing well, and will be a valuable simulation tool for soil and soil-structure interaction problems. The “open” available-to-all philosophy, and the broad range of structural and geotechnical contributions will make this a unique simulation environment. Planned Internet and parallel-processing (distributed computing) capabilities will further extend and facilitate use by all interested parties. The emphasis placed by PEER on calibration of available OpenSees soil models is among the main strengths (and distinguishing elements) from the geotechnical engineering point of view.

## **7 Summary and Conclusions**

At many sites, buildings, bridges, and lifelines are influenced by the presence of liquefiable soils. Liquefaction can strongly influence the seismic performance of such structures during earthquakes. The earthquake engineering literature contains many examples of the unsatisfactory performance of structures due to soil liquefaction. This chapter summarizes the main effects of liquefaction on the performance of structures, summarizes contemporary issues in liquefaction modeling, and describes PEER's contributions to improved liquefaction modeling. It also presents a series of conclusions regarding the modeling of liquefaction for performance prediction.

### **7.1 EFFECTS OF LIQUEFACTION ON PERFORMANCE**

Liquefiable soils can affect performance by influencing the amplitude, frequency content, and duration of the ground motions transmitted to the base of a structure. The generation of high porewater pressure associated with liquefaction produces a softening effect that can reduce the amplitude of high-frequency components of ground surface motions following the initiation of liquefaction; depending on when liquefaction is triggered, this effect can actually shield a structure from high ground surface accelerations. The low-frequency components of the motion, however, may produce large lateral ground surface (and subsurface) displacements.

Liquefaction can also produce permanent soil deformations that can influence the performance of structures. Permanent deformations are generally small on level-ground sites, but they can be substantial at sites that slope even very gently. The process of cyclic mobility is manifested in the field as lateral spreading, which can produce lateral displacements that vary from negligible to several meters. Because such deformations occur with an irregular spatial pattern, they can impose large differential displacements, and hence large loads, upon structures

and/or the foundations that support them. Flow slides can be triggered in sloping deposits of very loose saturated soil; though rare, the large distances and rapid speed of the soil movement in a flow slide can cause devastating damage to structures.

Because liquefaction can dominate the seismic performance of even very well-designed structures, prediction of its effects is an important part of the practice of performance-based earthquake engineering. As a result, PEER has worked toward the development of improved procedures and tools for estimating the effects of liquefaction on site response and the nature of liquefaction-induced ground failure.

## **7.2 CONTEMPORARY ISSUES**

Improvement of the earthquake engineering profession's ability to predict the performance of structures influenced by liquefiable soils requires improved understanding of the mechanical and hydraulic behavior of liquefiable soils. Over the years, considerable attention has been paid to the problems of liquefaction susceptibility and initiation of liquefaction; conservative procedures for evaluation of liquefaction potential are now available and widely used in earthquake engineering practice. The prediction of performance, however, is more closely related to the effects of liquefaction than to liquefaction potential. Research conducted over the past 10–15 years has illuminated several aspects of the behavior of liquefied soil that can strongly influence the effects of liquefaction.

The tendency of liquefiable soils to exhibit both contractive and dilative behavior during shear plays a strong role in determining seismic performance. The softening associated with contractive behavior can influence site response, but can also affect the level of permanent displacement in sloping ground. The stiffening that occurs under large strain excursions in the dilative regime can affect site response by producing significant acceleration spikes; this stiffening also tends to arrest the development of permanent downslope deformations in sloping ground. Relatively little experimental data are currently available from which to interpret the fundamental behavior of soils that have liquefied.

Geotechnical engineers have struggled with estimation of the residual strength of liquefied soil for many years. Laboratory- and field-based procedures for estimation of residual strength are available, but very large levels of uncertainty are associated with each. Part of the

practical difficulty in estimating residual strength lies in the complex behavior of soils of intermediate density, in which the tendency for contraction (at low shear strain levels) and dilation (at high shear strain levels) can lead to alternating periods of strain-softening and strain-hardening behavior. The strain-softening behavior can lead to a local minimum in shearing resistance at intermediate strain levels — this shearing resistance has been referred to as the quasi-steady-state strength. Depending on stress and density conditions, the quasi-steady-state strength may be slightly lower to much lower than the steady-state strength, which is only reached at very high strain levels. Case histories used to estimate residual strength by back-calculation, however, likely contain cases where both the quasi-steady-state strength and the steady-state strength were mobilized. The determination of residual strength, whether under quasi-steady-state or steady-state conditions, and identification of the factors that affect it, remain important issues in liquefaction research.

In numerous earthquakes liquefaction-induced flow slides have been observed to occur well after the cessation of ground shaking. Such slides result from the redistribution of excess porewater pressure that occurs both during and after earthquake shaking. Analytical and experimental research suggests that delayed failures tend to occur at sites with spatially variable permeability. In particular, the existence of low-permeability soils such as layers, or even lenses, of silt or clay can cause porewater pressure to increase and porewater to accumulate in their vicinities. The reduced effective stress associated with increased porewater pressure causes the soil skeleton to rebound, which reduces the available residual strength of the soil. Because residual strength is sensitive to soil density, relatively small degrees of rebound may lead to large reductions in residual strength. Additional research is needed to allow identification of the conditions under which delayed slides due to pore-pressure redistribution can occur, so that their potential effects on performance can be characterized and predicted.

### **7.3 PEER ACCOMPLISHMENTS**

Since its inception, PEER has devoted considerable resources to the problem of soil liquefaction in both its Core and Lifelines research programs. The research performed with this support has led to improved understanding of the mechanics of liquefiable soils, to improved constitutive

models for liquefiable soil, to new analytical tools for evaluation of liquefiable soil response, and to improved databases of actual liquefaction behavior.

The Core research program has focused on fundamental aspects of liquefiable soil behavior and on the development of tools that allow that behavior to be represented in dynamic site response and soil-structure interaction analyses. This work has included the development and validation of constitutive models capable of representing important aspects of liquefiable soil behavior (PI: Elgamal), experimental testing focusing on the post-liquefaction behavior of individual soil elements (PIs: Seed and Pestana), experimental model testing using a large geotechnical centrifuge with complementary constitutive model development (PIs: Kutter and Dafalias), and experimental/analytical investigation of the residual strength of liquefied soil (PI: Kramer). This work has been conducted in a collaborative manner; for example, element tests were performed at Berkeley at the request of constitutive modelers at San Diego, Davis, and Washington. The Core program, looking ahead to the development of performance-based procedures for liquefaction mitigation, has also supported investigations of the performance of various soil improvement techniques in actual earthquakes (PI: Sitar).

The PEER Lifelines research program has supported practical liquefaction research with demonstrable short-term benefits. A detailed, critical review and re-interpretation of the data on which empirical liquefaction potential evaluation procedures are based was combined with sophisticated statistical analyses to produce a probabilistic procedure for evaluation of liquefaction potential with greatly reduced uncertainty (PIs: Seed and Der Kiureghian). Additional Lifelines program research has led to an expanded and improved database of lateral spreading case histories, and to a straightforward procedure for probabilistic estimation of ground surface displacement (PI: Bardet). The Lifelines program has also supported field investigations of liquefaction sites in Turkey (PIs: Bray and Stewart), the high quality of which will add significantly to the total database of liquefaction case histories.

## **7.4 CONCLUSIONS**

Geotechnical engineers have been studying soil liquefaction intensely since its effects were so dramatically revealed in the 1964 Niigata and Alaska earthquakes. The profession has

developed reasonable procedures for evaluating the susceptibility of soils to liquefaction and for evaluating the level of loading required to initiate liquefaction.

Most liquefaction research to date has focused on the evaluation of liquefaction potential, i.e., on the behavior of the soil up to the point of initial liquefaction. Accurate prediction of the performance of structures founded on or near liquefiable soils requires the capability of modeling the most important aspects of the behavior of liquefiable soil, both up to and, particularly, after the initiation of liquefaction. Additional experimental work, involving both soil element and model testing, is needed to elucidate the response of liquefiable soils over a wide range of stress and strain conditions.

Because the behavior of liquefiable soils is complex, and because performance-based earthquake engineering seeks to predict a virtually continuous range of performance levels, the development and validation of numerical models of liquefiable soil are necessary. These models should be capable of representing the most important aspects of the behavior of liquefiable soils, i.e., they should realistically model nonlinear inelastic behavior, phase transformation behavior, quasi-steady-state and steady-state behavior, and porewater pressure redistribution/dissipation. To be useful, these models should be of a form that can be calibrated using the type of information that is commonly available to geotechnical engineers. The models should be validated by comparing their predictions with the results of laboratory element and model tests, and with full-scale behavior from well-documented case histories.

The existence of numerical models with these capabilities will benefit the development of performance-based earthquake engineering in several ways. They will, when implemented into an analytical platform such as OpenSees, allow direct analysis of soil-foundation-structure interaction involving liquefiable soils. They will also be useful, through sensitivity and uncertainty analyses, for identification of the parameters that most strongly influence performance. Such efforts can be used to identify the required parameters, and even the optimum mathematical form, for simplified, empirical (regression-based) performance prediction relationships. These models can also be used to guide the development of performance-based design procedures for liquefaction hazard mitigation by soil improvement.

PEER has taken a number of steps necessary to develop improved procedures and tools for evaluating performance at liquefiable soil sites, and is continuing work in that direction. Continuation and completion of this work will eventually result in more accurate, reliable, and

cost-effective procedures for evaluating and mitigating the effects of soil liquefaction on the performance of structures.

## References

- Adalier, K. (1992). Post-liquefaction behavior of soil systems. Masters thesis. Rensselaer Polytechnic Institute. Troy, N.Y.
- Adalier, K. (1996). Mitigation of earthquake induced liquefaction hazards. Ph.D. thesis. Troy, N.Y.: Department of Civil Engineering, Rensselaer Polytechnic Institute.
- Adalier, K., Elgamal, A.-W., and Martin, G. R. (1998). Foundation liquefaction countermeasures for earth embankments. *J. Geotechnical and Geoenvironmental Engineering* 124(6): 500–17. ASCE.
- Alarcon-Guzman, A., Leonards, G. A., and Chameau, J. L. (1988). Undrained monotonic and cyclic strength of sands. *J. Geotechnical Engineering* 114(10): 1089–1108. ASCE.
- Alshibli, K. A., Sture, S., Costes, N. C., Frank, M. L., Lankton, M. R., Batiste, S. N., and Swanson, R. A. (2000). Assessment of localized deformations in sand using X-ray computed Tomography. *Geotechnical Testing J.* 23(3): 274–99. ASTM.
- Ambraseys, N., and Sarma, S. (1969). Liquefaction of soils induced by earthquakes. *Bull. Seismological Society of America* 59(2): 651–64.
- Anandarajah, K. (1993). VELACS project: Elasto-plastic finite element predictions of the liquefaction behavior of centrifuge models no. 1, 3 and 4a. In *Procs., International Conference on the Verification of Numerical Procedures for the Analysis of Soil Liquefaction Problems, October 1–20, Davis, California, USA*. Rotterdam: Balkema Publishers. K. Arulanandan and R. F. Scott, eds., vol. 1, 45–66.
- Andrus, R. D., and Stokoe, K. H. II (1997). Liquefaction resistance based on shear wave velocity. In *Procs., NCEER Workshop on Evaluation of Liquefaction Resistance of Soils*, pp. 89–128. Buffalo, N.Y.: National Center for Earthquake Engineering Research, State University of New York at Buffalo.
- Ansal, A., Bardet, J. P., Barka, A., Baturay, M. B., Berilgen, M., Bray, J., Cetin, O., Cluff, L., Durgunoglu, T., Erten, D., Erdik, M., Idriss, I. M., Karadayilar, T., Kaya, A., Lettis, W., Olgun, G., Paige, W., Rathje, E., Roblee, C., Stewart, J., and Ural, D. (1999). *Initial geotechnical observations of the November 12, 1999, Düzce earthquake*. A report of the Turkey-US geotechnical earthquake engineering reconnaissance team.

- Arduino, P., Kramer, S., and Baska, D. (2001). UW-sand: a simple constitutive model for liquefiable soils. In *2001 Mechanics and Materials Summer Conference*, June 27–29, San Diego, CA.
- Arulanandan, K., Yogachandran, C., Muraleetharan, K. K., Kutter, B. L., and Chang, G. S. (1988). Laboratory flow slide during earthquake simulation. In *Centrifuge 88*, J.-F. Corte, ed., 539–44. Paris: Balkema Publishers.
- Arulanandan, K., and Scott, R. F., eds. (1993). *Procs., International Conference on the Verification of Numerical Procedures for the Analysis of Soil Liquefaction Problems, October 1–20, Davis, California, USA*. Rotterdam: Balkema Publishers. 2 vols.
- Arulmoli, K., Muraleetharan, K. K., Hossain, M. M., and Fruth, L. S. (1992). *VELACS: verification of liquefaction analyses by centrifuge studies, laboratory testing program, soil data report*. Report Project No. 90-0562. Irvine, Calif.: The Earth Technology Corporation.
- Ashford, S. A., and Rollins, K. (1999). *Full-scale behavior of laterally loaded deep foundations in liquefied sand: preliminary test results*. Report No. TR-99/03. San Diego, Calif.: Dept. of Structural Engineering, Univ. of California, San Diego.
- Aubry, D., Benzenati, I., and Modaressi, A. (1993). Numerical predictions for model no. 1. In *Procs., International Conference on the Verification of Numerical Procedures for the Analysis of Soil Liquefaction Problems, October 1–20, Davis, California, USA*, vol. 1, pp. 45–66. Rotterdam: Balkema Publishers.
- Balakrishnan, A., Kutter, B. L., and Idriss, I. M. (1997). *Liquefaction remediation at bridge sites — centrifuge data report for bam0*. Report UCD/CGMDR-97/10. Davis, Calif.: Center for Geotechnical Modeling, Univ. of California.
- Balakrishnan, A., and Kutter, B. L. (1999). Settlement, sliding and liquefaction of layered soil. *J. Geotechnical and Geoenvironmental Engineering* 125(11): 968–78. ASCE.
- Bard, Y. (1974). *Nonlinear parameter estimation*. New York and London: Academic Press.
- Bardet, J. P., and Proubet, J. (1991). A numerical investigation of the structure of persistent shear bands in granular media. *Géotechnique* 41(4): 599–613.
- Bardet, J. P., Huang, Q., and Chi, S. W. (1993). Numerical prediction for model no. 1. In *Procs., International Conference on the Verification of Numerical Procedures for the Analysis of Soil Liquefaction Problems, October 1–20, Davis, California, USA*, vol. 1, pp. 67–86. Rotterdam: Balkema Publishers.
- Bardet, J. P., Oka, F., Sugito, M., and Yashima, A. (1995). *The Great Hanshin Earthquake disaster*. Preliminary Investigation Report. Los Angeles: Dept. of Civil Engineering, Univ. of Southern California.

- Bartlett, S. F., and Youd, T. L. (1995). Empirical prediction of liquefaction-induced lateral spread. *J. Geotechnical Engineering* 121(4): 316–29. ASCE.
- Berrill, J. B., Christensen, R. J., Keenan, R. J., Okada, W., and Pettinga, J. R. (1997). Lateral spreading loads on a piled bridge foundation. In *Procs., Seismic Behavior of Ground and Geotechnical Structures*, Special Technical Session on Earthquake Geotechnical Engineering, “International. Conference on Soil Mechanics and Geotechnical Engineering,” pp. 173–83. Rotterdam: Balkema Publishers.
- Biot, M. A. (1956a). Theory of propagation of elastic waves in a fluid-saturated porous solid; i: Low-frequency range. *J. Acoustical Society of America* 28(2): 168–78.
- Biot, M.A. (1956b). Theory of propagation of elastic waves in a fluid-saturated porous solid; ii: higher-frequency range, *J. Acoustical Society of America*, 28(2): 179–91.
- Borja, R. I., Chao, H. Y., Montans, F., and Lin, C. H. (1999a). Nonlinear ground response at Lotung LSST site. *J. Geotechnical and Geoenvironmental Engineering* 125(3): 187–97. ASCE.
- Borja, R. I., Chao, H. Y., Montans, F., and Lin, C. H. (1999b). SSI effects on ground motion at Lotung LSST site. *J. Geotechnical and Geoenvironmental Engineering*, 125(9): 760–70. ASCE.
- Bouckovalas, G. D., Gazetas, G., and Papadimitriou, A. G. (1999). Geotechnical aspects of the 1995 Aegion, Greece, earthquake. In *Procs., 2<sup>nd</sup> International Conference on Earthquake Geotechnical Engineering*, vol. 2, pp. 739–48. Rotterdam: Balkema Publishers.
- Boulanger, R. W., Chan, C. K., Seed, H. B., Seed, R. B., and Sousa, J. B. (1993). A low-compliance bi-directional cyclic simple shear apparatus. *Geotechnical Testing J.* 16(1): 36–45. ASTM.
- Boulanger, R. W., and Seed, R. B. (1995). Liquefaction of sand under bidirectional monotonic and cyclic loading. *J. Geotechnical Engineering* 121(12): 870–78. ASCE.
- Boulanger, R. W., and Truman, S. P. (1996). Void redistribution in sand under post-earthquake loading. *Canadian Geotechnical J.* 33(5): 829–34.
- Boulanger, R. W., Mejia, L. H., and Idriss, I. M. (1997). Liquefaction at Moss Landing during Loma Prieta earthquake. *J. Geotechnical and Geoenvironmental Engineering* 123(5): 453–67. ASCE.
- Budhu, M. (1985). Lateral stresses observed in two simple shear apparatus. *J. Geotechnical Engineering* 111(6): 698–711. ASCE.

- Byrne, P. M., and McIntyre, J. (1994). Deformations in granular soils due to cyclic loading. In *Proceedings of Settlement 9, Texas*. Geotechnical Special Publication No. 40, pp. 1864–96. ASCE.
- Casagrande, A. (1936). Characteristics of cohesionless soils affecting the stability of earth fills. *J. Boston Society of Civil Engineers*, January: 13–33. Reprinted in *Contributions to soil mechanics 1925–1940*, vol. 1, pp. 257–76: Boston: Boston Society of Civil Engineers.
- Casagrande, A. (1975). Liquefaction and cyclic deformation of sands — a critical review. In *Procs., 5<sup>th</sup> Pan-American Conference on Soil Mechanics and Foundation Engineering, Buenos Aires, Argentina*; also published as *Harvard Soil Mechanics Series*, No. 88, January 1976. Cambridge, Mass.: [Harvard University].
- Castro, G. (1969). Liquefaction of sands. *Harvard Soil Mechanics Series 87*. Cambridge, Mass.: Harvard University.
- Castro, G., and Poulos, S. J. (1977). Factors affecting liquefaction and cyclic mobility. *J. Geotechnical Engineering Division 103 (GT6)*: 501–6. ASCE.
- Chan, A. H. C. (1988). A unified finite element solution to static and dynamic problems in geomechanics. Ph.D. dissertation. University College of Swansea, U.K.
- Chen, C. J., and Juang, C. H. (2000). Calibration of SPT- and CPT-based liquefaction evaluation methods. In *Innovations and applications in geotechnical site characterization*. Geotechnical Special Publication. ASCE.
- Dafalias, Y. F. (1994). Overview of constitutive models used in VELACS. In *Procs., International Conference on the Verification of Numerical Procedures for the Analysis of Soil Liquefaction Problems, Davis, California, USA, 17–20 October 1993*, K. Arulanandan and R. F. Scott., eds., vol. 2, pp. 1293–1304. Rotterdam: Balkema Publishers.
- Dafalias, Y. F., and Manzari, M. T. (1999). Modeling of fabric effect on the cyclic loading response of granular soils. In *Procs., ASCE 13<sup>th</sup> Engineering Mechanics Conference, 13–16 June, Baltimore, Maryland*.
- Davis, C. A., and Bardet, J. P. (1996). Performance of two reservoirs during the 1994 Northridge earthquake. *J. Geotechnical Engineering 122(8)*: 613–22. ASCE.
- Dobry, R., Taboada, V., and Liu, L. (1995). Centrifuge modeling of liquefaction effects during earthquakes In *Procs., 1<sup>st</sup> Int. Conference on Earthquake Geotechnical Engineering, Tokyo, Japan, 14–16 November 1995*, vol. 3, pp. 1291–1324. Rotterdam: Balkema Publishers.
- Dobry, R. and Abdoun, T. (1998). Post- triggering response of liquefied sand in the free field and near foundations. Keynote lecture. In *Procs., Geotechnical Earthquake Engineering and Soil Dynamics III, University of Washington, Seattle, Washington, August 3–6, 1995*. P.

Dakoulas, M. Yegian, and R. D. Holtz, eds., vol. 1, pp. 270–300. Geotechnical Special Publication No. 75. New York: ASCE.

Doroudian, M., and Vucetic, M. (1995). A direct simple shear device for measuring small-strain behavior. *Geotechnical Testing J.* 18(1): 69–85. ASTM.

Elgamal, A.-W., Dobry, R., and Adalier, K. (1989). Study of effects of clay layers on liquefaction of sand deposits using small-scale models. In *Procs., 2<sup>nd</sup> US-Japan Workshop on Liquefaction, Large Ground Deformation and Their Effects on Lifelines*, T. D. O'Rourke and M. Hamada, eds., vol. 1. pp. 145–60. Report NCEER-89-0032. Buffalo, N.Y.: SUNY-Buffalo.

Elgamal, A.-W., and Zeghal, M. (1992). Analysis of Wildlife site liquefaction during the 1987 Superstition Hills earthquake. In *Procs., 4<sup>th</sup> Japan-U.S. Workshop on Earthquake Resistant Design of Lifeline Facilities and Countermeasures against Soil Liquefaction, Tokai University Pacific Center, Hawaii, May 27–29, 1992*. Buffalo, N.Y.: NCEER, SUNY-Buffalo. Report No. NCEER-92-0019. M. Hamada and T. D. O'Rourke, eds., vol. 1, pp. 87–96.

Elgamal, A.-W., Zeghal, M., and Parra, E. (1996). Liquefaction of reclaimed island in Kobe, Japan. *J. Geotechnical Engineering* 122(1): 39–49. ASCE.

Elgamal, A.-W., Dobry, R., Parra, E., and Yang, Z. (1998). Soil dilation and shear deformations during liquefaction. In *Procs., 4th International Conference on Case Histories in Geotechnical Engineering, St. Louis, Missouri, March 8–15*. S. Prakash, ed., pp. 1238–59.

Fiegel, G. L., and Kutter, B. L. (1992). Liquefaction mechanism for layered soil. *J. Geotechnical Engineering* 120(4): 737–55. ASCE.

Finno, R. J., Harris, W. W., Mooney, M. A., and Viggiani, G. (1997). Shear bands in plane strain compression of loose sand. *Géotechnique* 47(1): 149–65.

Gill, P. E., Murray, W., and Wright, M. H. (1981). *Practical optimization*.: London; New York: Academic Press.

Hamada, M. (1992). Large ground deformations and their effects on lifelines: 1964 Niigata earthquake. In *Case studies of liquefaction and lifeline performance during past earthquakes*, T. D. O'Rourke and M. Hamada, eds., vol. 1, pp. 1–123. Technical Report NCEER-92-0002. Buffalo, N.Y.: National Center for Earthquake Engineering Research.

Hamada, M. (1999). Similitude law for liquefied ground flow. In *7th U.S. - Japan Workshop on Earthquake Resistant Design of Lifeline Facilities and Countermeasures against Liquefaction, August 15–17, 1999, Seattle, Washington*, T. D. O'Rourke, J. P. Bardet, M. Hamada, eds., pp. 191–205. Technical Report MCEER-99-0019. Buffalo, N.Y.: Multidisciplinary Center for Earthquake Engineering Research.

- Han, C., and Vardoulakis, I. (1991). Plane strain compression experiments on water-saturated fine-grained sand. *Géotechnique* 41(1): 49–78.
- Han, C., and Drescher, A. (1993). Shear bands in biaxial tests on dry coarse sand. *Soils and Foundations* 33(1): 118–32.
- Harder, L. F., and Stewart, J. P. (1996). Failure of Tapo Canyon tailings Dam. *J. Performance of Constructed Facilities* 10(3): 109–114. ASCE.
- Hill, R. (1950). *The Mathematical theory of plasticity*. London: Oxford University Press.
- Holzer, T. L., Youd, T. L., and Hanks, T. C. (1989). Dynamics of liquefaction during the 1987 Superstition Hills, California, earthquake. *Science* 244: 56–59.
- Housner, G. W. (1958). The mechanism of sandblows. *Bull. Seismological Society of America*, 48 (April): 155–61.
- Hushmand, B., Scott, R. F., and Crouse, C. B. (1992a). In-place calibration of USGS transducers at Wildlife liquefaction site, California, USA. In *Procs., 10<sup>th</sup> World Conference on Earthquake Engineering*, vol. 3, pp. 1263–68 Rotterdam: A.A. Balkema Publishers.
- Hushmand, B., Scott, R. F., and Crouse, C.B. (1992b). In-situ calibration of USGS piezometer installations. In *Recent advances in instrumentation, data acquisition, and testing in soil dynamics*, pp. 49–69. Geotechnical special publication no. 29. [Yokosuka, Japan]: ASCE.
- Iai, S. (1998). Seismic analysis and performance of retaining structures. In *Procs., Geotechnical Earthquake Engineering and Soil Dynamics III, Seattle, Washington, August 3–6*, P. Dakoulas, M. Yegian, and R. D. Holtz, eds., vol. 2, pp. 1020–44. Geotechnical Special Publication No. 75. New York: ASCE.
- Ishihara, K. (1984). Post-earthquake failure of a tailings dam due to liquefaction of the pond deposit. In *Procs., International Conference on Case Histories in Geotechnical Engineering, May 6–11, 1984, Univ. of Missouri-Rolla*, Shamsheer Prakash, ed., vol. 3, pp. 1129–43. St. Louis: Univ. of Missouri-Rolla.
- Ishihara, K. (1985). Stability of natural deposits during earthquakes. Theme lecture. In *Contributions to the 11<sup>th</sup> International Conference on Soil Mechanics and Foundation Engineering, San Francisco, 1985*, pp. 321–76. Norwegian Geotechnical Institute Publication 163 0078-1193. Oslo: Norges Geotekniske Institutt.
- Ishihara, K. (1996). *Soil behavior in earthquake geotechnics*. New York: Oxford University Press.
- Iwan, W. D. (1967). On a class of models for the yielding behavior of continuous and composite systems. *J. Applied Mechanics* 34: 612–17. ASME.

- Japanese Geotechnical Society (1996). *Soils and Foundations J.* Special issue on geotechnical aspects of the January 17, 1995 Hyogoken-Nambu earthquake. January, 1996. Tokyo.
- Juang, C. H., Rosowsky, D.V., and Tang, W. H. (1999). A reliability-based method for assessing liquefaction potential of sandy soils. *J. Geotechnical and Geoenvironmental Engineering* 125(8): 684–89. ASCE.
- Juang, C. H., Chen, C. J., Rosowsky, D. V. and Tang, W. H. (2000). A risk-based method for assessing liquefaction potential using CPT. *Géotechnique* 50(5): 583–92. Institution of Civil Engineers.
- Juang, C. H. and Jiang, T. (2000). Assessing probabilistic methods for liquefaction potential evaluation. In *Soil dynamics and liquefaction 2000, Procs., Geo-Denver 2000: August 5–8, 2000, Denver, Colorado*, Ronald Y. S. Pak, Jerry Yamamura, eds., pp. 148–62. Geotechnical Special Publication No. 107. Reston, Va.: American Society of Civil Engineers.
- Kammerer, A., Wu, J. Pestana, J., Riemer, M., and Seed, R. (2000). *Cyclic simple shear testing of Nevada sand for PEER Center Project 2051999*. Research report no. UCB/GT/00-02. Berkeley, Calif.: University of California.
- Kimura, T., Takemura, J., and Hirooka, A. (1993). Numerical prediction for model no. 1. In *Procs., International Conference on the Verification of Numerical Procedures for the Analysis of Soil Liquefaction Problems, Davis, California, USA, 17–20 October 1993*, K. Arulanandan and R. F. Scott, eds., vol. 1, pp. 141–52. Rotterdam: Balkema Publishers.
- Kimura, T., Kusakabe, O., and Takemura, J. (eds.) (1998). “Centrifuge 98,” *Procs., International Conference Centrifuge 98, Tokyo, Japan, September 23–25, 1998*. Brookfield, Vt.; Rotterdam: Balkema Publishers.
- Kokusho, T. (1999). Water film in liquefied sand and its effect on lateral spread. *J. Geotechnical and Geoenvironmental Engineering* 125(10): 817–26. ASCE.
- Kokusho, T., Kojima, T., and Nonaka, N. (1999). Emergence of water film in liquefied sand and its role in lateral flow. *Procs., 12<sup>th</sup> World Conference on Earthquake Engineering*, Auckland, New Zealand. No. 0946 (CD-ROM).
- Kovacs, W. D., and Salomone, L. A. (1982). SPT hammer energy measurement. *J. Geotechnical Engineering Division* 108(GT4): 599–620. ASCE.
- Kramer, S. L. (1996). *Geotechnical earthquake engineering*. Upper Saddle River, N.J.: Prentice Hall.
- Kramer, S., and Arduino, P. (1999). Constitutive modeling of cyclic mobility and implications for site response. In *Second International Conference on Earthquake Geotechnical Engineering, Lisbon, Portugal, 21–25 June 1999*, vol. 3, pp. 1029-1034. Brookfield, Vt.; Rotterdam: Balkema Publishers.

- Kutter, B. L., and Balakrishnan, A. (1998). Dynamic model test data from electronics to knowledge. Special Lecture. In *Procs. International Conference Centrifuge 98, Tokyo, Japan, September 23–25, 1998: “ISSMFE Centrifuge 98,”* T. Kimura, O. Kusakabe, and J. Takemura, eds., vol. 2, pp. 931–44. Rotterdam: Balkema Publishers.
- Kutter, B. L., and Wilson, D.W. (1999). De-liquefaction shock waves. In *Procs., Seventh U.S.-Japan Workshop on Earthquake Resistant Design of Lifeline Facilities and Countermeasures against Soil Liquefaction, Seattle, Washington, August 15–17, 1999*, pp. 295–309. Technical Report MCEER-99-0019. Buffalo, N.Y.: Multidisciplinary Center for Earthquake Engineering Research.
- Lacy, S. (1986). Numerical procedures for nonlinear transient analysis of two-phase soil system. Ph.D. dissertation. Princeton, N.J.: Princeton University.
- Lade, P. V., and Duncan, J. M. (1973). Cubical triaxial tests on cohesionless soil. *J. Soil Mechanics and Foundations Division* 99(SM10): 793–812. ASCE.
- Lade, P. V., and Yamamuro, J. A., eds. (1999). Physics and mechanics of soil liquefaction. In *Procs., International Workshop on the Physics and Mechanics of Soil Liquefaction, Baltimore, Maryland, September 10–11, 1998*. Rotterdam: A.A. Balkema.
- Lambe, T. W., and Whitman, R. V. (1969). *Soil mechanics*. New York: John Wiley & Sons.
- Lee, C.-J., Wu, B., Abdoun, T. and Dobry, R. (2000). *Centrifuge modeling of effects of liquefaction and lateral spreading on quay walls*. Troy, N.Y.: Dept. of Civil Engineering, Rensselaer Polytechnic Institute.
- Li, X. S. (1990). Free field response under multi-directional earthquake loading. Ph.D. dissertation. Dept. of Civil Engineering, University of California, Davis.
- Li, X. S. (1993). Numerical prediction for model no. 1. In *Procs., International Conference on the Verification of Numerical Procedures for the Analysis of Soil Liquefaction Problems, Davis, California, USA, 17–20 October 1993*, K. Arulanandan and R. F. Scott, eds., vol. 1, pp. 169–78. Rotterdam: Balkema Publishers.
- Li, X. S. (1997). Modeling of dilative shear failure. *J. Geotechnical and Geoenvironmental Engineering* 123(7): 609–16. ASCE.
- Li, X. S., Ming, H. Y., and Cai, Z. Y. (2000). Constitutive modeling of flow liquefaction and cyclic mobility. In *Computer Simulation of Earthquake Effects, Procs., Geo-Denver 2000: August 5–8, 2000, Denver, Colorado*, K. Arulanandan, A. Anandarajah, and X. S. Li, eds., pp. 81–98. Geotechnical Special Publication 110. New York: ASCE.
- Li, X. S., and Dafalias, Y. F. (2000). Dilatancy for cohesionless soils. *Géotechnique* 50(4): 449–60.

- Li, X. S. (2001). An anisotropic parameter for critical state modeling of sand response. In *2001 Mechanics and Materials Summer Conference, June 27–29, San Diego, California*.
- Liu, H. and Qiao, T. (1984). Liquefaction potential of saturated sand deposits underlying foundation of structure. In *Procs., 8th World Conference on Earthquake Engineering*, San Francisco, California, vol. III, pp. 199–206.
- Loret, B., and Prevost, J. H. (1990). Dynamic strain localization in elasto-(visco-)plastic solids, Part 1: General formulation and one-dimensional examples. *Computer Methods in Applied Mechanics and Engineering* 83: 247–73.
- Manzari, M. T. (1996). Finite deformation analysis of liquefaction-induced flow failures in soil embankments. *Intl. J. Geotechnical and Geological Engineering* 14(2): 83–110.
- Manzari, M. T., and Dafalias, Y. F. (1997). A critical state two-surface plasticity model for sands. *Géotechnique* 49(2): 252–72.
- Matsuoka H., and Sakakibara A. (1987). A constitutive model for sands and clays evaluating principal stress rotation. *Soils and Foundations* 27(4): 73–88.
- Mroz, Z. (1967). On the description of anisotropic work hardening. *J. Mechanics and Physics of Solids* 15: 163–75.
- Muraleetharan, K. K. (1993a). Numerical prediction for model no. 1. In *Procs., International Conference on the Verification of Numerical Procedures for the Analysis of Soil Liquefaction Problems, Davis, California, USA, 17–20 October 1993*, K. Arulanandan, and R. F. Scott, eds., vol. 1, pp. 187–96. Rotterdam: Balkema Publishers.
- Muraleetharan, K. K. (1993b). Numerical prediction for model no. 4a. In *Procs., International Conference on the Verification of Numerical Procedures for the Analysis of Soil Liquefaction Problems, Davis, California, USA, 17–20 October 1993*, K. Arulanandan, and R. F. Scott, eds., vol. 1, pp. 641–50. Rotterdam: Balkema Publishers.
- Muraleetharan, K. K., Mish, K. D., and Arulanandan, K. (1994). A fully coupled nonlinear dynamic analysis procedure and its verification using centrifuge test results. *Intl. J. Numerical and Analytical Methods in Geomechanics* 18: 305–25.
- Nemat-Nasser, S., and Tobita, Y. (1982). Influence of fabric on liquefaction and densification potential of cohesionless sand. *Mechanics of Materials* 1:43–62.
- Nemat-Nasser, S., and Okada, N. (2001). Radiographic and microscopic observation of shearbands in granular materials. *Journal Publication*.
- Nishi, K., and Kanatani, M. (1990). Constitutive relations for sand under cyclic loading based on elasto-plasticity theory. *Soils and Foundations* 30(2): 43–59.

- NRC (1985). *Liquefaction of soils during earthquakes*. Report by the Committee on Earthquake Engineering, National Research Council. Washington, D.C.: National Academy Press.
- Parra, E. (1996). Numerical modeling of liquefaction and lateral ground deformation including cyclic mobility and dilation response in soil systems. Ph.D. thesis. Troy, N.Y.: Dept. of Civil Engineering, Rensselaer Polytechnic Institute.
- Pastor, M., and Zienkiewicz, O. C. (1986). A generalized plasticity hierarchical model for sand under monotonic and cyclic loading. In [*Procs., 2<sup>nd</sup>*] *International Symposium on Numerical Models in Geomechanics, Ghent, 31st March–4th April, 1986*. G. N. Pande and W. F. Van Impe, eds., pp. 131–50. Cornwall, England: M. Jackson and Son Publisher.
- Peric, D., and Ayari, M. A. (2000). Influence of Lode's angle on generation of pore pressure in soils. In *Procs., Eighth International Symposium on Plasticity and Its Current Applications*, A.S. Khan, H. Zhang, and Y. Yuan, eds., pp. 312–14. Fulton, Md.: NEAT Press.
- Prevost, J. H. (1985). A simple plasticity theory for frictional cohesionless soils. *Soil Dynamics and Earthquake Engineering* 4(1): 9–17.
- Prevost, J. H. 1989. *DYNAID, A computer program for nonlinear seismic site response analysis: Technical Documentation*. Technical Report NCEER-89-0025. Buffalo, N.Y.: National Center for Earthquake Engineering Research, State University of New York at Buffalo.
- Proubet, J. (1991). Application of computational geomechanics to description of soil behavior. Ph.D. dissertation. University of Southern California, Los Angeles.
- Rauch, A. F. (1997). EPOLLS: An empirical method for predicting surface displacement due to liquefaction-induced lateral spreading in earthquakes. Ph.D. dissertation. Virginia Polytechnic Institute and State University, Blacksburg, Va.
- Reimer, M. F., and Seed, R. B. (1997). Factors affecting apparent position of steady-state line. *J. Geotechnical and Geoenvironmental Engineering* 123(3): 281–88. ASCE.
- Scott, R. F., and Zuckerman, K. A. (1972). Sandblows and liquefaction. In *The Great Alaska Earthquake of 1964*, pp. 179–89. Engineering Publication 1606. Washington, D.C.: National Academy of Sciences.
- Seed, H. B., and Lee, K. L. (1966). Liquefaction of saturated sands during cyclic loading. *J. of the Soil Mechanics and Foundations Division* 92(SM6): 105–34. ASCE.
- Seed, H. B., Lee, K. L., Idriss, I. M., and Makdisi, F. I. (1975). The slides on the San Fernando dams during the earthquake of February 9, 1971. *J. Geotechnical Engineering Div.* 101(7): 651–88. ASCE.

- Seed, H. B., (1979). Soil liquefaction and cyclic mobility evaluation for level ground during earthquakes. *J. Geotechnical Engineering Division* 105(GT2): 201–55. ASCE.
- Seed, H. B. and Idriss, I. M. (1982). Ground motions and soil liquefaction during earthquakes. Vol. 5 of Engineering monographs on earthquake criteria, structural design, and strong motion records. Berkeley, Calif.: Earthquake Engineering Research Institute.
- Seed, H. B. (1987). Design problems in soil liquefaction. *J. Geotechnical Engineering* 113(8): 827–45. ASCE.
- Seed, H. B., Seed, R. B., Harder, L. F., and Jong, H. L. (1989). *Reevaluation of the slide in the lower San Fernando Dam in the 1971 San Fernando earthquake*. Report No. UCB/EERC-88/04. Berkeley, Calif.: University of California.
- Seed, R. B., Dickenson, S. E., Riemer, M. F., Bray, J. D., Sitar, N., Mitchell, J. K., Idriss, I. M., Kayen, R. E., Kropp, A., Hander, L. F. Jr., and Power, M. S. (1990). *Preliminary report on the principal geotechnical aspects of the October 17, 1989, Loma Prieta earthquake*. Report No. UCB/EERC-90/05. Berkeley, Calif.: Earthquake Engineering Research Center, University of California.
- Sitar, N., ed. (1995). Geotechnical reconnaissance of the effects of the January 17, 1995, Hyogoken-Nanbu earthquake Japan. Report No. UCB/EERC-95/01. Berkeley, Calif.: Earthquake Engineering Research Center.
- Stark, T. D., S. M. Olson, W. H. Walton, and G. Castro (2000). 1907 static liquefaction flow failure of the north dike of Wachusett Dam. *J. Geotechnical and Geoenvironmental Engineering* 126(12): 1184–93. ASCE.
- Sture, S. (1999). Constitutive issues in soil liquefaction. *Procs., International Workshop on the Physics and Mechanics of Soil Liquefaction, September 10–11, 1998, Baltimore, Maryland*, P.V. Lade and J.A. Yamamuro, eds., pp. 133–43. Rotterdam: A.A. Balkema.
- Taboada, V. M. (1995). Centrifuge modeling of earthquake-induced lateral spreading in sand using a laminar box. Ph.D. thesis. Troy, N.Y.: Rensselaer Polytechnic Institute.
- Tan, T. S., and Scott, R. F. (1985). Centrifuge scaling considerations for fluid-particle systems. *Géotechnique* 35(4): 461–70.
- Tateishi, A., Taguchi, Y, Oka, F. and Yashima, A. (1995). A cyclic elasto-plastic model for sand and its application under various stress conditions. In *Procs., 1st International Conference on Earthquake Geotechnical Engineering, Tokyo, Japan, 14–16 November, 1995*, vol. 1, pp. 399–404. Rotterdam: Balkema Publishers.
- Thomas, P. A., and Bray, J. D. (1999). Capturing nonspherical shape of granular media with disk clusters. *J. Geotechnical and Geoenvironmental Engineering* 125(3): 169–78.

- Tobita, Y., and Yoshida, N. (1995). Stability of mechanically well-behaved constitutive model in liquefaction analysis of saturated sands. In *Procs., 1st International Conference on Earthquake Geotechnical Engineering, Tokyo, Japan, 14–16 November, 1995*, vol. 1, pp. 429–34. Rotterdam: Balkema Publishers.
- Toprak, S., Holzer, T. L., Bennett, M.J., and Tinsley, J.C. III (1999). CPT- and SPT-based probabilistic assessment of liquefaction potential. In *Procs., Seventh U.S.-Japan Workshop on Earthquake Resistant Design of Lifeline Facilities and Countermeasures against Soil Liquefaction* pp. 69–86. Technical Report MCEER-99-0019. Buffalo, N.Y.: Multidisciplinary Center for Earthquake Engineering Research.
- Vaid, Y. P., Chung, E. K. F., and Kuerbis, R. (1990). Stress path and steady state. *Canadian Geotechnical J.* 27(1): 1–7.
- Vaid, Y. P., and Thomas, J. (1995). Liquefaction and postliquefaction behavior of sand. *J. Geotechnical Engineering* 121(2): 163–73. ASCE.
- Vaid, Y. P., and Sivathayalan, S. (1999). Fundamental factors affecting liquefaction susceptibility of sands. In *Physics and Mechanics of Soil Liquefaction*, P. V. Lade and J. A. Yamamuro, eds., pp. 105–120. Rotterdam: Balkema Publishers.
- Vardoulakis, I., and Sulem, J. (1995). *Bifurcation analysis in geomechanics*. London: Blackie Academic and Professional.
- Verdugo, R., and Ishihara, K. (1996). The steady state of sandy soils. *Soils and Foundations* 36(2): 81–92.
- Wang, Z. L., Dafalias, Y. F., and Shen, C. K. (1990). Bounding surface hypoplasticity model for sand. *J. Engineering Mechanics* 116: 983–1001. ASCE.
- Yang, Z. (2000). Numerical modeling of earthquake site response including dilation and liquefaction. Ph.D. dissertation. Dept. of Civil Engineering and Engineering Mechanics, Columbia University, New York.
- Yang, Z., and Elgamal, A. (2001). Influence of permeability on liquefaction-induced shear deformation. *J. Engineering Mechanics*. ASCE (In Review).
- Yoshimine, M., and Ishihara, K. (1998). Flow potential of sand during liquefaction. *Soils and Foundations* 38(2): 189–98.
- Youd, T. L., and Holzer, T. L. (1994). Piezometer performance at the Wildlife liquefaction site." *J. Geotechnical Engineering* 120(6): 975–95. ASCE.
- Youd, T. L., Hansen, C., and Bartlett, S (1999). Revised MLR equations for predicting lateral spread displacement. In *7th U.S.-Japan Workshop on Earthquake Resistant Design of Lifeline Facilities and Countermeasures against Soil Liquefaction, August 15–17, 1999*,

*Seattle, Washington*, T. D. O'Rourke, J. P. Bardet, M. Hamada, eds., pp. 99–114. Technical Report MCEER-99-0019. Buffalo, N.Y.: Multidisciplinary Center for Earthquake Engineering Research, State University of New York.

Youd, T. L., Idriss, I. M., Andrus, R. D., Arango, I., Castro, G., Christian, J. T., Dobry, R., Finn, W. D. L., Harder, L. F., Hynes, M. E., Ishihara, K., Koester, J. P., Liao, S. S. C., Marcuson, W. F. III, Martin, G. R., Mitchell, J. K., Moriwaki, Y., Power, M. S., Robertson, P. K., Seed, R. B., and Stokow, K.H. II (2001). Liquefaction resistance of soils: Summary report from the 1996 NCEER and 1998 NCEER/NSF workshops on evaluation of liquefaction resistance of soils. *J. Geotechnical and Geoenvironmental Engineering* 127(10): 817–33.

Zeghal, M., and Elgamal, A.-W. (1994). Analysis of site liquefaction using earthquake records. *J. Geotechnical Engineering* 120(6): 996–1017. ASCE.

Zeghal, M., Elgamal, A. -W. and Parra, E. (1996). Identification and modeling of earthquake ground response II: Site liquefaction. *Soil Dynamics and Earthquake Engineering* 15: 523–47.

Zeng, X., and Arulanandan, K. (1995). Modeling lateral sliding of slope due to liquefaction of sand layer. *J. Geotechnical Engineering* 121(11): 814–16. ASCE.

Zienkiewicz, O. C., Chan, A. H. C., Pastor, M., Paul, D. K., and Shiomi, T. (1990). *Static and dynamic behavior of soils: A rational approach to quantitative solutions: I. Fully saturated problems*. Royal Society London, A 429, 285–309.